FOURIER TRANSFORM PHOTOLUMINESCENCE SPECTROSCOPY

OF

DONOR BOUND EXCITONS IN GaAs AT HIGH MAGNETIC FIELDS

by

Douglas J.S. Beckett

B.Sc., University of Waterloo, 1984

M.Sc., University of Ottawa, 1986

THESIS SUBMITTED IN PARTIAL FULFILLMENT OF

THE REQUIREMENTS FOR THE DEGREE OF

DOCTOR OF PHILOSOPHY

in the Department

of

PHYSICS

SIMON FRASER UNIVERSITY

December 1990

APPROVAL

Name: Douglas J.S. Beckett

Degree: Ph.D. (Physics)

Title of Thesis: Fourier Transform Photoluminescence Spectroscopy of Donor Bound Excitons in GaAs at High Magnetic Fields

Examining Committee: Chairman: Dr. E.D. Crozier

Dr. M.L.W. Thewalt
Senior Supervisor

Dr. G. Kirczenow

Dr. J.C. Irwin

Dr. R.F. Frindt

Dr. E.S. Koteles
External Examiner
GTE Laboratories
Waltham, Massachusetts

Date Approved: December 18, 1990

PARTIAL COPYRIGHT LICENSE

I hereby grant to Simon Fraser University the right to lend my thesis, project or extended essay (the title of which is shown below) to users of the Simon Fraser University Library, and to make partial or single copies only for such users or in response to a request from the library of any other university, or other educational institution, on its own behalf or for one of its users. I further agree that permission for multiple copying of this work for scholarly purposes may be granted by me or the Dean of Graduate Studies. It is understood that copying or publication of this work for financial gain shall not be allowed without my written permission.

Title of Thesis/Project/Extended Essay

Fourier Transform Photoluminescence Spectroscopy

of Donor Bound Excitons in GaAs at High Magnetic Fields

Author: _____
(Signature)

Douglas J.S. Beckett
(Name)

December 20, 1990
(Date)

ABSTRACT

As a means of studying semiconductor photoluminescence, Fourier transform interferometry offers resolution and signal throughput capabilities which are superior to those of conventional dispersive spectroscopy. In this thesis, Fourier transform photoluminescence spectroscopy studies of the donor bound exciton in GaAs will be presented. The behaviour of the donor related photoluminescence transitions is studied as a function of magnetic field strength, orientation and excitation wavelength.

Furthermore, the application of Fourier transform photoluminescence to donor species identification in GaAs at high magnetic field is demonstrated. The energies of the various species-dependent transitions important for characterization are measured with unprecedented precision, and should provide a standard for such studies.

Finally, a straightforward and reliable method, using resonant excitation, is developed for donor identification in less pure materials. This method is based on results obtained for high purity epitaxial GaAs. The resonant technique is demonstrated for bulk semi-insulating GaAs.

ACKNOWLEDGEMENTS

I would like to thank my supervisor, Dr. Mike Thewalt for creating a first class research environment.

The donation of high-purity epitaxial GaAs samples by Dr. Simon Watkins of American Cyanamid Company, and a variety of semi-insulating GaAs samples by Dr. Maria Maciaszek of Johnson-Matthey Electronics is gratefully acknowledged.

I would also like to thank the Natural Sciences and Engineering Research Council, the B.C. Advanced Systems Foundation, Simon Fraser University and Dr. M.L.W. Thewalt for financial support.

I would like to thank Emily, Stéphanie and Michèle for having a graduate student for a Dad.

TABLE OF CONTENTS

LIST OF TABLES

LIST OF FIGURES

LIST OF FIGURES (CONTINUED)

LIST OF ABBREVIATIONS

APD	avalanche photo-diode
BE	bound exciton
FE	free exciton
FIEAS	far infrared exciton absorption spectroscopy
FIR	far infrared
FTPL	Fourier transform photoluminescence
FTPLE	Fourier transform photoluminescence excitation
MOCVD	metal-organic chemical vapour deposition
MPL	magneto-photoluminescence
NIR	near infrared
PL	photoluminescence
PLE	photoluminescence excitation
PMT	photomultiplier tube
PTIS	photo-thermal ionization spectroscopy
RK	Rühle and Klingenstein, in reference [78R1]
SBCC	Skromme, Bhat, Cox, and Colas, in reference [89S1]
SI	semi-insulating
SNR	signal to noise ratio
TES	two electron satellite

CHAPTER 1. INTRODUCTION

1.1 Rationale

Photoluminescence (PL) is one of the most widely used techniques for studying semiconductors. Its applicability to this field derives from the precise measurements of transition energies which it can provide, and the importance of these measurements in studying both the fundamental and technologically important properties of these materials. The topics of fundamental physics and materials characterization are often closely related, as the detailed study of impurities and defects can reveal both their structure and their effect upon the electrical properties of the semiconductor. Since the utility of semiconductors in electronics is based on their electrical characteristics, it follows that materials characterization plays a crucial role in the development of the industry as a whole.

The particular interest in the characterization of GaAs stems from its widespread use in the field of optical devices, and its suitability for high-speed electronics. It has even been opined that GaAs would eventually replace silicon in even conventional electronic applications, but because of the the advanced state of Si processing technology, the superiority of Si for device processing, and recent advances in Si-based heterostructures, this has not yet happened, and probably never will. However, due to its direct band gap, GaAs is the material used for a large number of electro-optical applications, especially in the telecommunications and recording industries. Also, the higher electron mobilities attainable in GaAs make it the choice material for ultra-fast

semiconductor devices.

The interest in donor related photoluminescence in GaAs does not arise solely from its applicability to the semiconductor industry. It is also due to its suitability as a test of unconventional (for PL) spectroscopic techniques, *i.e.* Fourier transform interferometry, because of the high resolution required to study the rich donor bound exciton spectrum. Furthermore, there is a fundamental interest in the behaviour of this bound exciton system in the presence of a magnetic field, as well as the challenge presented by one of the most difficult problems in the characterization of semiconductors by optical techniques.

1.2 Background

Later chapters of this thesis require understanding of the basics of semiconductor physics. Descriptions of the properties of semiconductors are given in many textbooks (e.g. Kittel [86K1]), and a knowledge of what is meant by such terms as band gap, donor and acceptor, *etc.* will be assumed. A more in-depth understanding of some topics such as impurity energy levels, excitons and bound excitons is also needed. This section will be devoted to a review of such subjects.

The momentum dependence of the electron and hole energies gives a dispersion relation for the energy bands. Most electronic and optical properties depend on the behaviour of electrons (holes) which have the minimum allowable energies, having relaxed by scattering with lattice phonons, to the band extrema. For many calculations, the bands are assumed parabolic at these extrema, and we can calculate their energies as if they were free electrons (holes) with

$$E(\mathbf{k}) = \frac{\hbar^2 k^2}{2\, m_{eff}} \qquad (1.1)$$

where: $m_{eff} = \left(\frac{\partial^2 E}{\partial \mathbf{k}^2} \right)^{-1}$ is the effective mass of the electron (hole).

This is usually a good assumption near the the band extrema, and m_{eff} is simply the inverse of the curvature of the band in the E-**k** diagram. Thus sharply curved bands will have lighter effective masses (and therefore higher intrinsic mobilities) than bands with less curvature. The equation for the effective mass may be tensorial in nature, which means that anisotropic band edges will result in effective masses which vary depending on the direction of carrier motion.

Much of the success of semiconductor physics derives from the analogies which can be made between impurity spectra and atomic physics. The analogy with hydrogen is exploited fully when studying shallow donors (acceptors) [81R1], where the charged impurity core weakly binds an electron (hole). The weak nature of the bond, relative to atomic hydrogen, is due mostly to the screening effect of the high-dielectric-constant semiconductor (ε = 12.56 in GaAs [71S1]). The energy levels of such donors are thus only slightly below the free-electron states which form the conduction band. Acceptor energy levels behave in a similar manner. Because weakly bound impurity states can be represented as a linear combination of states taken near the band extrema, they exhibit an effective mass similar to the free carriers at the band edges. This

effective mass must also be considered in calculating the hydrogen-like ionization energy. The energy levels are calculated theoretically (called effective mass theory) to give:

$$E_n = - \frac{m_{eff} e^4}{2\varepsilon^2 n^2 \hbar^2} \qquad (1.2)$$

where m_{eff} = effective mass (~0.07 m_0 for e in GaAs)

ε = dielectric constant

These result in a theoretical donor ionization energy of 31.27 meV in Si and 5.715 meV in GaAs. The actual values observed in far infrared (FIR) absorption, vary between 30 and 45 meV for shallow donors in Si depending on the chemical identity. The differences in the observed values are due to the so-called central-cell potential V_c, which is usually considered as a perturbation to effective-mass theory. This is an effect of the different environment existing for different chemical species, even though they are all donors. In this case the charge of the bound particle, ρ_c, in the vicinity of V_c causes an increase in the ionization energy E_i of the impurity states (whose energy is given by eq. 1.2) by an amount [73D1,76B1]

$$\Delta E_i = V_c \rho_c \qquad (1.3)$$

The shift of the ionization energy is *different* for each energy

level, as the amount of charge in the central-cell region will decrease as the wavefunctions become more extended. Such a species dependent difference in ionization energy allows the use of FIR absorption or PL measurements to determine donor impurity identities in Si.

However, in GaAs, experimental ionization energies vary only over the range of 5.752 to 5.913 meV. Such donors are said to be "effective-mass-like", because the Bohr-radius (~50 Å in GaAs [81R1]) extends over many lattice spacings (~6 Å [82L1]) and ΔE_i in eq. 1.3 is small, even for the lowest states. This insensitivity of the binding energy to the nature of the chemical identity of the donor atom in GaAs is the reason why donor identification by spectroscopic means is so difficult.

In analogy with the donor case, shallow acceptor bound holes take on the effective mass of the valence band, resulting in effective-mass-like energy levels. Because the effective mass (curvature) of the valence band is different from that of conduction band, the ionization energy for acceptors are different than for donors. In GaAs, the effective mass theory gives 26.0 meV [90S1] for the acceptor ionization energies. The experimentally measured values are 26 to 40 meV.

The basis of optical characterization in semiconductors is the impurity- or defect-specific nature of energy levels within the forbidden energy gap of the semiconductor. These energy levels are also responsible for the electrical behavior, which is of primary interest in these materials. By observing the emission or absorption of light due to transitions between these levels, or associated levels such as bound excitons, a great deal of information can be obtained.

The technique used throughout this work is photoluminescence, in which optical excitation is used to populate higher energy states of the crystal. The luminescent decay of the these excited states is then monitored. The photoluminescence of excitons bound to donors in GaAs is the subject of this thesis.

As discussed in the preceding section, simple donors and acceptors form energy levels within the energy gap and close to the band edges. Such levels are called "shallow". Energy levels closer to the middle of the band gap can also exist, caused by the presence of other impurities and defects (or combinations thereof). These levels within the band gap can also have major effects on the electrical and optical properties of the material. However, in this thesis, only the shallow donor bound excitons will be considered.

The simplest form of photoluminescence is performed by exciting an electron from deep within the valence band to high in the conduction band. The resulting energetic, mobile electron and hole then relax to the band edges by emission of phonons (i.e. they cool down or "thermalize"). The electron and hole can then recombine, giving off a photon in luminescence, whose energy is equal to the band gap energy. At room temperature, this is the dominant photoluminescence process. The electron and hole can also recombine via non-radiative paths, especially if the defect or impurity concentration is high.

If the temperature is lowered to near 0 K, (e.g. by immersing the sample in liquid helium), other processes can occur. In the regime of reduced thermal excitations, carriers will lower their energy by binding to impurities, defects, or other particles. One of the most important

processes is the case where electrons and holes bind together in a hydrogen-like entity called an exciton. The binding energy is small due to the small effective masses and high dielectric constant as was the case for shallow donors and acceptors. In addition, because it is made up of *two* light particles (unlike donors and acceptors) the effective mass used in calculating the energy spectrum must be the reduced effective mass μ of the electron and hole given by:

$$\frac{1}{\mu} = \frac{1}{m_e} + \frac{1}{m_h} \qquad (1.4)$$

where: m_e = electron effective mass

m_h = hole effective mass

This results in a lower binding energy than for a donor or acceptor, and is the reason why even lower temperatures are required to form excitons than to trap carriers onto ionized donors and acceptors. At high temperature excitons would be dissociated by the thermal lattice vibrations (phonons). The free exciton (FE) is a mobile, neutral, hydrogen-like particle, but like positronium, the constituents of the exciton recombine within a finite lifetime, giving luminescence at a characteristic energy

$$E_{FE} = E_g + E_X + E_{kin} \qquad (1.5)$$

where: E_g = the semiconductor energy band gap

$E_x = -\frac{\mu e^4}{2\varepsilon^2 n^2 \hbar^2}$ is the hydrogen-like bound state energy spectrum

E_{kin} = the kinetic energy

The kinetic energy term reflects the fact that the FE is made up of mobile electrons and holes and will display a thermal distribution. In Si, the kinetic energy is very well represented by the classical Boltzmann distribution. In GaAs, the direct-gap results in complicated behaviour for $E_{kin} \rightarrow 0$, because of the exciton polariton effect.

Since excitons are mobile, they are free to diffuse through the crystal, and can become localized onto impurities, a process which further lowers their energy. This localized particle is a bound exciton (BE). The recombination of a bound exciton would result in photons of even lower energy:

$$E_{BE} = E_{FE}\Big|_0 - E_{loc} \qquad (1.6)$$

where: $E_{FE}\Big|_0$ = the minimum FE energy (*i.e.* n = 1, $E_{kin} = 0$)

E_{loc} = the BE localization energy

Like impurity ionization energies, the localization energy may also display impurity dependence, due to the effect of the central-cell potential V_c on the charge associated with the BE wavefunction. The impurity specific differences in E_{BE} can be related to eq. 1.3 through

$$E_{loc} = a\, E_i + b \qquad (1.7)$$

which is an empirical relation called Haynes' rule [60H1].

A schematic diagram of some possible excitonic transitions is shown in Fig. 1.1. For shallow donors and acceptors in Si and GaAs, the localization energy is about 1/10 the donor or acceptor ionization energy (*i.e.* a = .1), while b ~ 0. Thus, if the donors or acceptors due to different chemical species have different ionization energies, then the recombination luminescence of their BE's will be impurity specific as well. This forms the basis for much of the optical characterization of semiconductors by PL. It should be noted that in contrast to FE luminescence, the BE recombination transitions are very narrow, as the binding eliminates the kinetic energy distribution associated with free particles.

The BE luminescence was described above as if there were only one possible initial state and one possible final state. However, as depicted in Fig. 1.1, the bound exciton has an excited-state spectrum, as do the binding centers which form the final states in such recombination transitions. In the case of donor or acceptor binding centers, the spectrum of the final state is that described earlier for such impurities.

The initial state may thus in general be any one of the possible BE energy levels. The population of the initial levels is usually determined by the temperature, as such systems often reach thermal equilibrium before recombination. However, for centers exhibiting very

Figure 1.1

Schematic diagram of the important BE photoluminescence transitions. The excited states for the binding center *and* the bound exciton are shown. Two-electron satellites refers to donor BE, for acceptor BE the corresponding transitions are referred to as two-hole satellites.

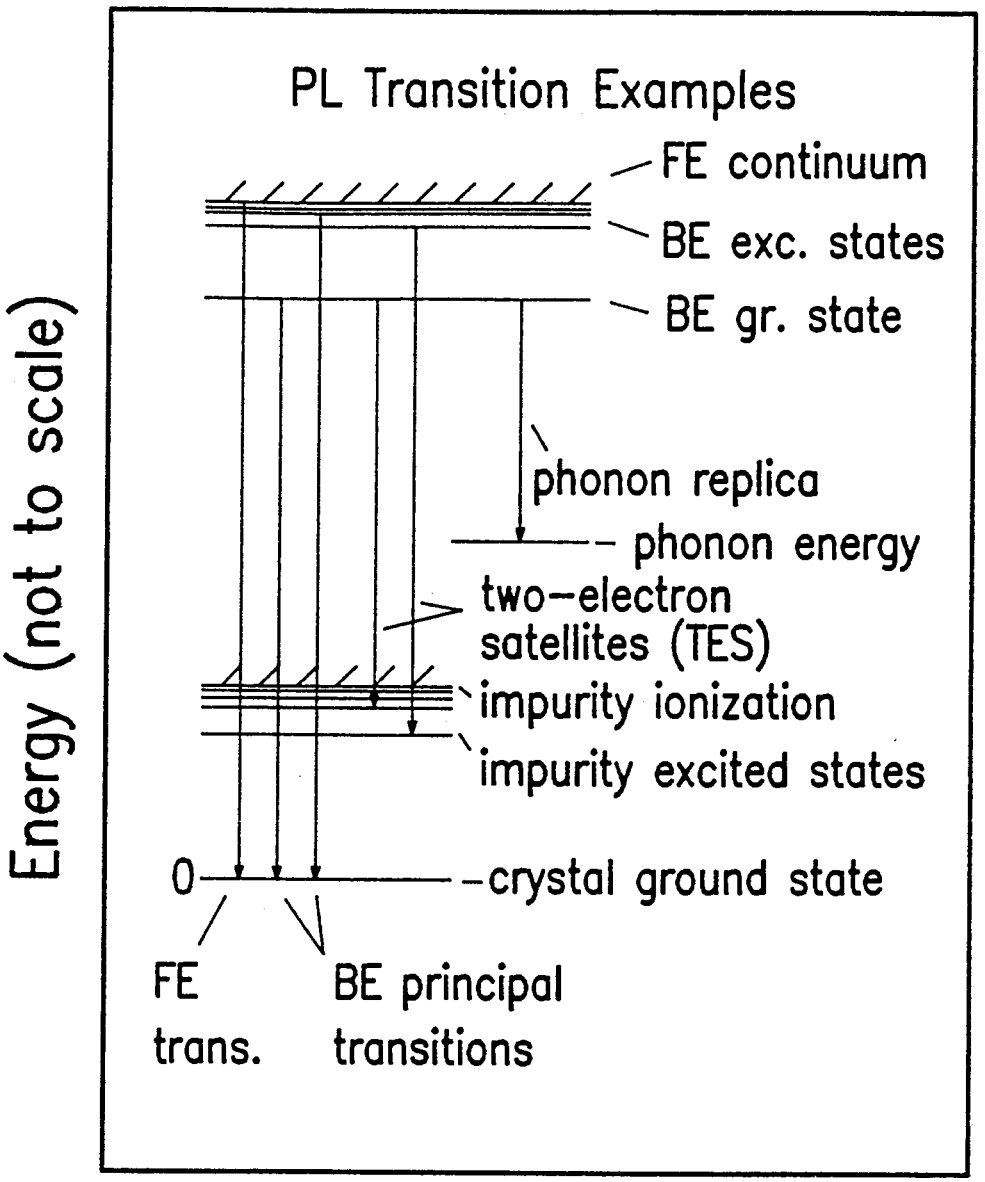
PL Transition Examples
Energy (not to scale)
FE continuum
BE exc. states
BE gr. state
phonon replica
phonon energy
two-electron satellites (TES)
impurity ionization
impurity excited states
0
crystal ground state
FE trans.
BE principal transitions

fast recombination, the excited states may represent a greater proportion of the initial state population than that dictated by the thermal distribution in equilibrium.

These thermally depopulated BE excited states can be better observed in more complicated experiments. The most common is photoluminescence excitation (PLE) spectroscopy, where the BE is created directly by absorption of a photon at one of its excited state energies, and then relaxes to the BE ground state. The luminescence of the ground state recombination transition is detected. The dependence of the ground state luminescence intensity on the excitation energy gives the BE excited state spectrum. There are many examples of the use of this technique. Two of the earliest are by Faulkner and Dean [70F1] and Cohen and Sturge [77C1].

Another approach developed recently by Thewalt and co-workers [84L1,85T1] is far infrared exciton absorption spectroscopy (FIEAS). In this technique, the bound excitons are created by near band gap excitation, and the BE ground state to excited state absorption spectrum is measured in the FIR, in analogy with impurity FIR absorption.

These two methods provide complementary information, as the selection rules result in the creation of BE in the even parity excited states for PLE and odd parity for FIEAS. However, FIEAS may be restricted to systems which have a long BE ground state lifetime, such as isoelectronic BE in Si, in order to increase the probability of such a two-step process. For this reason, the technique was not attempted for the donor BE in GaAs.

In addition to the complications of the excited initial state, the

final state of the transition may also be an excited state of the impurity binding center. Such PL transitions are often referred to as two-electron transitions or satellites (TES) for donors, since both electrons in the donor BE complex take part in the transition. For acceptors, the label two-hole transition or satellite is used. Such transitions are shown in Fig. 1.1. The occurrence of such excited final state transitions is governed both by conventional selection rules as well as the spatial overlap of the initial state wave function with that of the final state.

The result of such an excited-final-state transition is a luminescence photon whose energy has been reduced (compared to the ground state to ground state, or principal transition energy) by the impurity excitation energy. Thus a series of luminescence lines to lower energy can often be observed, converging to an ionization energy equal to that observed in the far infrared absorption spectrum of the binding center. The observation of such transitions in the PL spectrum provides definitive proof that a luminescence transition corresponds to a particular binding center seen in FIR absorption, and thus such transitions are important for characterization studies.

1.3. Donor Identification in III-V Semiconductors by Photoluminescence

As explained in section 1.1, the donors in GaAs are almost perfectly described by effective-mass theory. The small conduction band effective mass results in wavefunctions which extend over many lattice spacings and thus exhibit very little sensitivity to the identity of the binding center. As such, donors have very little chemical-species-dependant

shift, which makes them difficult to identify, even by optical means.

It has been found that the application of a strong magnetic field enhances the central-cell splitting, allowing the species dependent resolution of the FIR transitions of different donors. This enhancement is due to the compression of the donor wavefunction in the magnetic field and the consequent increased dependence of the ground state energy on the chemical identity of the binding center.

A variant of FIR absorption called photo-thermal ionization spectroscopy (PTIS) has been applied very successfully to this problem. PTIS is a photo-conductivity technique in which the FIR optical excitation of an electron (in the case of a donor) from the impurity ground state to one of the lower excited states is followed by thermal ionization of the impurity. This ionization results in an increase in the conductivity which is very sensitive to the energy of the incident FIR photons. PTIS has a predicted sensitivity of as low as 10^8 impurities/cm^{-3}, well beyond the purity level of any semiconductor ever grown.

As described previously, the donor energy spectrum, which is in the FIR spectral region, can also be observed in the near infrared (NIR) PL by means of the TES of the donor BE. When carried out at the same magnetic field, the TES are separated from the lowest PL principal transition by the same energy as measured by PTIS (less the energy of an electron spin-flip, due to selection rules). In addition, there is a slight augmentation of the TES central-cell splitting over that observed in PTIS, due to a magnetic-field-induced central-cell splitting of the donor bound exciton *initial* state. For very pure samples, species

dependent splittings can be observed even in the principal BE transitions.

The BE spectrum for GaAs (and InP) is complicated by the existence of excited hole states. These states are analogous with those of the hydrogen molecule, and the BE can be modeled as a nonrigid rotator [78R1]. This model, due to Rühle and Klingenstein (RK), is successful in explaining the observed luminescence transitions of the donor BE. The model classifies the states according to the rotational quantum number ℓ_{rot}, and gives the following zero-field spectrum (valid for small ℓ_{rot}):

$$E_{\ell_{rot}} = \frac{-(2m_h a^2/\hbar^2)D^2}{\left\{ \frac{1}{2} + \left[\left(\ell_{rot} + \frac{1}{2} \right)^2 + (2m_h a^2/\hbar^2)D \right]^{\frac{1}{2}} \right\}^2} \qquad (1.8)$$

where: a and D are distance and energy parameters of the potential well used in the model

m_h is the hole effective mass.

The value of energy for $\ell_{rot} = 0$ is calculated using the *mean* effective hole mass (as is used to calculate the acceptor ionization energy in the effective mass approximation). This is the ground state, with the non-zero energy being the zero-point energy in the potential used in the model. However, the quantities which are most relevant are the energy separations for levels with different ℓ_{rot}.

It is useful to note that different values for the hole effective mass (m_h) are used for $\ell_{rot} > 0$. The so-called heavy and light holes are identified with the $m_j = \pm\frac{3}{2}$ and $m_j = \pm\frac{1}{2}$ projections respectively, of the $j = \frac{3}{2}$ angular momentum of the 4-fold degenerate valence band edge. The degeneracies of the hole angular momentum (and hence the effective masses) are lifted by the quantizing axis of the rotational angular momentum in the nonrigid rotator model. This will be of some significance in Chapter 4.

This thesis will be concentrated in two areas. One is the study of the energy levels involved in the donor bound exciton (D^0,X) recombination transitions in GaAs at high magnetic fields. The second is the investigation of the use of magneto-photoluminescence (MPL) as a technique for donor identification in both epitaxial and bulk GaAs, with emphasis placed on the role of Fourier transform interferometry.

One of the most attractive features of photoluminescence characterization is that it is one of the most sensitive techniques for identifying impurities in semiconductors which are pure enough to be technologically important. A comparison of other common techniques for impurity identification techniques gives the following minimum detectable impurity concentrations: PL lower than 10^{11} cm^{-3}; secondary ion mass spectroscopy (SIMS) high 10^{13} cm^{-3}; local vibrational mode (LVM) infrared absorption mid $10^{14}cm^{-3}$; atomic absorption spectroscopy mid $10^{14}cm^{-3}$; and glow discharge mass spectroscopy $10^{15}cm^{-3}$. Thus only PL and PTIS are sensitive enough to reach the low impurity levels of the purest semiconductors, which can be less than 10^{11} cm^{-3}.

Another important advantage of all-optical characterization is its

inherent non-destructive nature. This is in contrast with conductivity techniques such as PTIS, which require the application of ohmic electrical contacts. This is obviously undesirable in cases where other processing is to follow, such as on a piece of substrate material.

One area in which PL techniques have been difficult to apply, however, is to donor identification in III-V materials. The very small species-dependent central-cell shifts, combined with the reduction of this shift for BE implied by Haynes' rule, makes the donor BE PL lines occur at very nearly the same energy in GaAs. Even with the application of a high magnetic field, resolving the different donor transitions is very difficult, and until now has been limited by the dispersive spectroscopic methods normally used for GaAs PL. It will be shown that FTPL removes this limitation.

The course of action taken in this research has been to follow the best of the previous work with a comprehensive and exhaustive study of the transitions upon which donor identification by PL is based. This has required the study of very high quality epitaxial GaAs films. Hopefully, this work has set the standard for such characterization in the future, has resulted in some meaningful insight into donor bound exciton physics in III-V semiconductors, and has also allowed the clarification of a number of important controversies related to the high-field technique itself. In addition, the information gained in the study of high quality epitaxial material has allowed the application of the technique to the systematic and unambiguous identification of donors in bulk semi-insulating (SI) GaAs.

1.4 Spectroscopy

Every spectrum obtained for this thesis was collected by a method which is quite new to GaAs PL spectroscopy, namely Fourier transform interferometry. Special attention will be given to the role played by this technique, as without its use, this work could simply not have been completed.

The advantages of interferometry can be loosely classified as those intrinsic to the technique, or those which are due to technical and convenience limitations which are much less constraining for interferometry than for dispersive spectroscopy. In the first category are the the multiplex, or Fellgett advantage, and the throughput, or Jacquinot advantage [72B1,86G1]. The Fellgett advantage arises from the fact that in FT spectroscopy, every spectral resolution element is being collected simultaneously. This means that, for N spectral elements, this is equivalent to spending a factor of N times as much time on each spectral element as would be the case for the dispersive technique. This is only an advantage however, when the major source of noise is detector noise, which is often the case for spectral regions where photomultiplier tubes (PMT) are unavailable: *i.e.* at wavelengths longer than 1.2μm. The multiplex advantage in the signal-to-noise ratio (SNR) is expected to be $\sqrt{N}$ in this case.

A different situation occurs when the dominant noise is in the actual light signal. The shot-noise limit has noise which is proportional to the square-root of the signal intensity, and the multiplex advantage is exactly canceled. However, if there is noise which is directly proportional to the signal, e.g. as caused by unstable

excitation power, then there is a $\sqrt{N}$ *disadvantage* in using FT techniques. This underlines the need for highly stable laser sources for FTPL.

In the case of near gap GaAs PL, FT spectroscopy should offer no multiplex advantage, as the wavelengths are well within the range of PM tubes. However the throughput advantage still makes FTPL a superior choice, as demonstrated in the example given by Thewalt *et al.* [90T1], comparing an interferometer with a high quality dispersive (grating) spectrometer under identical conditions. For a 1 m double spectrometer, with f/8 optics and 1800 groove/mm gratings operated at 0.1 cm^{-1} resolution, the entrance slit would be 30 μm wide, and 20 mm high giving an area of 0.6 mm^2. This represents a ~600:1 length:width ratio, and is very difficult to utilize fully. A typical interferometer at this resolution has a *circular* entrance aperture 1.7 mm in diameter, or 2.3 mm^2 in area.

The other advantages of interferometry, are detailed in ref. 90T1. They include spectral capabilities from the FIR to the ultraviolet (UV), the ability to perform very wide spectral scans with no collection time penalty, high spectral accuracy (with no calibration!) and high flexibility in choosing the tradeoffs between SNR and resolution.

Perhaps the most important feature of interferometry as it relates to this thesis, is its unparalleled high resolution capability, which is achieved without sacrificing signal strength. The resolution is simply a function of the distance over which the scanning mirror is moved, and the quality of the optics used. In the instrument used in this work, spectral energy:resolution ratios of 500 000:1 are possible, which

translates into a best resolution of 0.024 cm^{-1} in the GaAs excitonic PL region.

Due to the exclusive use of interferometric techniques in this work, reciprocal wavelength (wavenumbers or cm^{-1}) will be used as the energy units. These units are the most accurate, as the spectral data is referenced during collection against the interference signal of a single mode, frequency stabilized HeNe laser. In addition, using wavenumbers obviates the need for conversion factors, which may change as international standards are updated. For reference purposes, the conversion factor from cm^{-1} to the more customary (for PL) meV is:

$$\text{value in meV} = (\text{value in } cm^{-1}) \times \frac{hc}{e} \times 10^5$$

(with h, c and e in SI units).

$$= (\text{value in } cm^{-1}) \times 0.1239813$$

or 1 meV = 8.065541 cm^{-1} using the latest values for h, c and e [90C1].

CHAPTER 2. LITERATURE REVIEW

2.1 Introduction

In Chapter 1, the physics of hydrogen-like shallow donors was described, as were the basics of donor identification by PL. In this chapter, a review of the literature is presented, outlining the achievements of previous workers. A short review of the use of FT spectroscopy for PL will also be given.

2.2 PTIS

As described in the previous chapter, photo-thermal ionization spectroscopy is an FIR photoconductivity technique, in which the conductivity signal arises from the ionization of the neutral donor by a combination of an FIR photon and thermal energy [77K1]. The temperature must be controlled so that the thermal energy is large enough to ionize the donor from its excited states, but not high enough to cause transitions from its ground state. The conductivity is then strongly dependent on FIR absorption at the ground-state-to-excited-state energies. In contrast with the more conventional FIR absorption, the PTIS signal can be shown to *increase* with decreasing impurity concentration [77K1]. This makes PTIS less useful for less pure materials such as bulk SI GaAs, but an extremely sensitive technique for high purity epitaxial material. Aside from being a useful method of donor identification in III-V semiconductors in its own right, PTIS has also played an important role in the development of PL as a technique for this application.

PTIS was first used for studying shallow impurities in Ge, as described in a review of the early use of this technique [77K1]. Stillman and coworkers extended the technique to GaAs [69S1, review 77S1] where the near-perfect effective-mass-like behaviour of donors in GaAs was verified. The observation of the chemical dependence of transition energies for different donor species in GaAs was first reported by Fetterman *et al.* [71F1] in a PTIS-like technique, in which the magnetic field was varied and a fixed-frequency FIR laser was used as the light source. As summarized by Skromme *et al.* [85S1], most of the shallow donor species have since been correlated with 1s to $2p_-$ (*i.e.* 1s to m_ℓ = -1 Zeeman split level of 2p) hydrogenic transition observed in PTIS by selectively back-doping high purity epitaxial material.

While PTIS is a sensitive technique for donor identification, the variety of samples which can be successfully analyzed is somewhat limited. PTIS is a majority-carrier technique [87B1], and thus is limited to n-type samples for donor identification. In addition, a serious problem encountered in PTIS measurements is the so-called "absorbance saturation" effect. It has been shown [85S2] that the complex refractive index at the FIR transition energies is very dependent on the donor concentration. In less pure samples, this can result in broadened, or even notched spectral features, and is a hindrance to the unambiguous identification of donors by PTIS. The absorbance saturation effect can be overcome in some cases by thinning the sample, but is thus completely destructive, and not feasible for higher impurity concentrations. Thus for p-type and SI samples, donor

identification by PTIS is precluded.

2.3 Donor Identification by Photoluminescence

In this thesis, donor identification measurements by PL were performed at a magnetic field of 12T. In order to make a direct comparison with PTIS, transition energies at the same field are required. Following the example of Skromme, Bhat, Cox and Colas (SBCC) [89S1], PTIS values at B=12 T were extracted from graphs in the work of Afsar *et al.* [80A1,80A2,81A1], with the currently accepted donor identities being assigned to the corresponding transition energies. This work has proven very useful as a check that the energy difference measured in PL between the 1s and $2p_-$ transitions corresponds with the PTIS energies at this high field. It also serves as a way of confirming the electron spin-flip energy, as the 1s to $2p_-$ energy differences observed in PL in Faraday configuration differ from the PTIS values by that amount.

The first published results demonstrating the use of the TES for donor identification in GaAs were by Almassy *et al.* [81A2]. These were zero field measurements of the TES of the (D^0,X) second excited rotator states. Zero field results have also been reported by Watkins *et al.* [87W1], in which resonant excitation of one of the rotator states was used. Such resonant excitation removes the interference caused by other rotator state TES. The laser excitation was sufficiently narrow in this latter study to demonstrate species dependent absorption energies in the principal transitions, although this splitting was unresolved in PL. At zero field, however, the TES of different donor species are still very

closely spaced, making resolution of different species only possible for the more widely spaced transitions (e.g. Ge and Si) and only in very pure material.

Since the resolution of different donor species by PTIS was aided by the application of a magnetic field, a logical step was to do the same with PL. This was in fact done by Reynolds *et al.* [83R1,84R1], and showed the effect of the magnetic field in narrowing transitions and increasing the separation between transitions. In ref. 84R1, the first report of donor identification by optical techniques in p-type GaAs was given.

The advantages of even higher magnetic fields were first explored in experiments on InP [84D1]. The application of higher fields to GaAs followed, in the first experiments on donor identification in bulk material [86H1,88H1]. Additional work on epitaxial material was also reported in these references, as it was by Bose *et al.* [87B1]. For these studies, PTIS and PL were performed on the same samples, providing an important check on the PL species assignments.

Reynolds *et al.* [83R1], Bose *et al.* [87B1], Shastry *et al.* [88S1] and Watkins *et al.* [88W2] found that the TES had larger central-cell shifts for a given donor species than did the PTIS transitions. These enhanced shifts, as well as the species dependent excitation energies observed at zero-field by Watkins *et al.* [88W1], and high field by Harris *et al.* [86H1,88H1] were explained by SBCC as being due to central-cell splitting of the donor bound exciton states. The observation of this (D^0,X) central-cell splitting in actual PL spectra of the principal transitions was first reported by SBCC. These authors

also reported resonant narrowing of the TES when exciting into the principal transitions.

The validity of PL as a donor identification technique has been well proven in the above literature. However, there still remains some controversy as to which (D^0,X) principal transitions correspond to the $2p_-$ TES used in donor identification.

The behaviour of the donor BE states in a magnetic field is little understood, although some models have been proposed. One is that of a simple 4-fold degenerate donor BE rotator state split by the magnetic field, put forward by Reynolds *et al.* [89R1], but this completely ignores the complications of the existence of many rotator states. In a more involved theoretical treatment developed for InP, Rorison *et al.* [84R2] model the donor bound exciton as a free exciton orbiting a neutral-donor. This model implies, and even builds on, the inequivalence of the two electrons in the donor BE complex, and is thus somewhat counterintuitive. Neither model incorporates the non-rigid rotator model of RK, who themselves use MPL to confirm the symmetries of the rotator states in their zero-field model. However, RK say that the rotator model does not extend to high fields, as the high field tends to allow the mixing of normally forbidden states.

Given the paucity of theoretical models, we must turn to experiment as a step toward a better understanding of this system. This requires both higher resolution spectroscopy and better signal-to-noise, such as is offered by FTPL. The former requirement comes about because of the small splittings which must be resolved if any useful information is to be obtained, and the latter due to the vast number of spectra which must

be collected in such a study. (Certainly any one spectrum can be averaged for an arbitrary period to obtain the desired SNR, but to collect hundreds at a resolution of 0.1 cm^{-1} and better would be impossible on a dispersive instrument, even if time were the only consideration.)

Taking full advantage of the power of interferometric PL, it is hoped that this present study will both provide new insight into the physics of the (D^0,X) system in GaAs under the application of high magnetic fields, as well as set a standard for donor identification by PL.

2.4 FTPL

Having stated the importance of FTPL to this work, it must be said that the use of interferometry is not new in the field of semiconductor PL spectroscopy [87C1,88R1]. There are even commercial interferometric systems specifically configured for PL characterization work, offered by such companies as Midac and Bio-Rad. What is new in this and recent work by Thewalt and co-workers [this work,90T1,90B1] is the application of FTPL to GaAs spectroscopy, which until now has been considered the preserve of dispersive spectrometers and photomultipliers. Also, the exploitation of the unparalleled combination of resolution and signal throughput achieved with FTPL [90T1,90N1,90T2] has not been reported by others. The advantages of FTPL will be explained further in Chapter 3 and demonstrated throughout this thesis.

CHAPTER 3. EXPERIMENTAL PROCEDURE

3.1 Introduction

The standard photoluminescence set-up consists of an above-band-gap light source, a light detector, as well as some type of spectrometer with which to analyze the luminescence as a function of energy. For impurity-specific studies, a cryostat is necessary to maintain the sample at low temperature. The list of equipment grows rapidly as the requirements for more control of the many parameters of excitation, detection and sample environment increase. Thus the best equipped photoluminescence laboratory will have many lasers, detectors, spectrometers, cryostats, magnets, optical filters, and more. In addition, a vast array of electronics is required with which to control equipment, and collect, analyze and store data.

In collecting the data for this thesis, most of the items in the above list were utilized. In the following sections a description of the equipment and the reasons for its use will be given.

3.2 Fourier Transform Interferometry and Photoluminescence

The goal of experimental spectroscopy is to obtain data with a very high signal-to-noise ratio without compromising the spectral resolution. As explained in Chapter 1, there are many advantages to using interferometric techniques to achieve this. Fourier transform spectroscopy has long been recognized as being superior for spectroscopy in the far- and mid-infrared, where detector noise is often the limiting factor. Due to the throughput advantage, as well as the higher

attainable spectral resolution, FT interferometry is superior even in the spectral region where low-noise photomultipliers tubes operate. However, until recently, technological limitations have prevented the application of this technique to spectral regions with wavelengths in the near-infrared (NIR) and shorter. This problem is evident when one considers that a high resolution (0.02 cm^{-1}) spectrum requires that two mirrors must be kept parallel within a fraction of the wavelength of interest, while one of these mirrors is moved a distance of 25 cm. As the wavelength decreases, the difficulty in maintaining alignment increases. Recent advances in this area, involving clever optical and mechanical alignment techniques, have resulted in the commercial availability of FT interferometers which are useful into the UV region of the spectrum.

The interferometer used for this thesis was a BOMEM model DA3.02 interferometer system, with some simple external additions. A schematic diagram of the optical setup for FTPL is given in Fig. 3.1. This is basically a Michelson interferometer. The light path chosen for PL is actually the reverse of that normally used for this instrument, which enables the internal interferometer light sources to be used to align the collection optics onto the sample: a very convenient feature.

Two features distinguish the Bomem machine from other commercial systems: the use of real-time numerical filtering while collecting data, and its active optical alignment system [89B1]. The first feature enables very rapid data collection and subsequent Fourier transform calculation. The second gives the Bomem its short-wavelength high-resolution capability. This system uses a single-mode HeNe laser

Figure 3.1

Schematic diagram of the interferometric PL apparatus. Central to this technique is the Bomem DA3.02 interferometer, which features dynamic alignment of the "fixed" mirror with respect to the scanning mirror. This allows the alignment to be maintained during high resolution scans. Also shown are the internal light sources which can be imaged backwards along the PL collection path to allow for simple alignment onto the sample.

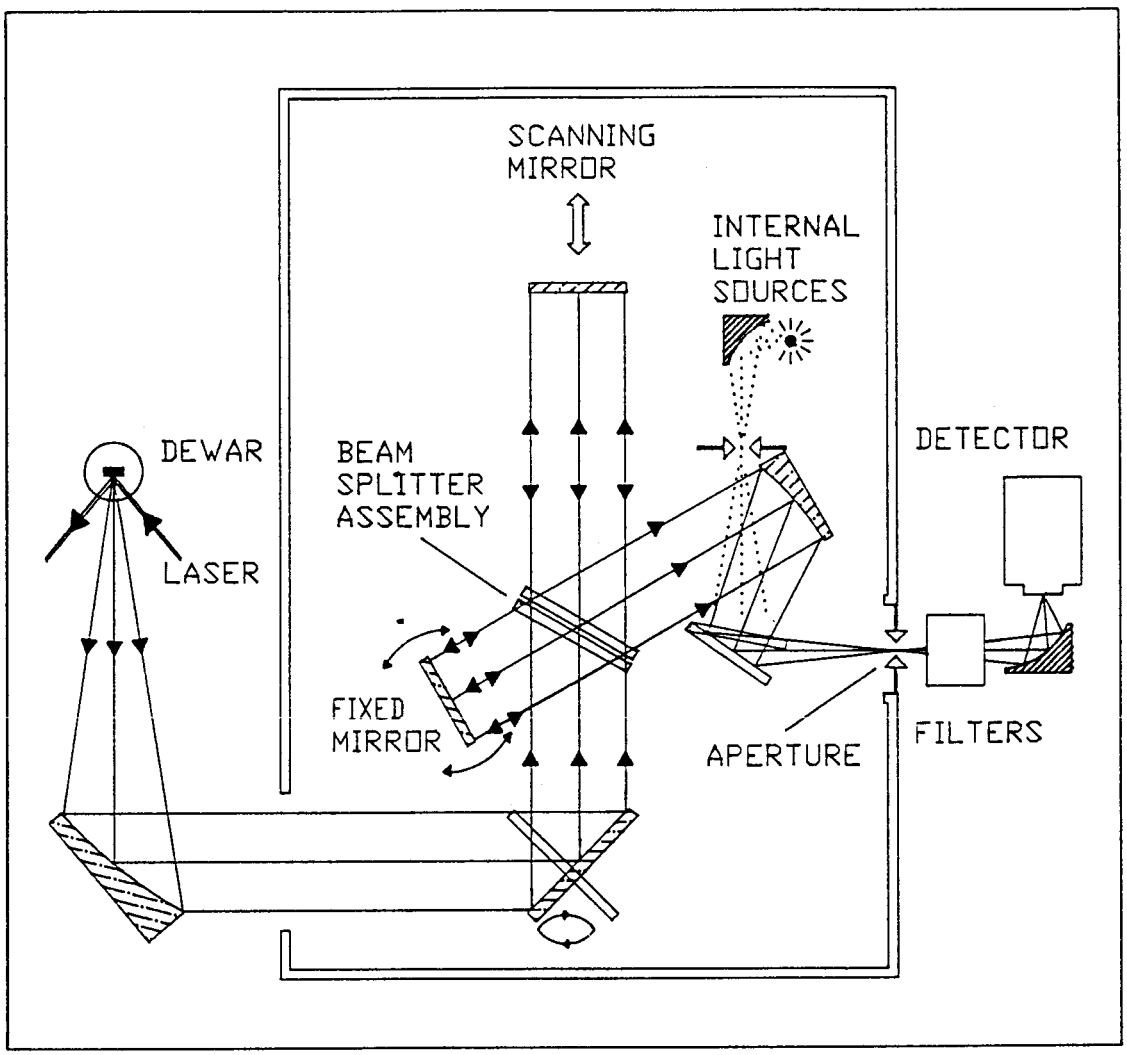
SCANNING
MIRROR
INTERNAL
LIGHT
SOURCES
DEWAR
LASER
BEAM
SPLITTER
ASSEMBLY
DETECTOR
FIXED
MIRROR
APERTURE
FILTERS

(λ ~ 633nm) which is guided onto the interferometer optical path by a system of prisms. The interference pattern (interferogram) due to the laser is optically filtered from light related to the experiment and fed onto an array of detectors. The modulation level of the laser interference signal is maximized through the use of feedback circuits driving galvanometric motors on the so-called "fixed" mirror. In this way the fixed mirror is kept parallel to the scanning mirror. This causes the maximum amount of modulation in the signal interferogram as well, which translates directly into signal level.

The PL is collimated before being directed into the interferometer through a 4 inch quartz window. For some of the preliminary zero field work, an off-axis paraboloidal mirror was used for collimation, with the cryostat placed beside the interferometer. For the magneto-PL, the collimation was performed with a simple plano-convex lens, and directed over the 4 m path to the interferometer with aluminized front surface plane mirrors. The 14.5 T magnet was placed at this distance to avoid magnetic interference with the interferometer.

In all cases the samples were immersed in superfluid He (T between 1.6 and 2.2 K).

3.3 Magneto-photoluminescence

High magnetic fields are required to remove the degeneracies in the donor and donor bound exciton states, increase the sensitivity of the BE wavefunction to the binding center central-cell potential, and resolve the transitions due to different donors and due to different states. For this purpose a 14.5T Oxford Instruments hybrid NbTi/Nb_3Sn

superconducting solenoid was used. The magnet cryostat was designed and built at Simon Fraser University. In addition to the high field capability, this magnet also features a large (2 inch) bore. This permits a large optical aperture (~f/4) even with the reduction imposed by having the sample-chamber separate from the magnet reservoir.

The uniformity of the magnetic field was rated at 10^{-4} in a 1 cm^3volume around the center of the field. The accuracy of the field was verified by comparing various transition energies with those of other workers. This will be discussed further in Chapter 4. Line broadening or shifting due to field inhomogeneity or day-to-day changes were never observed, provided care was taken to place the samples at the same position in the magnet, and to avoid the use of potentially ferromagnetic materials in the sample holder.

3.4 Excitation sources

The excitation conditions have been shown to have a large effect on both the strength and width of the PL transitions in the GaAs excitonic system. The intensity is enhanced greatly by pumping nearer the band edge. This effect is due to the larger excitation volume obtained with longer wavelengths, as the absorption length increases. In addition, the cooler, less dense excited electron and hole populations will tend to form excitonic species rather than recombine via other paths. For resonant excitation studies, the laser source should exhibit ease of tuning, narrow linewidth and high power.

The Al_2O_3:Ti (Ti doped sapphire or Ti-sapphire) laser is a near ideal laser for this application. This laser has made conventional dye

lasers obsolete in the 700-1000 nm range. In addition, the Ti-sapphire laser can be tuned to at least 1150 nm, limited at present only by the available cavity mirror sets. This tuning range is well beyond any available dye. Even in the range accessible by dyes, the Ti-sapphire laser is more powerful by about a factor of 10. It should be noted that sapphire makes an excellent laser host medium. It is inert, rugged, and has a very high thermal conductivity.

The Ti-sapphire laser used in this study was a Spectra-Physics model 3900, pumped with a 20 W Spectra-Physics model 171 Ar^+-ion laser. Such a combination is capable of producing up to 3 W of tunable laser output at 800 nm, well above any normal semiconductor spectroscopic requirements. The laser system is shown schematically in Fig. 3.2. The present full tuning range of 700 nm to 1150 nm can be obtained with only 3 different mirror sets. For the purposes of GaAs donor identification, wavelengths from 720 nm to 820 nm were used. This tuning range could be obtained using a single mirror set.

For resonant excitation, narrowed laser linewidths of approximately 0.03 cm^{-1} were achieved by using an etalon in the laser cavity. Tuning over a 5 cm^{-1} range was obtained by tilt-tuning the etalon, while coarse tuning was controlled by the 3-plate birefringent tuner supplied with the laser.

3.5 Wavemeter

A device which proved invaluable to this work, especially for the resonant and excitation spectra, was the Laser Technics model 100F Fizeau wavemeter. With this instrument the wavelength of the tunable

Figure 3.2

Schematic diagram of the Ti-sapphire laser system used for this study. The use of the wavemeter and the power stabilizer are explained in the text. The laser could be tuned from 700 to 1150 nm, with linewidths as narrow as 0.03 cm^{-1}.

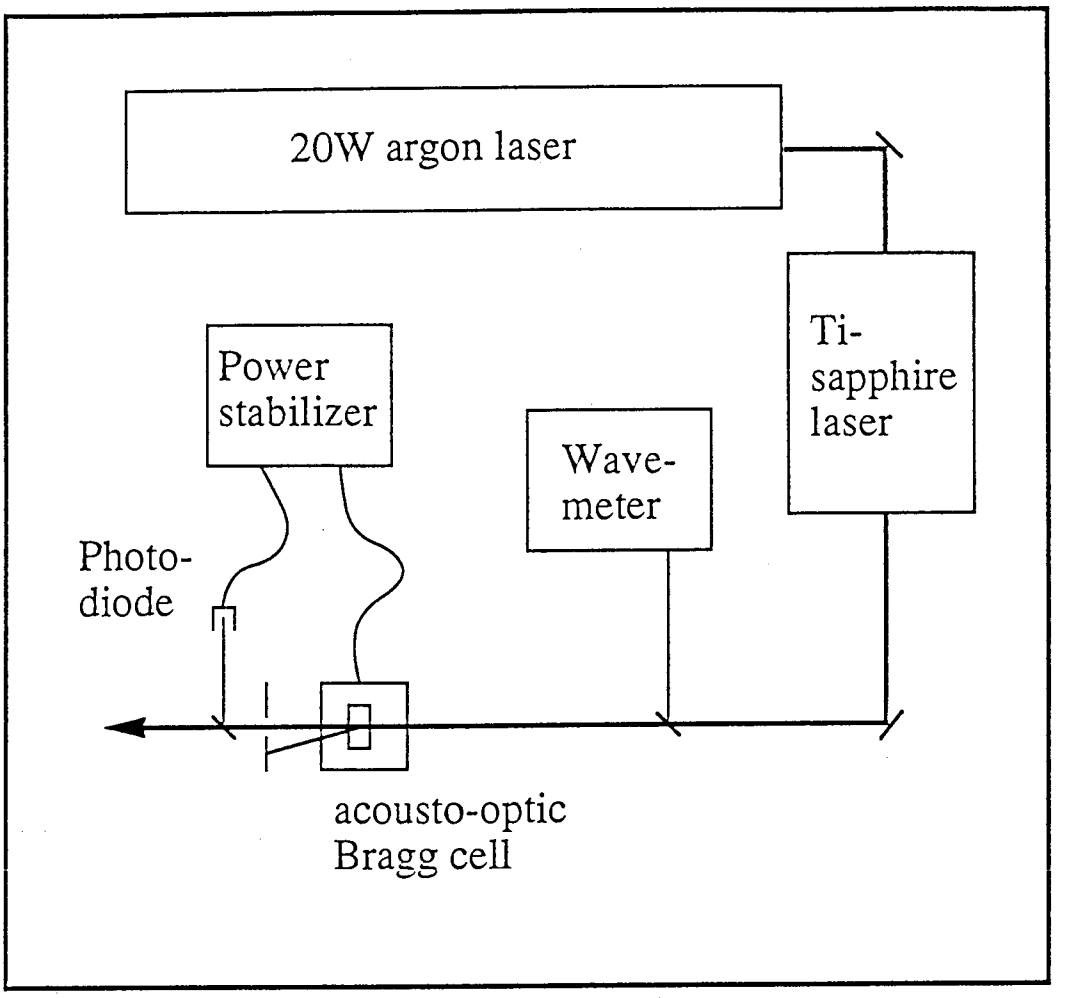
20W argon laser
Ti-
sapphire
laser
Power
stabilizer
Wave-
meter
Photo-
diode
acousto-optic
Bragg cell

Ti-sapphire laser could be continuously monitored, with a precision of better than 3 parts in 10^6. Calibrating the wavemeter against the interferometer allowed for convenient setting of the laser wavelength, to an accuracy within the laser linewidth or the interferometer resolution, whichever was larger.

The precision and accuracy of the wavemeter are remarkable considering that no moving parts are required for the wavelength measurement. This is accomplished by using a wedge (Fizeau) interferometer formed by two optically flat glass plates, near but not exactly parallel to one another. The spatial interference pattern is formed by the change in optical path across the plates. This pattern is imaged onto a 1024-element silicon photodiode array and digitized. By using a fitting algorithm and careful calibration, the intensity distribution falling on the array is translated into a value for the wavelength. A pick-off beam-splitter was placed in the laser beam path to direct a small fraction of the laser light into the wavemeter, as shown in Fig. 3.2.

3.6 Noise-Eater

In Chapter 1, the need for stable laser power was outlined, as the multiplex advantage of interferometry becomes a disadvantage when noise proportional to the signal is present. To reduce variations in the laser intensity, a power-stabilizer was used in the laser light path. The output laser power, as measured using a photo-diode, was compared with an adjustable set-point, and variations were compensated for by controlling the radio-frequency power being fed back to an acousto-optic

Bragg-cell deflector. The laser power is thus controlled by the amount of light which is diffracted out of the beam by the standing-wave-induced variation in the refractive index of the cell. The stabilizer is also shown in Fig. 3.2.

3.7 Photoluminescence Excitation

In conventional excitation spectroscopy using grating spectrometers, a single transition is monitored while the wavelength of a tunable excitation source (tunable laser or monochromatized white light) is continuously varied. The response of the monitored transition due to absorption into its related excited states is then obtained.

When using an interferometer for PLE, however, a different approach must be taken. This is because there is no way of continuously monitoring only one wavelength, as an interferometer has no intrinsic means of wavelength selection or rejection. Fourier transform PLE (FTPLE) *can* be performed by interferometrically modulating a white light source over the excited state spectral region [90T1] while monitoring the ground state response, as above. As with dispersive PLE, this is very difficult for weak transitions, or those which occur very close to other transitions since a sequence of optical filters or dispersive spectrometers must be used to both select the ground state transition and reject the modulated interferometer light at the the ground state energy. This introduces the resolution and throughput deficiencies of dispersive technique, and is not the method of choice when a tunable laser source is available in the spectral region of interest.

For this reason, a brute force method was chosen for the excitation

spectroscopy in this work. A spectrum of the $2p_-$ TES region was recorded for over two hundred laser pump wavelengths corresponding to energies in the principal transition region. The PLE spectrum for a given $2p_-$ transition was then constructed by plotting the intensities of that transition from each of the recorded spectra as a function of the excitation energy. (Care must be taken to maintain the sample conditions constant throughout the experiment.)

For such a method to be feasible, rapid collection time is required. Interferometry offers an immediate advantage in this regard. Rapid collection time necessitates a fast detector so that the scanning mirror speed can be increased without sacrificing detector response. For a given resolution, the time to collect a spectrum is determined by the mirror velocity (in cases where the SNR requires only a single scan), which in turn determines the electronic frequencies present in the interferogram. Rapid tuning of the laser wavelength was also necessary to reduce the time required for collecting such PLE spectra. The wavemeter was thus an essential component in the collection of the PL spectra used for PLE.

Collecting and constructing a PLE spectrum in this manner is somewhat tedious, but has the advantage of allowing the construction of a PLE spectrum for any feature in the collection passband. It also enables the monitoring of the evolution of the various spectral features as the excitation energy is changed.

3.8 Detectors

For some of the earlier MPL work, an InGaAs photoconductive detector

(Epitaxx model ETX 1000 TV) was used to convert the luminescence interferogram signal into an electrical signal to be fed into the interferometer analog-to-digital converter. This detector was mounted in a liquid nitrogen (LN_2) cooled cold-finger cryostat plate, as was a 2N6483 dual channel J-FET and 100 MΩ feedback resistor configured to be compatible with a Cincinnati Electronics detector/amplifier (model EEH-100).

Later, a Si avalanche photo-diode (APD) (RCA model C30872) was used in the same manner, but biased with a variable battery-powered high-voltage supply. This proved to be a superior detector configuration. For equal collection times, spectra obtained with the APD exhibited a SNR which was approximately three times higher than with the InGaAs diode. Similar results were obtained when comparing the APD to a GaAs-cathode photomultiplier tube. This is not surprising, as in most cases the luminescence was in the high signal limit *i.e.* shot-noise limited. In this limit, the SNR is increased more by improving the photon detection probability (>50% for the APD, <20% for the PMT) than by decreasing the detector background noise. Even with this higher efficiency, the APD also had a higher electronic bandwidth (~ 6kHz, determined by the size of the feedback resistor) than the InGaAs diode (~1 kHz) enabling more rapid collection of spectra.

3.9 Optical Filters

A drawback of interferometry, as compared to dispersive spectroscopy, is the total lack of rejection of light in spectral regions which are outside the range of interest. Such rejection is

often necessary, not only to avoid detector saturation, e.g. from scattered laser light, but also to reduce noise. This is because noise on the signal occurring in one spectral region affects other regions as well, and is particularly detrimental when trying to observe weak features, while also collecting light from much more intense regions. Thus, indispensable components of the resonant and excitation spectroscopy setups were the optical interference filters used to reject the scattered laser light and pass the spectral regions of interest. In particular, a high performance four cavity interference filter from Andover Inc. was most useful for the GaAs $2p_-$ TES transitions at 12T. This filter has a 1 nm pass band, centered at 820 mm when at normal incidence. A 3nm-wide passband filter centered at 818.5 nm was also used to select the excitonic region in GaAs while rejecting the near-gap laser excitation.

Each of these filters could be tilt-tuned in a specially made light-tight box placed between the interferometer and the detector. Lenses were used to ensure that the luminescence was collimated while passing through the filter, which is necessary for optimum performance. The filter itself was mounted in a removable holder on a wormscrew driven turntable to enable tilt-tuning, and the tilt-angle was calibrated against an external dial setting. It was found that the filter could be set most conveniently, however, by simply tuning the laser to the desired filter setting and maximizing the signal due to scattered laser light.

For above gap excitation (always at 720 nm in this work) a Schott RG780 colour glass filter was used for laser rejection. For

polarization studies, iodine-dyed stretched-film sheets laminated between polished glass (Oriel model no. 27300) were used as linear polarizers. Birefringent polymer sheets, also laminated between glass plates (Oriel model no. 27520), were used as quarter-wave retarders required to analyze circularly polarized light. Both of these materials are available as sheets or in mounted format.

Chapter 4 RESULTS and DISCUSSION I: Donor Bound Excitons in GaAs at High Magnetic Field

4.1 Introduction

In this chapter, photoluminescence spectra will be presented showing the many transitions associated with the recombination of excitons bound to donors in GaAs. The dependence of the transition energies and intensities on magnetic field strength, excitation energy, crystal orientation and polarization will be shown. These results will be used to provide insight into the nature of the bound exciton states responsible for the luminescence. The relationship of the PL transitions with those observed in PTIS will be given, although results relating strictly to donor identification will be presented in Chapters 5 and 6. The spectra presented in Chapters 4 and 5 were obtained from high quality epitaxial GaAs grown by metal-organic chemical vapour deposition (MOCVD).

4.2 Zero-field Transitions

The use of FTPL enables the rapid collection of high resolution spectra. An example of this is given in Fig. 4.1(a), where the excitonic region of GaAs at zero magnetic field is shown. The need for high resolution is evident, when one considers that the two lowest rotator states [78R] are separated by only 0.3 cm^{-1} (0.04 meV). This spectrum was collected at a resolution of 0.1 cm^{-1}, a moderate resolution on the interferometer used in these studies. The wide-band spectrum of the near-gap PL shown in Fig. 4.1(b) demonstrates the

Figure 4.1

(a) Photoluminescence spectrum of the excitonic region in high purity GaAs at zero magnetic field, taken at a resolution of 0.1 cm^{-1}. (b) Wider view of the same spectrum as in (a). There is no collection time penalty in increasing the spectral coverage. The labels are described on page 41.

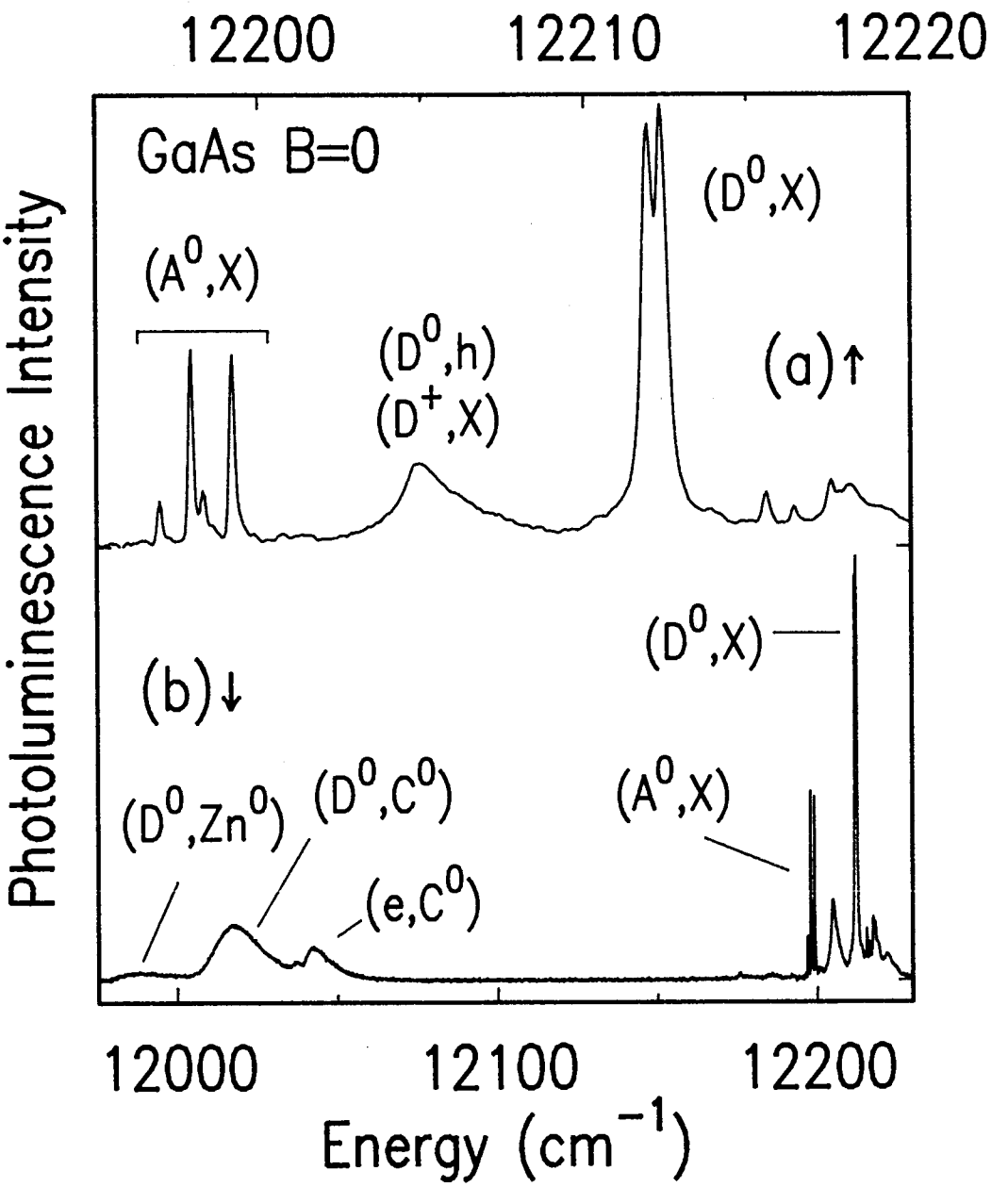
12200
12210
12220
GaAs B=0
(A0,X)
(D0,h)
(D+,X)
(D0,X)
(a)↑
(b)↓
(D0,X)
(D0,Zn0)
(D0,C0)
(e,C0)
(A0,X)
Photoluminescence Intensity
12000
12100
12200
Energy (cm-1)

advantage of parallel collection. There is no collection-time penalty for increasing the energy-range of a spectrum at a given resolution. There is of course a time penalty in performing the Fourier transform, but this is of little consequence with the capabilities of modern computers and software, and the numerical filtering technique.

The various labels of Fig. 4.1 indicate the following recombination transitions:

(D^0,X) - neutral donor bound exciton;
(A^0,X) - neutral acceptor bound exciton;
} principal transitions

(D^+,X) - ionized donor bound exciton;

(D^0,h) - free hole to neutral donor;

(e,C^0) - free electron to neutral carbon acceptor;

(D^0,C^0), (D^0,Zn^0) - donor-acceptor pairs involving C and Zn acceptors respectively

The spectra of Fig. 4.1 are given for comparison with spectra in the next section, where the (D^0,X) system will be studied under the application of a magnetic field.

An example of the resolution capabilities of FTPL is given in Fig. 4.2, where the two lowest (D^0,X) rotator states are shown for two samples known from magneto-PL studies (Chapter 5) to contain mostly Ge (top), and mostly Sn/Se/Si (bottom). Sn and Se are referred to together because they have very similar ionization energies, and have never been resolved by PTIS or PL. Si can only be resolved from Sn/Se at high magnetic field. The energy of the lowest two rotator states has a species-dependent shift of 0.186 ± 0.010 cm^{-1}. This is the first

Figure 4.2

High resolution photoluminescence spectra of GaAs at zero magnetic field, taken at a resolution of 0.025 cm^{-1} for (a) a sample known to contain mostly Ge donors, and (b) a sample known to contain mostly Sn and Si donors. On the left in each case is the luminescence due to carbon acceptor bound excitons, which demonstrates the spectral accuracy of the interferometer, and the species-dependence of the (D^0,X) energies.

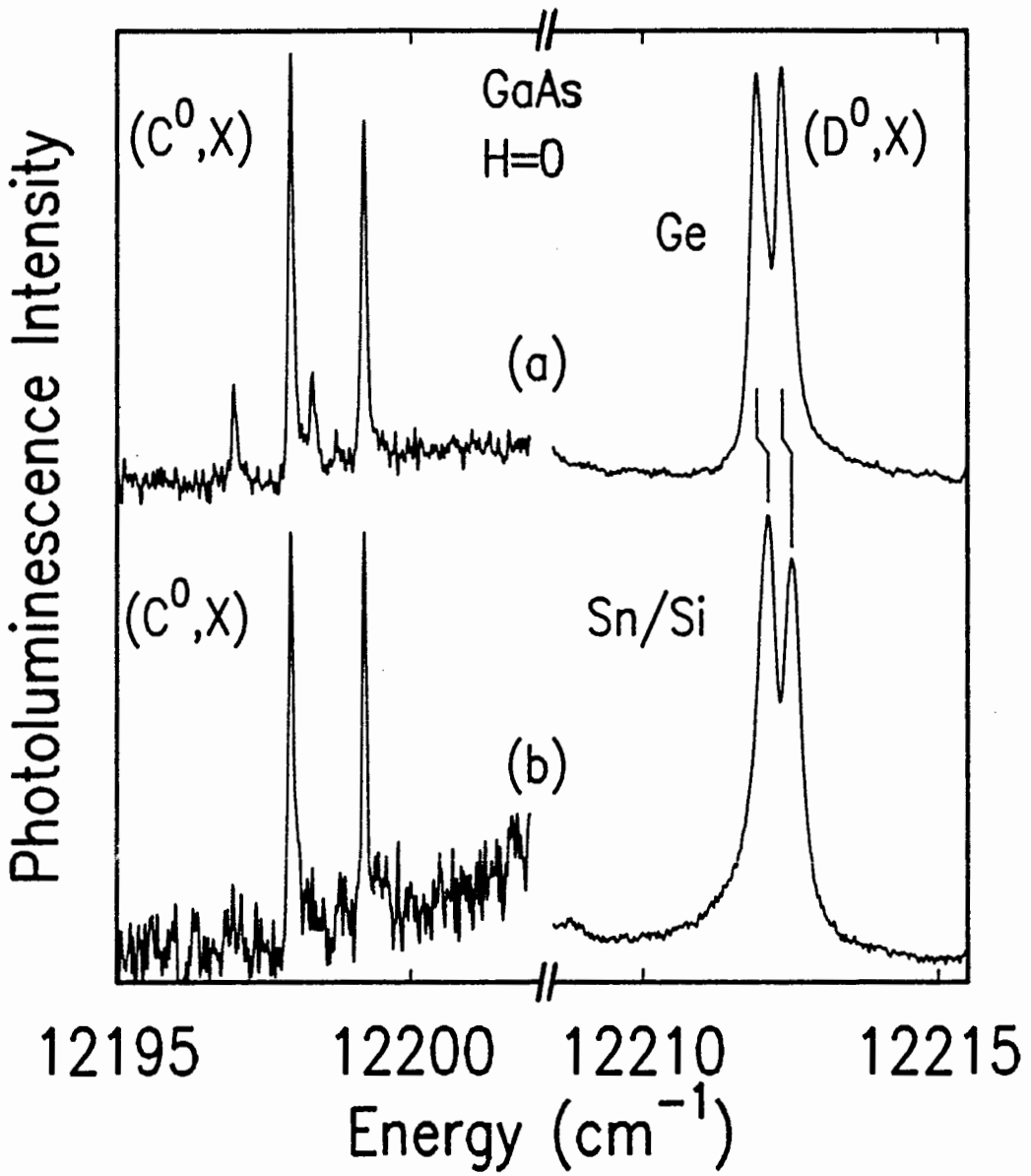
GaAs
H=0
(C^0,X)
(D^0,X)
Ge
(a)
(C^0,X)
Sn/Si
(b)
Photoluminescence Intensity
12195
12200
12210
12215
Energy (cm^{-1})

direct observation by PL of such a shift at zero magnetic field, and is a demonstration of the resolution and spectral accuracy of FTPL. This is verified by comparison of the neutral carbon acceptor BE (C^0,X) transitions for the same two samples, whose energies agree within the measurement limits of the instrument (0.005 cm^{-1}). The (C^0,X) transitions are shown on the left hand side of Fig. 4.2. The (species-dependent) rotator state transition energies are given in Table 4.1.

4.3 Donor Bound Excitons at High Magnetic Field

The behavior of the donor bound excitons in the presence of a magnetic field is a subject of both fundamental and applied interest. Until now, the studies of this system in a magnetic field have produced little more than general observations, rather than definitive conclusions regarding the origin of the field-split transitions. This absence of information is due to the proximity of the transitions, both at zero and higher magnetic fields. Because of the close spacing of the luminescence transitions, high quality material is required to produce narrow transition linewidths, and very high resolution spectroscopy is required to resolve them.

High quality material has been available for a number of years, produced by a number of epitaxial techniques. However, the spectroscopy has been limited by the SNR and resolution available with dispersive instruments. With the use of interferometric techniques, the limitation has now been shifted back to the actual linewidths of the transitions. In most cases, these can be shown to be limited by strains or impurity

Table 4.1 Transitions energies for the various rotator states of excitons bound to Ge and Sn/Si in GaAs at zero magnetic field.

rotator ℓ_{rot}	Transition Energy (cm^{-1})			
	Ge	Sn/Si	ΔE (Sn/Si-Ge)	ΔE (Ge_ℓ-Ge_0)
0	12211.949 ± 0.010	12212.135 ± 0.015	0.19 ± 0.03	0
1_h	12212.365 ± 0.010	12212.526 ± 0.015	0.16 ± 0.03	0.416 ± 0.012
1_l	12215.584 ± 0.015	12215.62 ± 0.02	0.04 ± 0.03	3.64 ± 0.02

levels in the samples. However, some evidence will be given which will show that the observed transition linewidths are under some conditions limited by the finite life-times of the states.

A representative spectrum of GaAs at 12T is given in Fig 4.3. Unless otherwise specified, all spectra shown in this thesis will be for **B** ∥ <100>. The spectrum of Fig. 4.3 is taken in Voigt configuration (*i.e.* the collected luminescence is emitted perpendicular to the field direction) for an MOCVD-grown sample with very low acceptor concentration. Fig 4.3(a) is a wide spectrum showing the (D^0,X) principal lines as well as the $2p_-$ and $2p_0$ TES transitions.

The principal 1s region is shown on an expanded scale in part (b) of the same figure, while Fig 4.3(c) shows the $2p_-$ TES on an expanded scale. These expanded spectra are from the same spectrum as in part (a). The strongest features visible in the principal region are due to the different field-split energy levels of the (D^0,X) manifold. More precisely in this sample, the strong features are all due to the recombination of excitons bound to Sn/Se or Si donors, while some of the weaker features are due to other impurities. Such splitting between different donor species is observable even in the principal region, as was reported previously by SBCC.

The structure visible in the $2p_-$ TES (Fig 4.3(c)) is due to both the different donors species and to different BE initial states, with the strong doublet due to the resolution of Se/Sn from Si. The different occurrences of this doublet (as well as the repetition of features due to other donor species) arise from the different initial and final states of the three-particle recombination process.

Figure 4.3

Photoluminescence spectra of high-purity GaAs taken in Voigt configuration at a magnetic field of 12 T. (a) wide spectrum showing the principal and donor TES transitions. (b) expanded view of the principal region from part (a). (c) expanded view of the $2p_-$ TES region from part (a). The labels are explained in the text.

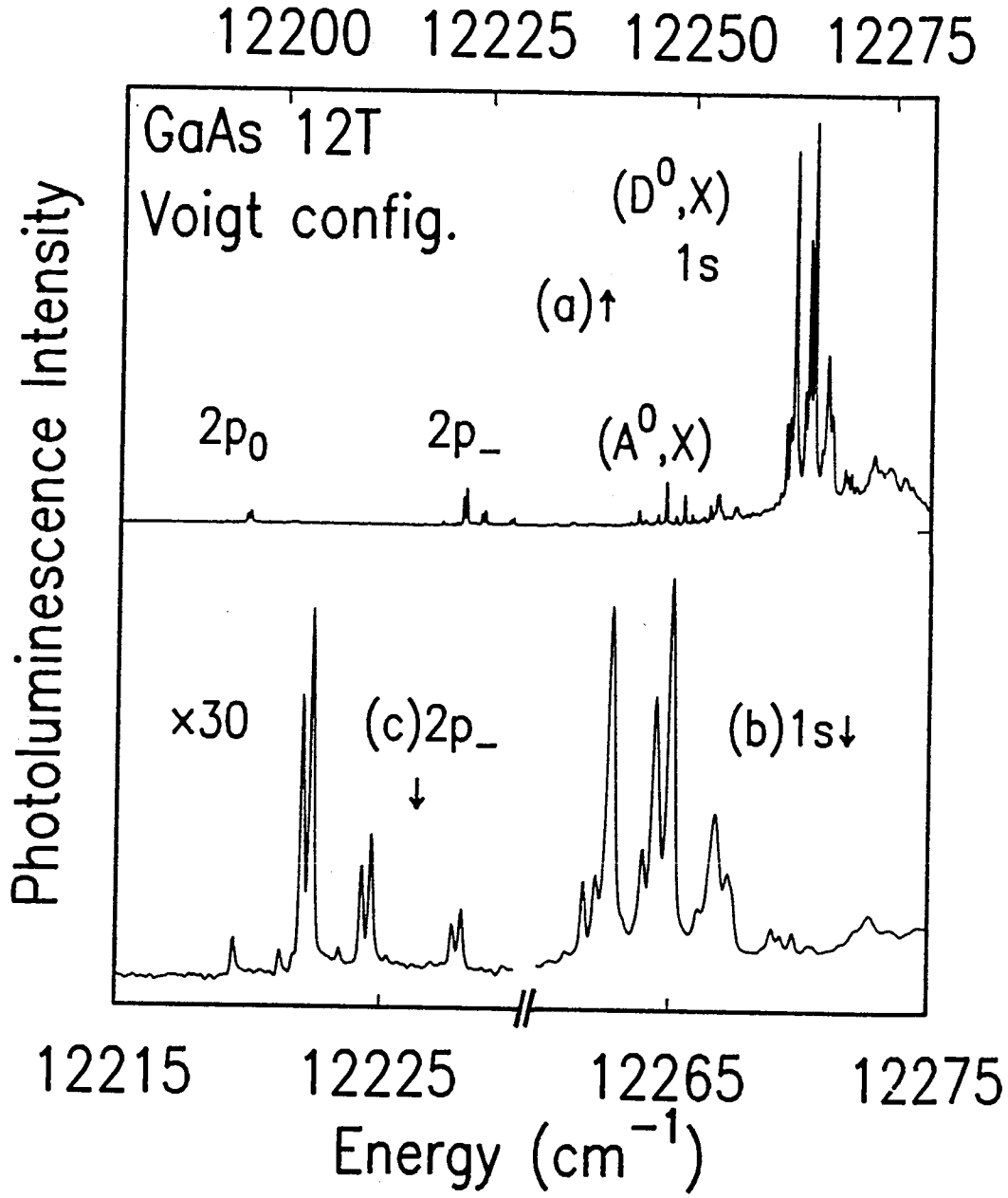
12200 12225 12250 12275
GaAs 12T
Voigt config.
(D0,X)
1s
(a)↑
2p0
2p_
(A0,X)
x30
(c)2p_
(b)1s↓
Photoluminescence Intensity
12215 12225 12265 12275
Energy (cm-1)

In the following discussion, certain spectral features will be referred to repeatedly. The labelling system will be systematic, although based on the one used previously by SBCC. In this scheme, the following conventions will be used:

(1) Transitions from the same initial state will use the same letter, upper-case for principal transitions, and lower-case for the TES transitions, which in this study only involve 2p final states.

(2) To retain compatibility with the labelling scheme of SBCC, we retain some of the subscripted principal transitions where this is not in conflict with (1) (e.g. A_0, B_1, E_1, E_2), but these subscripts have no physical significance. On the other hand, the TES label subscripts will be "-" and "0" for the $2p_-$ and $2p_0$ final states respectively, e.g. principal transition A and TES transitions $2p_-$ a_- and $2p_0$ a_0 all have the same initial state. (A_0 is an unrelated transition);

(3) The superscript "*" will be used to indicate transitions which leave the donor in a spin ground state. This is a higher energy PL transition than those resulting in a spin excited state, which will carry no superscript. e.g. A and A^* are two transitions from the same BE initial state, but A is to the spin excited donor 1s state, while A^* is to the ground spin state of 1s. The spin-flip energy at 12T is of the order of 2 cm^{-1}, while the splitting between 1s, $2p_-$ and $2p_0$ is 30 to 40 cm^{-1}.

An example of this labelling scheme is given in Fig. 4.4 for the lowest (D^0,X) level. This level is seen to be the initial state for

Figure 4.4

Schematic diagram showing the labelling convention used in this thesis for PL transitions originating from the same initial state. The up and down arrows on the right of the neutral donor (D^0) states indicate spin projections of $+\frac{1}{2}$ and $-\frac{1}{2}$ respectively. The bi-directional arrows for the 1s transitions indicates that these transitions may also be observed in absorption via PLE type experiments. The higher D^0 states would not be thermally populated at the temperatures used in this work.

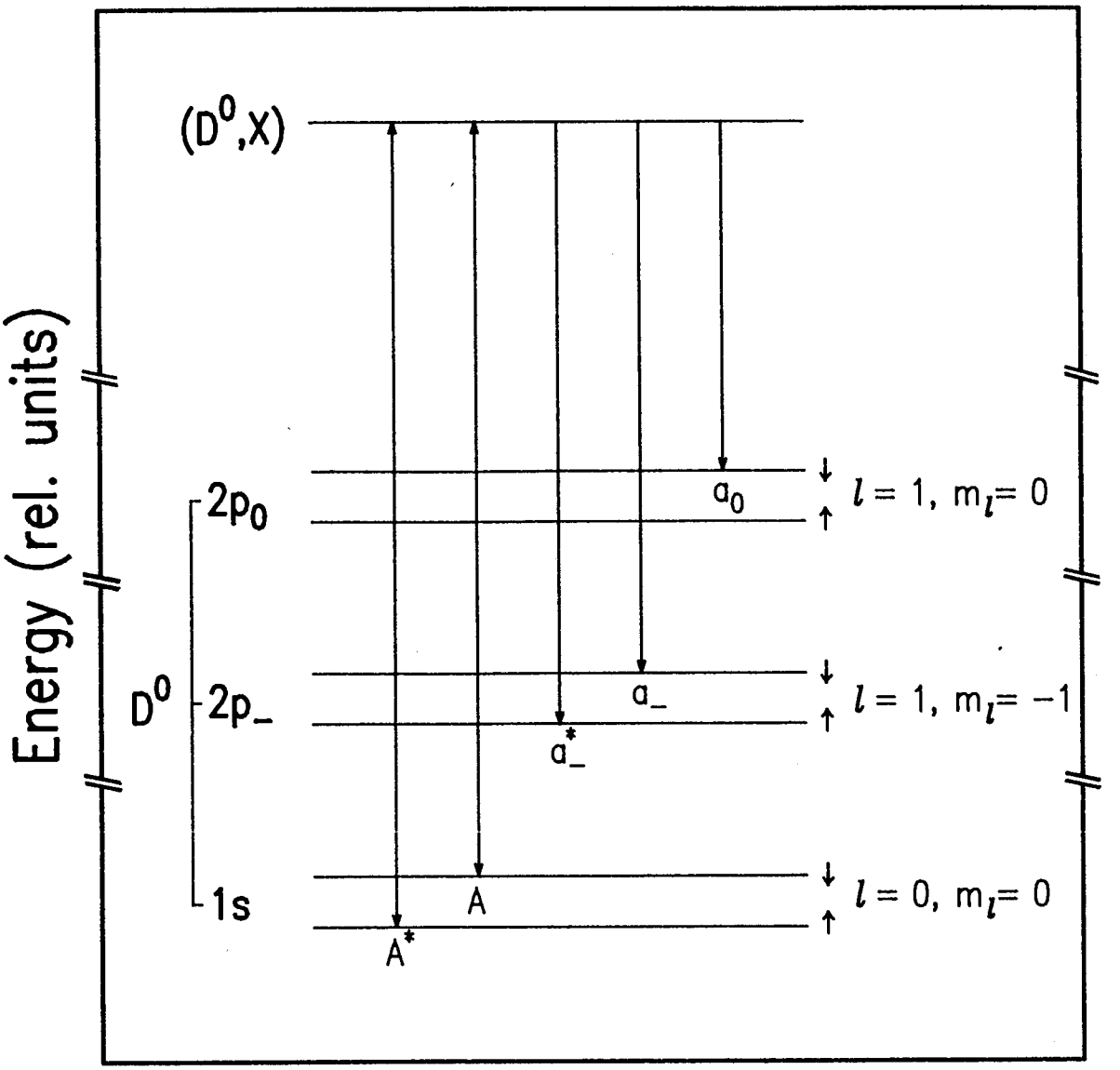
Energy (rel. units)
(D⁰,X)
2p₀
D⁰
2p₋
1s
a₀
a₋
a*₋
A
A*
l = 1, m_l = 0
l = 1, m_l = −1
l = 0, m_l = 0

five observable PL transitions: A^*, A, a_-^*, a_- and a_0 in order of decreasing energy. The labels for most of the observed states are given in Table 4.2, along with the previous labels of SBCC. These transitions will be discussed later.

An expanded view of the principal 1s BE PL region is given in Fig. 4.5, where part (a) shows the spectrum for Voigt configuration, while part (b) shows the same sample in Faraday configuration (*i.e.* the collected luminescence is emitted parallel to the magnetic field direction). The inset will be discussed in a following section. All of the transitions visible in Faraday configuration are also visible in Voigt configuration, which in addition includes the π-polarized transitions which are invisible in the Faraday configuration. The transitions observed in Voigt configuration are seen to be linearly polarized, and can be of either π polarization ($E \parallel B$) or σ polarization ($E \perp B$). This can be compared to the spectra collected in Faraday configuration, in which case, the observed polarizations are right- or left-circularly polarized (RCP or LCP) and are labeled σ^- and σ^+ respectively.

These polarizations and labels derive from atomic spectroscopy, where the polarizations arise from transitions between states with different projections m_ℓ of the orbital angular momentum ℓ on the magnetic field direction. π polarization corresponds to transitions with $\Delta m_\ell = 0$, while $\Delta m_\ell = \pm 1$ results in $\sigma^\pm$ polarization respectively. The linear σ polarization observed in Voigt configuration is a linear combination of the two circularly polarized components observed in Faraday configuration, while π polarized transitions are not observed in

Table 4.2 Labels used in this thesis for the various (D^0,X) transitions observed at B = 12 T. PL transitions sharing the same initial state are placed in the same row. Related TES transitions are given, as are the previous assignments of SBCC.

Labels		
Principal transitions	Skromme *et al.*† princ. trans.	Related TES transitions
A, A^*	A, --	a^*_-, a_-, a_0
A_0, A^*_0	A_0, B_2	
B_1, B^*_1	B_1, --	
$B_,$ B^*	--, --	b^*_-, b_0, b^*_0
C	C	
E^*_1	E_1	
E_2	E_2	
E	--	
D^*	D	d^*_0
F^*	F	f^*_-, f_-, f^*_0

† The "--" indicates transitions which were not previously reported.

Figure 4.5

12 T magneto-photoluminescence spectra of the same sample as in Fig. 4.3, taken at a resolution of 0.1 cm^{-1} to compare (a) Voigt configuration and (b) Faraday configuration. The labelled transitions in part (a) are all π polarized. The σ polarization labels in part (b) are explained in detail in the text. The inset is a higher resolution version of part of spectrum (a), and shows the similarity of the A and A^* transitions.

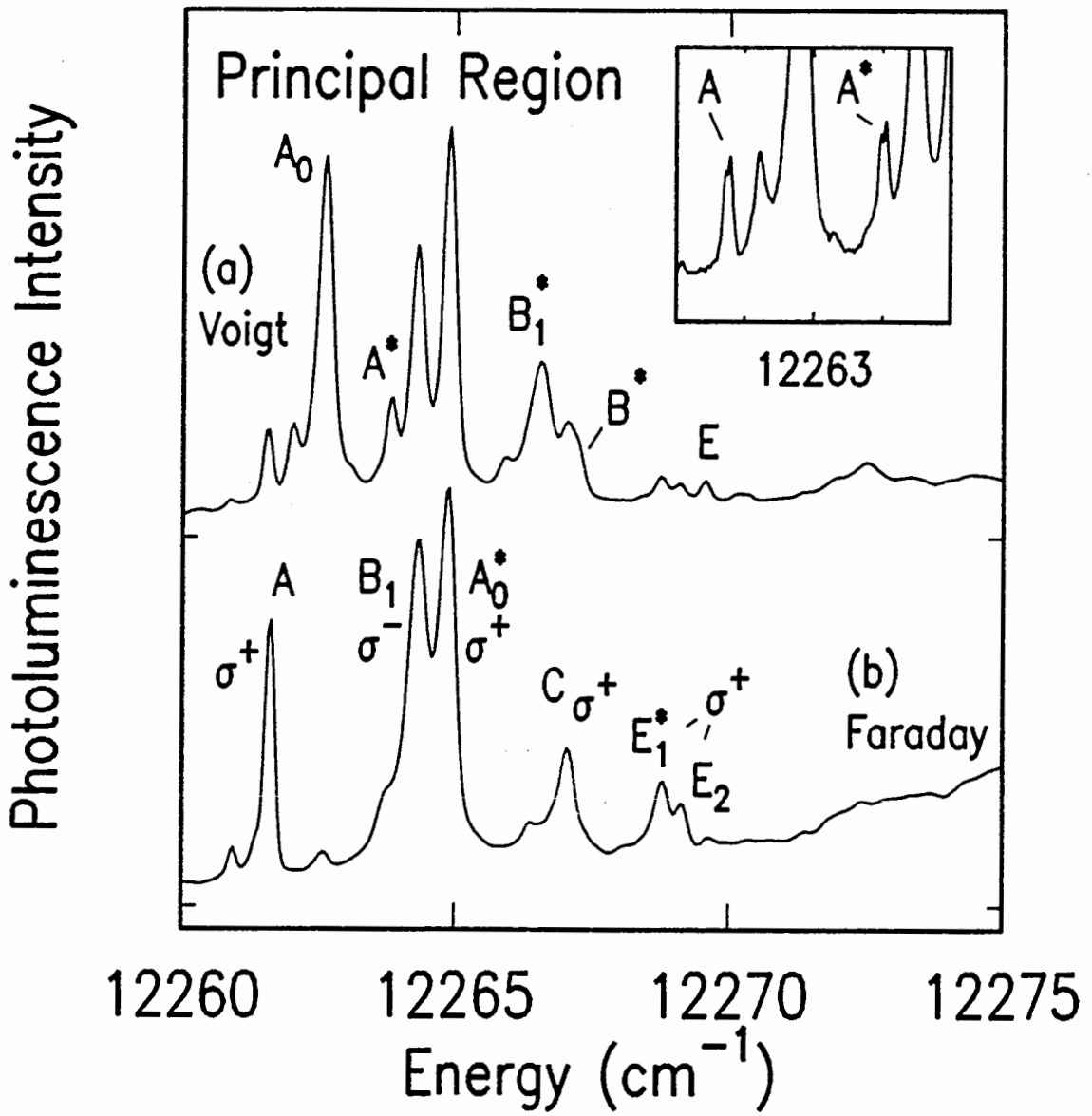
Principal Region
A
A*
12263
A0
(a)
Voigt
A*
B1*
B*
E
A
B1
A0*
σ+
σ−
σ+
Cσ+
E1*
σ+
E2
(b)
Faraday
Photoluminescence Intensity
12260
12265
12270
12275
Energy (cm−1)

Faraday configuration, as this would require the polarization of the emitted light to be along the direction of propagation.

The Faraday configuration is experimentally more convenient in magnets where the optical access is along the bore, as is the case for high field solenoids. The spectra collected in this direction also contain fewer lines, as the π-polarized transitions are absent. For these reasons, the majority of the spectroscopy performed was in the Faraday configuration. However, the results obtained were most useful when compared with selected spectra obtained in Voigt configuration.

The TES for both configurations are shown in Fig. 4.6 for transitions which result in the donor being left in the excited $2p_-$ state. The corresponding spectra for the $2p_0$ TES region are given in Fig 4.7. These spectra show the impurity-specific transitions in the same sample as shown previously in Fig. 4.3. In addition, the TES recombinations involving higher (D^0,X) initial states can also be seen. These transitions can be enhanced by resonant excitation, which is the most useful method of determining their relation with principal lines. An example of resonant excitation will be given in a later section.

The problem addressed in this chapter is the identification of the various energy levels responsible for the different transitions. The observed splittings may arise from two sources: the splitting of the rather complicated (two electrons and one hole) bound exciton (D^0,X) initial state, or the splitting of the final D^0 state (one electron) in the magnetic field. As discussed previously, the splitting of the final state consists of the different possible ℓ and m_ℓ values of the donor electron, *i.e.* 1s, $2p_-$ or $2p_0$, leading to the principal or TES

Figure 4.6

12 T magneto-photoluminescence spectra in the same manner as Fig. 4.5, but for the $2p_-$ TES region. The prominent doublets are due to identical transitions involving Sn/Se donors (lower E component) and Si donors (higher E component). The weaker features which do not show the same doublet structure are due to Ge and S donors, as will be discussed in Chapter 5.

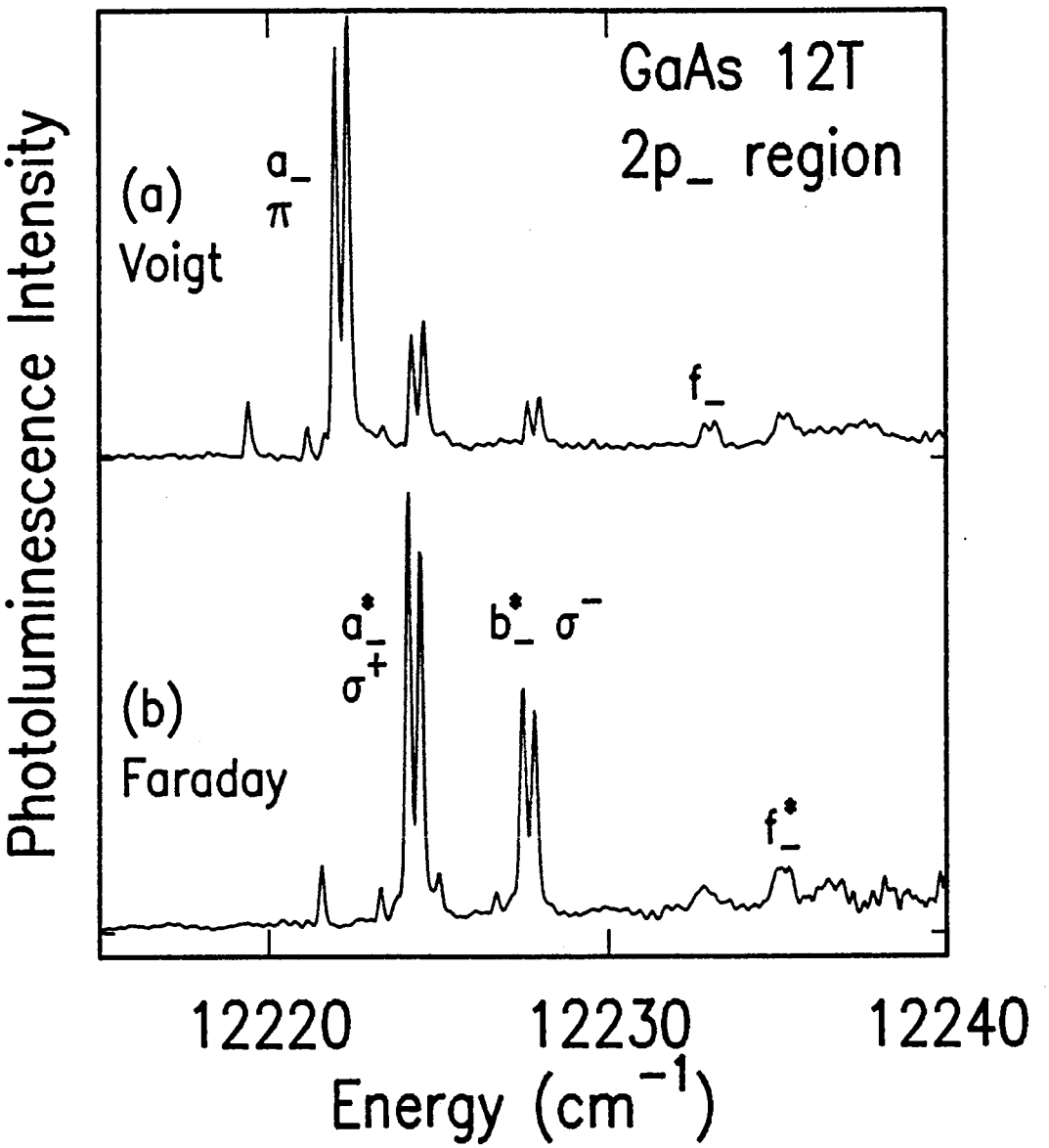
GaAs 12T
2p_ region
(a)
Voigt
a_
π
f_
(b)
Faraday
a*_
σ+
b*_ σ−
f*_
Photoluminescence Intensity
12220
12230
12240
Energy (cm−1)

Figure 4.7

12 T magneto-photoluminescence spectra in the same manner as Fig. 4.6, but for the $2p_0$ TES region. As in Fig. 4.6, the labelled peaks are π-polarized in (a) and σ-polarized in (b).

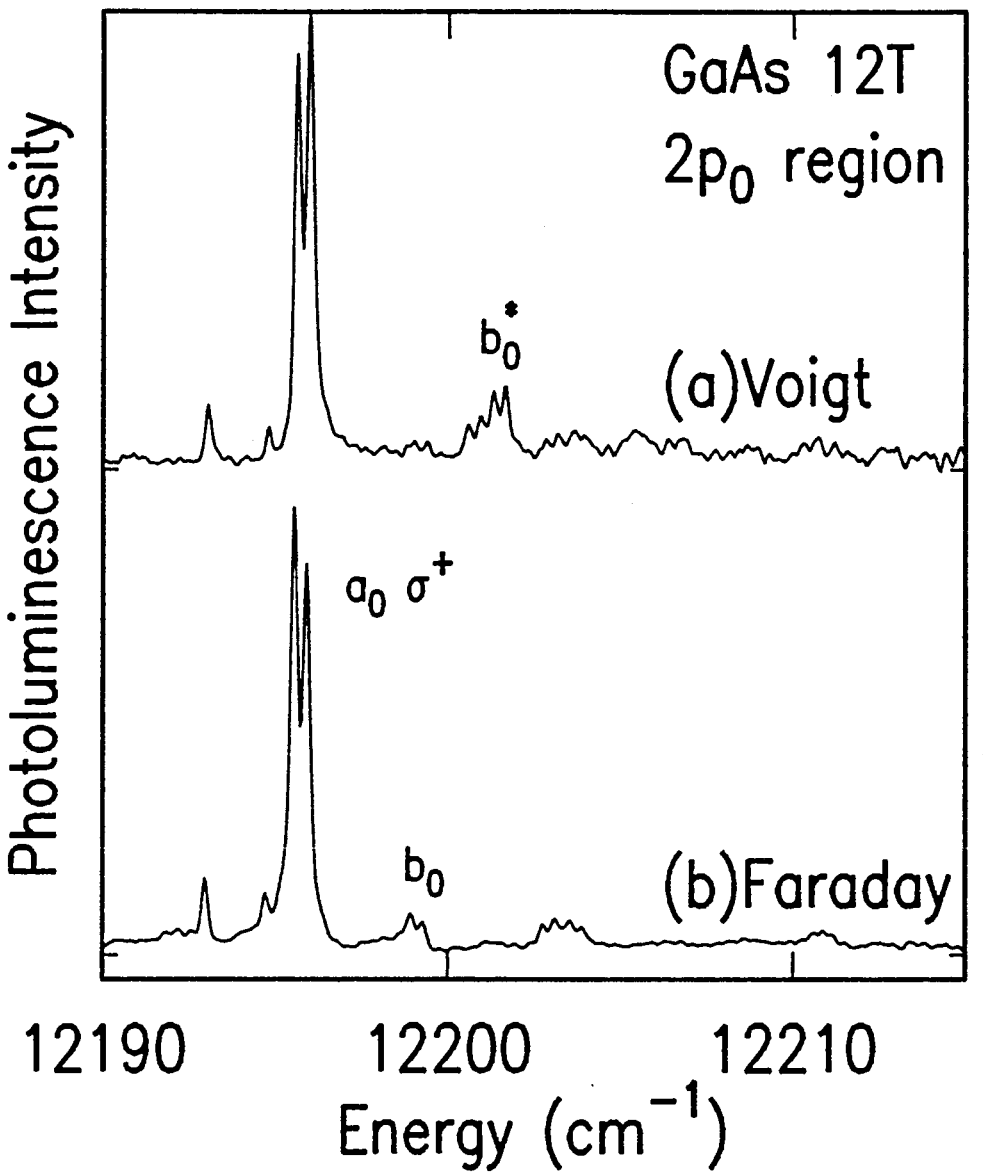
GaAs 12T
2p0 region
b0*
(a)Voigt
a0 σ+
b0
(b)Faraday
Photoluminescence Intensity
12190
12200
12210
Energy (cm-1)

transitions. In addition, the electron spin may be aligned parallel or anti-parallel to the B-field, with corresponding differences in energy.

The magnitude of this electron spin-flip energy in the final state will now be discussed. An important result of this work has been the precise measurement of the energy of an electron spin flip, and as a consequence, the value of the GaAs electron g-factor, g_e. Values of g_e in the literature range from -0.46 ± 0.02 as measured for the deep Sn acceptor BE by Schairer *et al.* [76S1] to -0.43 ± 0.05 measured earlier by White *et al.* [72W1] for the same transitions. The value measured by electron spin resonance experiments [82L1] is -0.44 ± 0.2 in agreement with the above values. In the present experiments g_e is found to be :

$$g_e = -0.402 \pm 0.008 \qquad (4.1)$$

in agreement with White *et al.*

This value was obtained by identifying PL transitions which are spin flip pairs, such as A and A^* in the Fig. 4.4. The g_e value is then calculated from the difference ΔE in these transition energies using the relation:

$$\Delta E = 2|m_s|\, g_e \mu_B B \qquad (4.2)$$

where B= magnetic field strength

$m_s = \pm\frac{1}{2}$

μ_B = Bohr magneton

= 9.2740154 J T^{-1} [90C1]

$= 0.466864\ cm^{-1}\ T^{-1}$ in wavenumber units.

The *observed* spin flip pairs are given in Table 4.2: (A, A^*); (a_-, a_-^*); (A_0, A_0^*); (B_1, B_1^*); (b_0, b_-^*) and (f_-, f_-^*). The most important of these transitions are the A series seen in Fig. 4.4, since as the lowest initial state, these are observed most easily by PL and PLE. The A and A^* transitions also have narrower linewidths than any of the other principal transitions. In this work, the identification of spin flip pairs was made first with these transitions, and the pairing of other transitions followed.

The assignment of A, A^*, a_- and a_-^* to the same initial state is made using spectra such as those shown in Figs. 4.5 and 4.6. The emergence of the A^* transition in Voigt configuration (Fig. 4.5(a)) at an energy 2.26 cm^{-1} above the A transition is accompanied by the simultaneous emergence of a_- (Fig. 4.6(a)) 2.26 cm^{-1} *below* the a_-^* transition. This in itself is strong evidence that these states share the same initial state, and are related as shown in Fig. 4.4.

Furthermore, the A and A^* transitions are seen in the inset to Fig. 4.5 to have similar appearance and narrow linewidths, narrow enough to resolve Sn/Se from Si even though these are principal transitions. These linewidths are smaller by a factor of 5 from those of the nearby A_0 and B_1 transitions. These similarities in A and A^* support the pairing of these transitions. (Full-width at half maximum is $\Delta E \sim 0.06$ cm^{-1} for A or A^*, and $\Delta E \sim 0.3\ cm^{-1}$ for B_1. This suggests that the A_0 and B_1 linewidths may in fact be transform limited.)

Further evidence that the electron spin flip energy is 2.26 cm^{-1} at B =

12T is given by comparing the A to a_-^* separation to the 1s to $2p_-$ separation measured for the same donor by PTIS. The two values should differ by the energy of an electron spin flip [89S1]. The only high-field PTIS measurements found in the literature are given in a series of papers by Afsar and co-workers [80A1,80A2,81A1]. Following the procedure of SBCC, the PTIS transition energies of the various impurities were interpolated from graphs in these references, and given the currently accepted impurity assignments. A comparison of these values with the A to a_-^* separation measured by FTPL (the subject of Chapter 5) gives agreement only if the electron spin flip energy at 12T is 2.26 ± 0.05 cm^{-1}, in agreement with the value of g_e = -0.402 ± 0.008.

The evidence is thus very convincing that the pairing of (A, A^*) and (a_-, a_-^*) is correct, and repeated measurements of these PL transitions in a number of samples then give a precise value of the spin flip energy as 2.255 ± 0.006 cm^{-1}. This in turn gives a value of g_e = -0.4024 ± 0.0011.

The final value for g_e can not be quoted with the same relative error, however, due to the inability to confirm the accuracy of the magnetic field strength B. Comparison with PL transition energy values from SBCC, and the PTIS measurements discussed above, does allow an estimate of ± 1.8% as an upper bound on the accuracy of the magnetic field. Using this value for the relative error, the value of g_e is calculated to be -0.402 ± 0.008 as given in eq. 4.1. Due to the near-perfect effective-mass-like behaviour of the donor-bound electron [71S1], this value also represents the g-factor of the conduction band.

4.4 Fan Diagram

To investigate the nature and zero-field origin of the high field energy levels, the spectral positions of transitions in the 1s-manifold were measured as a function of magnetic field strength. The line positions obtained from this set of measurements are plotted in Fig. 4.8. The spectra for this fan diagram were recorded in Voigt configuration. In order to reduce the effects of the diamagnetic shift of the luminescence energy, the plotted transitions energies are not absolute but rather measured relative to the A transition. This is the lowest energy transition and is seen to be separated, even at low fields, from the remainder of the transitions, making it a good reference for relative energy measurements.

Although using relative measurements results in a removal of the diamagnetic shift for the A line, there is still a relative diamagnetic shift between the various energy levels. This effect has been reported previously for the deep Sn acceptor bound exciton system in GaAs [76S1] where the $m_j = \pm 1/2$ hole states were found to shift differently than the $m_j = \pm 3/2$ states. Surprisingly, there is no observed state whose separation from the (A, A^*) state is completely linear in B. Thus there is no obvious centroid around which to center the Zeeman split states. Hence, in addition to reducing the effect of diamagnetic shift by measuring transition energies relative to the A line, the points in Fig 4.4 have been shifted linearly according to $\Delta E\ (cm^{-1}) = -.375 \times B\ (T)$. This value is arbitrary and is done only to aid in the tracking of the various transitions as the field is varied, by roughly centering the fan diagram around $\Delta E = 0$.

Figure 4.8

Graph of peak energies *versus* magnetic field strength for the principal (D^0,X) transitions in GaAs. The peaks are measured relative to the A transition, in Voigt configuration. In addition, the energies have been arbitrarily shifted by $-0.375 \times B$, in order to roughly center the fan diagram around $\Delta E = 0$. This shift is helpful when visually connecting related points, as shown by the solid lines. The origins of some of the high-field components can be traced back to the zero-field rotator states, which are shown on the left, where 1_h and 1_ℓ indicate the heavy and light hole $\ell_{rot} = 1$ nonrigid rotator excited states of (D^0,X) respectively. The light and heavy hole masses are used separately in eqn. 1.8 for $\ell_{rot} \neq 0$, as the different masses correspond to different projections of the hole angular momentum on the rotational angular momentum vector. For the other states, additional information must be used to assign the shown labels.

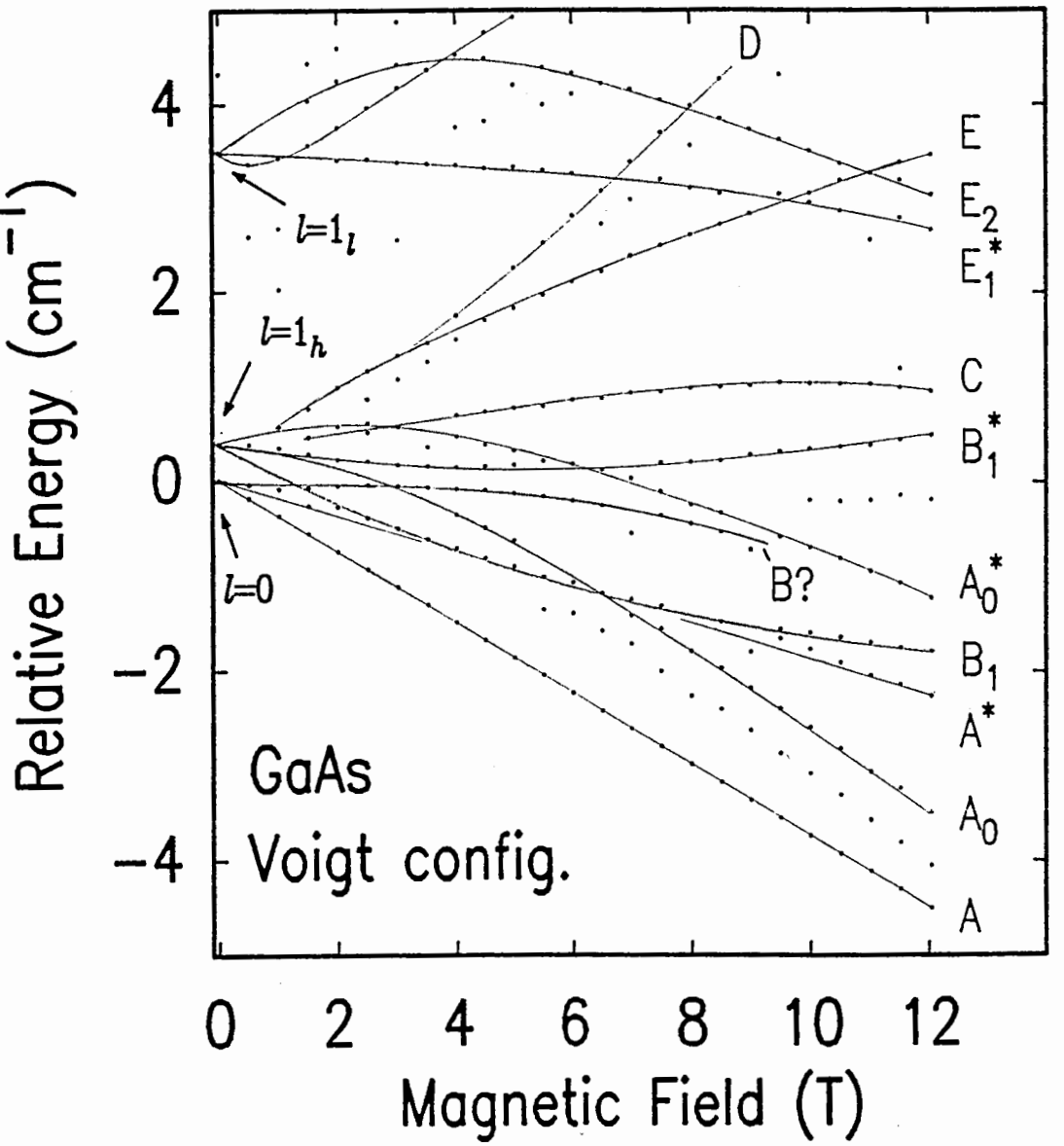
Relative Energy (cm^{-1})
4
2
0
−2
−4
0
2
4
6
8
10
12
Magnetic Field (T)
D
E
E_2
E_1^*
C
B_1^*
B?
A_0^*
B_1
A^*
A_0
A
l=1$_l$
l=1$_h$
l=0
GaAs
Voigt config.

The difficulties in making such measurements are evident when one considers that the entire fan diagram shown spans only 10 cm^{-1} (or about 1.25 meV). Even the high resolution of FTPL and the narrow linewidths of the sample are not sufficient to give unambiguous results in all cases. However, by using the polarization dependence, the (corrected) electron spin flip energy, and the orientation dependence of the transitions (to be shown later) a self-consistent picture of the field dependence of the various transitions may be realized. The lines shown in Fig. 4.8 represent the information gleaned from hundreds of spectra recorded in many different conditions of orientation, polarization, magnetic field, temperature and excitation.

The non-rigid rotator model of the (D^0,X) states in InP and GaAs [78R1] successfully explains the observed energy of the various transitions at zero-field, even though the authors, Rühle and Klingenstein, express surprise at this success, given the approximations made. The purpose of constructing the fan diagram was to study the evolution of the various (D^0,X) rotator states as the magnetic field was increased. It was hoped that by doing so, some picture could be developed which would help to explain the selection rules and polarization dependence of both the principal and TES transitions. Comments regarding such a picture will be made in section 4.7, but unfortunately the results are not conclusive. Even with FTPL, the behaviour of the various components at fields less than 3T is still unresolvable in GaAs. Thus choices as to which rotator state the transitions belong is based on an extrapolation of the high-field behaviour. In retrospect, such a study would perhaps have been more

informative if the Zeeman experiments of Rühle and Klingenstein on InP had been repeated using the higher resolution of FTPL and the higher purity samples now available.

Despite these difficulties, the following assignments can be made. The (A,A^*) state is clearly seen to evolve from the $\ell_{rot} = 0$ rotator state. The (B_1,B_1^*) state is seen to evolve from the $\ell_{rot} = 1$ heavy hole state ($\ell_{rot} = 1_h$) based on the extrapolation of B_1^* to zero field.

The origin of the other states is less certain, although C seems to originate from $\ell_{rot} = 1_h$ as well. In Fig. 4.8 there is a transition labelled "B?" which is resolved from A_0^* below B = 9T, and is also separated from C by slightly *less* than the energy of an electron spin flip for 6T < B < 9T. This transition clearly extrapolates to $\ell_{rot} = 0$, and is significant because in the next section it will be assigned the same initial state as the b_-^* TES transition. Further observations of the fan diagram reveal that the E transition (seen in PL in Fig. 4.5(a)) and the D^* transition (seen in PLE) originate from the lowest two rotator states.

The E_1^* and E_2 states (seen in PL in Fig. 4.5(b)) are the lowest observed transitions which clearly originate from the $\ell_{rot} = 1$ light hole state ($\ell_{rot} = 1_\ell$). The fact that these transitions have very little TES response when resonantly excited (aside from enhancing transitions from lower energy (D^0,X) states) indicates that the ℓ_{rot} value may play some role in determining the strengths of TES replicas. This will be discussed further in section 4.7.

4.5 Orientation Dependence

The identification of the principal transitions which share the initial state with the b_-^* TES transition has been the subject of some discussion [89S1]. Energetically, the b_-^* transition is separated from the a_-^* transition by an energy which is very slightly (less than 0.2 cm^{-1}) *higher* than the A to A_0^* separation in the principal region. It is tempting to dismiss this small discrepancy and assign b_-^* and A_0^* same initial state. However, the evidence of section 4.3 is very convincing that the A transition is made to a spin excited final state, (being paired with the A^* transition) while the A_0^* transition, paired with A_0, is to the 1s spin ground state. This is important when making the state assignment for b_-^*.

Based on the assignment of A and A_0 to spin excited final states and the energy separation of a_-^* and b_-^*, the (A_0, A_0^*) transition pair and the b_-^* TES can not share the same initial state. The b_-^* transition must share an initial state whose spin excited final state principal transition would appear very slightly above the A_0^* transition energy. The spin ground state principal transition from this energy level (labelled B^*) would be very slightly above the C transition energy. This transition is indeed observed as the high energy π-polarized shoulder on the C-line in Fig 4.5(a). In addition, the transition which is obscured by A_0^* may well be the transition labelled "B?" in the fan diagram, Fig. 4.8.

Additional evidence for this interpretation is obtained from the plot of transition energies versus crystal orientation which is given in Fig 4.9(a), (b) and (c) for the three spectral regions corresponding to

Figure 4.9

Graph of peak energies *versus* the angle between the <110> crystal axis and the magnetic field for (a)the principal 1s, (b) the $2p_-$ TES and (c) the $2p_0$ TES regions. The <100> crystal direction is 45° from <110>. The energies are on the same scale for all three regions. Points representing transitions which are discussed in the text have been connected to aid the eye.

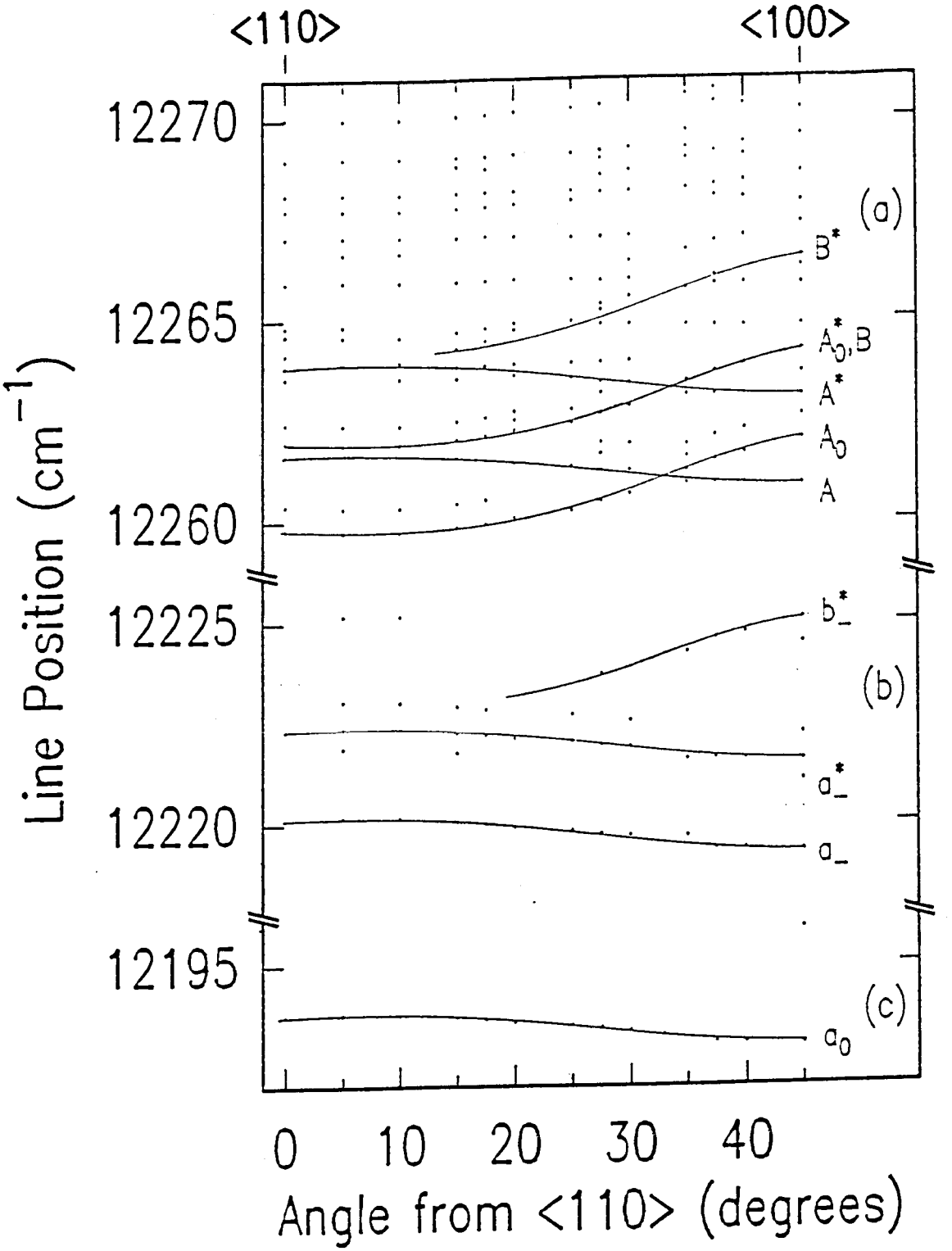
<110>
<100>
12270
12265
12260
12225
12220
12195
Line Position (cm^{-1})
(a)
B*
A*$_0$,B
A*
A$_0$
A
(b)
b*$_-$
a*$_-$
a$_-$
(c)
a$_0$
0
10
20
30
40
Angle from <110> (degrees)

1s, $2p_-$ and $2p_0$ final states respectively. Observation in Fig 4.9 of the orientation dependence of the (A,A^*) and (a_-,a_-^*) pairs and the lone $2p_0$ TES transition (a_0) again supports the interpretation given previously that these five states all originate from the same initial state. Unfortunately, the SNR in the $2p_0$ TES region was insufficient to observe transitions other than a_0.

The orientation dependence of the b_-^* transition is more complex. Superimposing the (a_-,a_-^*) curves from Fig. 4.9(b) onto those for (A,A^*) in Fig. 4.9(a) supports the claim that b_-^* is not from the same initial state as A_0^*, *i.e.* b_-^* aligns with neither A_0 nor A_0^*. However, the b_-^* orientation dependence (which admittedly mirrors that of (A_0,A_0^*)) is also seen in a transition to higher energy, in exactly the correct position to correspond to the B^* transition. From this and the previous arguments based on energy separations, b_-^* is judged to have the same initial state as (B,B^*), rather than (A_0,A_0^*) as previously assigned by SBCC.

It is worth mentioning that the (A_0,A_0^*) state becomes the lowest energy state as the crystal is turned toward <110> ∥ **B**. Even though this should energetically favour the population of this state, no TES transitions are observed which would correspond to this level. The differences in the (D^0,X) luminescence when the sample is rotated from **B** ∥ <100> to **B** ∥ <110> are shown in Fig. 4.10. These spectra are represented by the end points in part (a) of Fig. 4.9. The changes in transition energies is attributed to the anisotropy of the hole wavefunctions with respect to the various crystal directions [76S1].

Figure 4.10

Spectra showing the difference in PL for the principal (D^0,X) transitions when the magnetic field **B** is aligned (a) parallel to one of the <100> crystal axes, and (b) parallel to one of the <110> crystal axes. The lowest energy transition changes from A to A_0 on going from **B** ∥ <100> to **B** ∥ <110>.

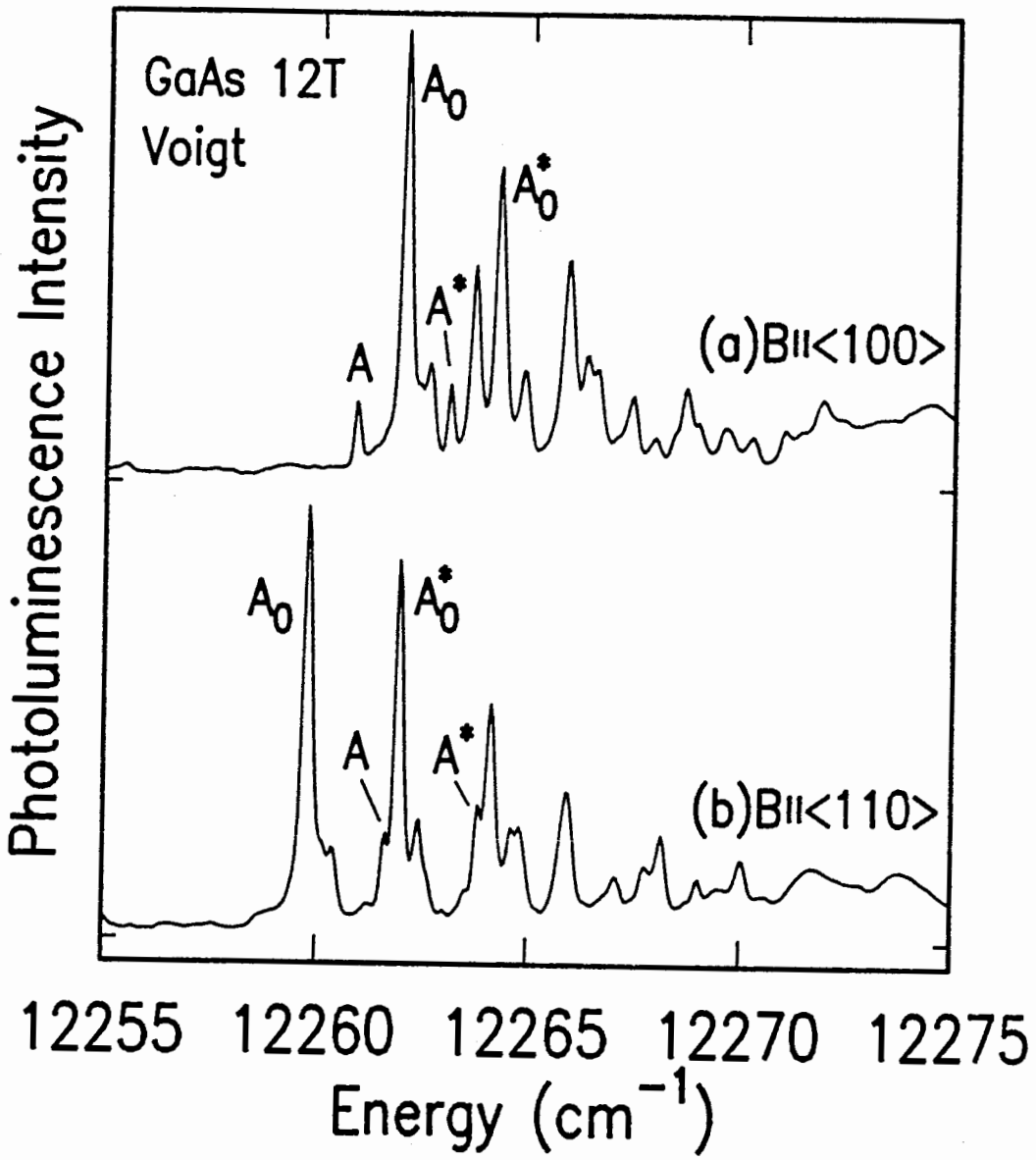
GaAs 12T
Voigt
A_0
A_0^*
A^*
A
(a)B∥<100>
A_0
A_0^*
A
A^*
(b)B∥<110>
Photoluminescence Intensity
12255
12260
12265
12270
12275
Energy (cm^{-1})

4.6 Resonant and Excitation Spectroscopies

Further information can be obtained by studying the $2p_-$ TES response as each of the principal transitions are resonantly excited using the tunable laser source. In the manner described in Chapter 3, a PLE spectrum was constructed out of over 200 separate spectra. This PLE spectrum is given in Fig. 4.11, and shows how the intensity of the a^*_- TES transition for the Ge donor varies as the excitation energy is scanned over the principal region. Such a spectrum is particularly informative for the higher energy portion of the principal region, as most of these states are weak in normal PL spectra due to thermal depopulation.

Enhancements are most evident for the D^* and F^* transitions. From the fan diagram of Fig 4.8, the D^* transition is seen to originate from one of the two lowest energy rotator states at zero field. It is unclear at this time what is the origin of the F^* transition, although one of the $\ell_{rot} = 2$ rotator states is a good possibility. The F^* transition is not seen in the fan diagram of Fig. 4.8 as it is weak in PL and is also obscured by the FE luminescence.

Another interesting result which comes out of the PLE spectrum of Fig. 4.11 is the complete absence of the "G" line reported in PLE by SBCC. A reasonable explanation could be that the G line is really due to excitation into the FE and this can be strongly dependent on the sample used. The most important result of this PLE data however, relates to donor identification and the impurity-specific nature of the PLE transitions. This will be dealt with further in Chapter 5.

A precursor to the construction of the PLE spectrum of Fig. 4.11

Figure 4.11

Photoluminescence excitation (PLE) spectrum for the Ge $2p_-$ a^*_- TES transition. The spectrum has been constructed by extracting the Ge a^*_- intensity from a series of over two hundred PL spectra, collected as the excitation energy was stepped through the principal transition spectral region.

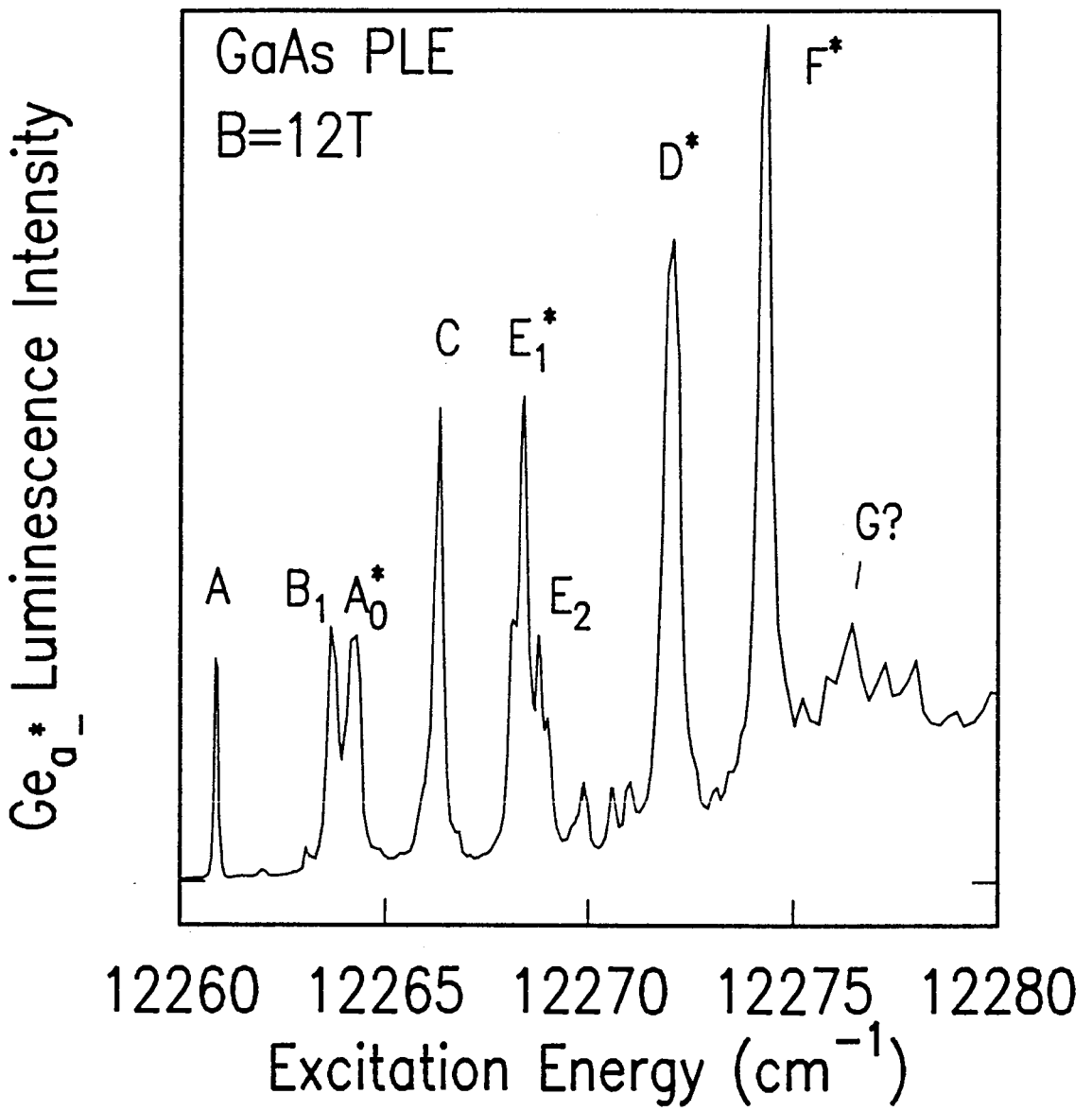
GaAs PLE
B=12T
F*
D*
C
E1*
G?
A
B1
A0*
E2
Ge_a* Luminescence Intensity
12260
12265
12270
12275
12280
Excitation Energy (cm-1)

was the collection of a number of resonant spectra. Such spectra are shown in Fig. 4.12(b)-(d) for a sample in which the dominant donor impurity is Ge. For purposes of indicating the resonant excitation energies, a PL spectrum of the principal 1s region is shown in Fig. 4.12(a). The excitation energy for parts (b),(c) and (d) of Fig. 4.12 are shown with arrows labelled "(b)", and "(c),(d)".

Spectrum (b) is of the $2p_-$ TES region while exciting near the A_0^* and B states. Although the spectrum seems crowded, each and every transition can be positively identified as one of several TES replicas of different donor species. (In this case, transitions due to the lower concentrations of S, Sn/Se and Si have been selectively enhanced with respect to the dominant Ge donor.) Another resonant $2p_-$ TES spectrum from the same sample is shown in Fig. 4.12(c), for excitation at the energy of the F^* transition seen in PLE in Fig. 4.11. This time the Ge donor is selectively pumped. The $2p_0$ TES region from the same spectrum is shown on the same energy scale in Fig. 4.11(d), and is positioned to align the a_0 and a_-^* transitions.

The horizontal arrow under Fig.4.12(a) indicates the energy separation of the laser from the principal A transition. The same separation from the respective a_-^* and a_0 transitions is shown by the horizontal arrow between Fig. 4.12(c) and (d). The enhanced TES transitions (f_-^*, f_-, and f_0) are assigned to the same initial state as the F^* transition.

This assignment may require some explanation, as the f_- transition is *two* times the spin flip energy below the translated laser position, as indicated by the multi-bracket element in Fig. 4.12(c). However, one

Figure 4.12

Resonant photoluminescence spectra of the TES regions at B = 12T. Fig. 4.12(a) gives a non-resonant principal 1s spectrum in which the labelled arrows refer to the features excited to give: (b) the $2p_-$ region while pumping primarily S/Sn/Si of the A_0^* transition, *and* simultaneously S of the B transition so that the TES spectrum has separate contributions from S, Sn/Se, Si, and Ge (since Ge is dominant, it appears strongly even though it is not resonantly pumped); (c) the $2p_-$ region and (d) the $2p_0$ region while pumping at the Ge F^* transition energy, resulting in the complete dominance of Ge in the TES spectra. The significance of each spectrum as well as the multibracket element in (c) and the horizontal arrows under (a) and (c) is discussed in the text.

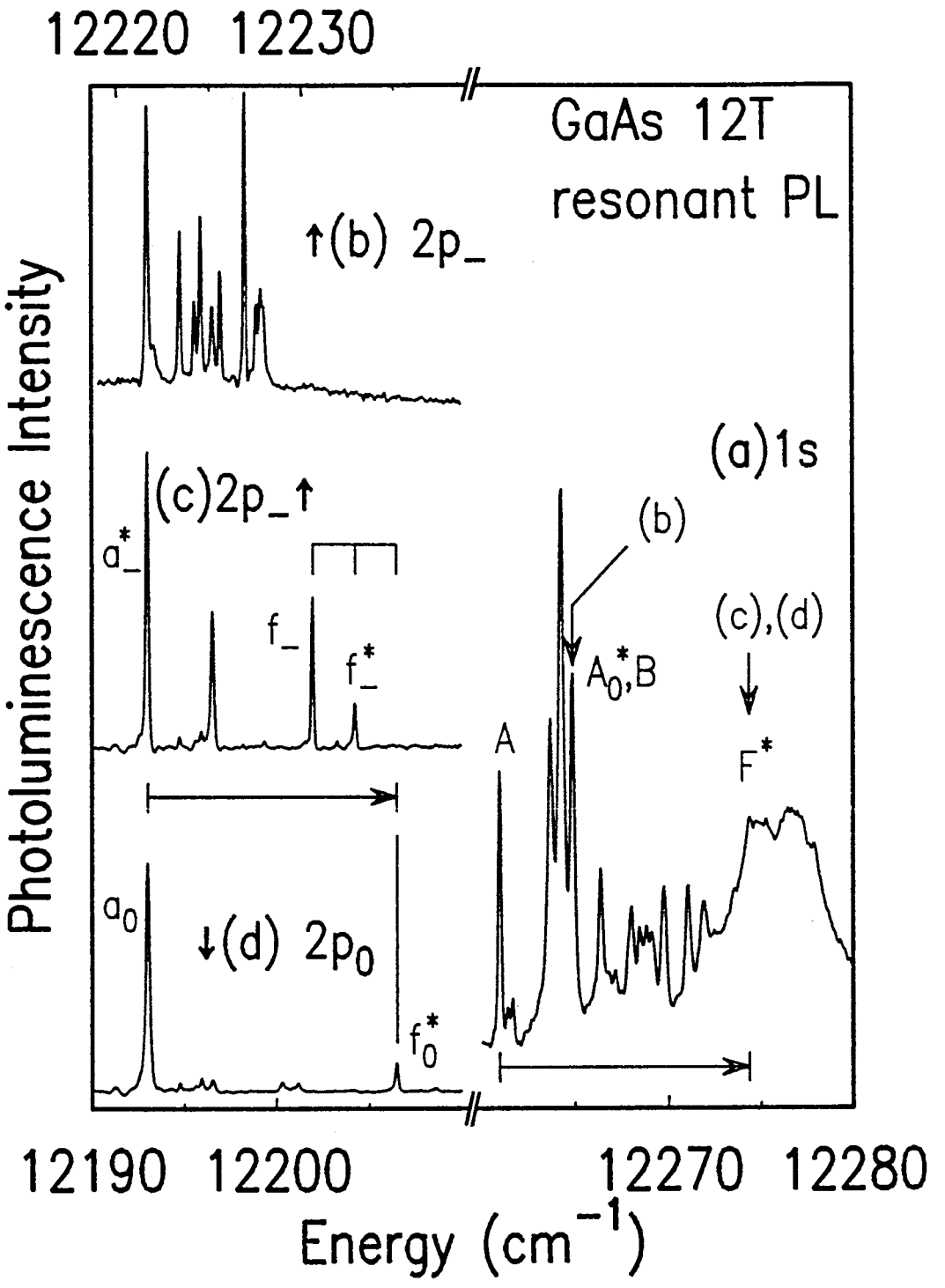
12220 12230
GaAs 12T
resonant PL
↑(b) 2p_
(a)1s
(c)2p_↑
(b)
(c),(d)
a_-^*
f_-
f_-^*
A_0^*,B
A
F^*
a_0
↓(d) $2p_0$
f_0^*
Photoluminescence Intensity
12190 12200
12270 12280
Energy (cm^{-1})

spin flip is accounted for since A is to a spin excited final state and if F^* is not. The other spin flip is accounted for if f_- is to a spin excited state, since a_-^* is not. Using the above information, the a_0 transition must also be identified as the transition leaving the donor in the excited spin state of $2p_0$. Thus with one spectrum, three transitions can be assigned the correct final state. Unfortunately, not all spectra taken for this thesis were so informative!

4.7 Energy levels

Using the information presented in Sections 4.1 - 4.6, an energy level diagram has been constructed for the (D^0,X) transitions in GaAs at 12T. This level scheme, shown in Fig. 4.13, is the first such detailed diagram reported for this system. In addition, the most important TES transitions are also shown. Most of these transitions have already been discussed. The levels with strong TES transitions are grouped together in Fig. 4.13(a). These levels can be placed with the greatest degree of confidence, using arguments such as the one in the previous section.

The next group of states, Fig. 4.13(b), is made up of the remaining levels which originate from the lowest two rotator states. These levels do not display strong TES transitions. The placement of the C transition is somewhat uncertain, as it is the only one to be observed from that (D^0,X) state. The other two states in (b) are placed with greater confidence, since two transitions are observed from each state.

The E_1^* and E_2 levels are shown separately in Fig. 4.13(c) as they are clearly observed to originate from the higher $\ell_{rot} = 1_\ell$ rotator state. The assignment of spin excited or spin ground final states is

Figure 4.13

Energy level diagram of the (D^0,X) states in GaAs at B = 12T showing (a) transitions to the D^0 1s, $2p_-$ and $2p_0$ states for states which have been observed to have strong TES transitions; (b) for the transitions not shown in (a) which can be seen to originate from the lowest two zero-field rotator states; and (c) the states which are seen to originate from the $\ell_{rot} = 1_\ell$ light hole rotator state. The energy within each vertically separated section is to the same scale. The placement of the levels is based on arguments made in the text. Transitions terminated by arrows at the upper ends are those which can be resonantly excited, since both spin states of the donor 1s state will be thermally populated at liquid helium temperatures (in contrast, none of the donor 2p states will be populated).

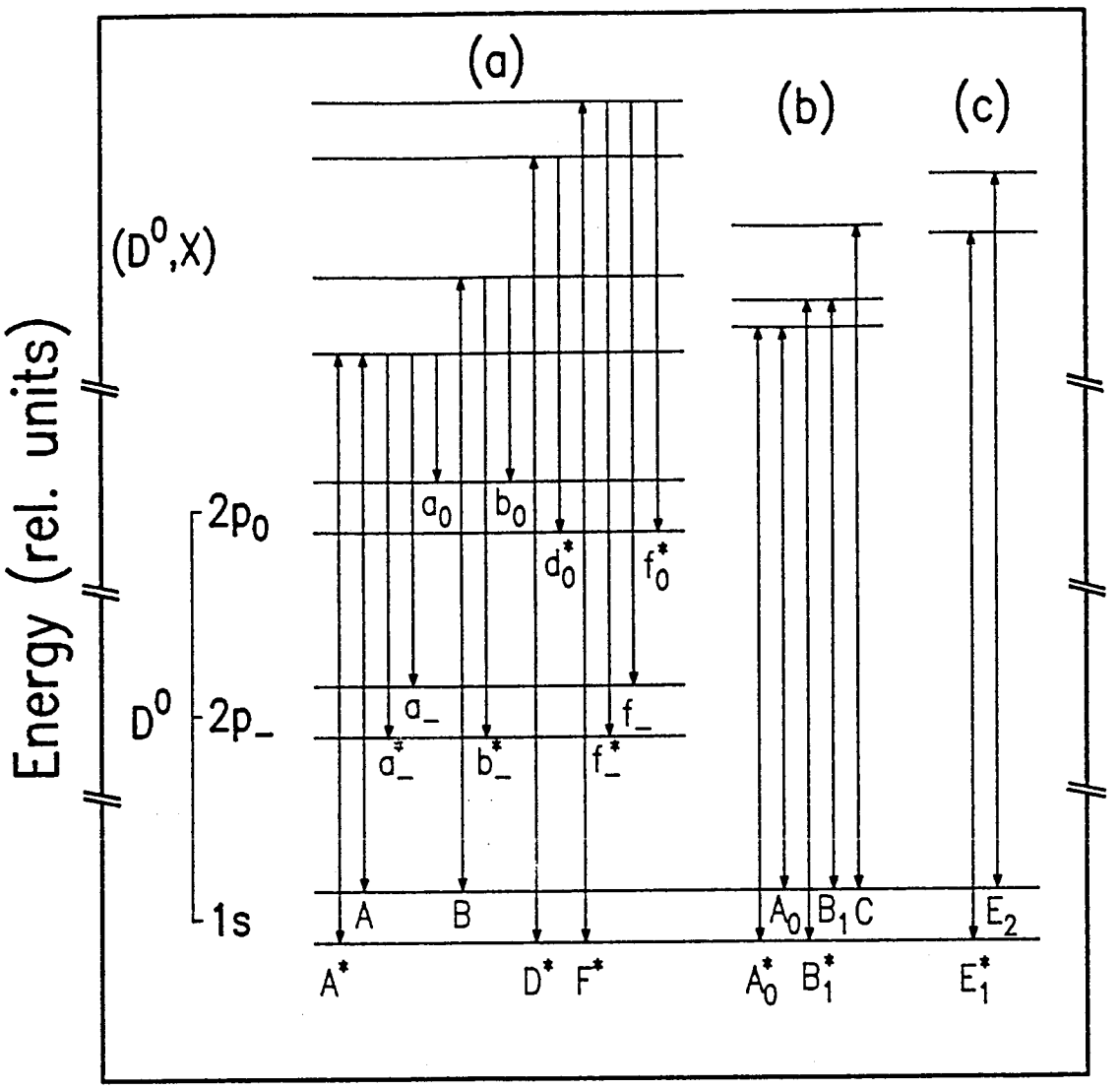
(a)
(b)
(c)
Energy (rel. units)
(D⁰,X)
D⁰
2p₀
2p₋
1s
a₀
b₀
d₀*
f₀*
a₋
f₋
a₋*
b₋*
f₋*
A
B
A₀
B₁
C
E₂
A*
D*
F*
A₀*
B₁*
E₁*

based on the difference in strength of these transitions as observed in PLE *versus* PL. Note that while the (D^0,X) states may not be in thermal equilibrium due to their short lifetimes, the D^0 states, which are the initial states of PLE transitions, will certainly be in thermal equilibrium. Since E_2 is much weaker in PLE, it is judged to come from the spin excited 1s donor state, as this state would have a lower thermal population than would the 1s spin ground state. (The population ratio of spin excited:ground states would be ~0.45 using T = 2K and the spin flip energy of 2.26 cm^{-1}.)

The selection rules for transitions from these (D^0,X) levels to donor ground and excited states seem to be strongly governed by angular momentum selection rules, judging from the polarization behavior, and the complete absence of π-states in Faraday configuration. However, proposing a scheme for assigning angular momentum quantum numbers to the states in Fig. 4.13 is a challenging task. It is doubtful that the non-rigid rotator model holds at high magnetic field, as admitted by the authors of the model. But as outlined in Chapter 1, no alternative theoretical model exists which successfully predicts the behaviour of this complicated system in a magnetic field.

Despite this lack of theoretical models, some phenomenological observations can be made regarding the selection rules and angular momentum properties of the (D^0,X) states, based on the known values of the D^0 final states. Consider for example the A series of PL transitions, shown in Fig. 4.4. The polarization behaviour of all but the A^* state can be explained if the (D^0,X) state (initial state in PL) has a total angular momentum projection on the field of $m_J = -\frac{3}{2}$. This

is seen, for example, by considering the σ^+ polarization of the A transition, which has as a final state $\ell = 0$, $m_s = -\frac{1}{2}$ (remember g_e is negative, so the spin excited state has $m_s = -\frac{1}{2}$ rather than $+\frac{1}{2}$). By arbitrarily adding the projections m_ℓ and m_s to obtain a value of m_J for the final state, we obtain $\Delta m_J = +1$, in agreement with the observed polarization of this transition. Extending this model further, the (D^0,X) initial state would then come from the $\ell_{rot} = 0$ and $m_J = -\frac{3}{2}$ rotator and hole states respectively, given the observed evolution of the A transition in the fan diagram of Fig. 4.8.

Similar calculations for a_-^*, a_- and a_0 agree with this simple scheme. The A^* state would violate this selection rule ($\Delta m_J = +2$), but then A^* is weaker in PL than the other π polarized transitions, and could be due to a higher order transition induced in the presence of the strong magnetic field.

This simplistic model is contrary to the rules governing the relation between angular momentum quantum numbers of the ℓ, s representation and the J representation. Normally, one would expect that the angular momentum and spin would be coupled at low magnetic field, *i.e.* where the spin-orbit interaction energy is comparable to the scale of the interaction with the external field. This justifies the use of the total angular momentum (J) representation, and one would expect the various projections m_J of J on the magnetic field to be the determining factor in the polarization and selection rules. At higher fields, ℓ and s are uncoupled and treated independently, so the use of selection rules for m_J is contraindicated.

In this case, however, the use of total angular momentum

projections constructed from the independent orbital and spin projections does seem to produce the correct polarizations for many of the transitions, and it does provide a starting point for further models. Hence, a tentative selection rule argument is proposed, in which the following postulates are used:

(1) The projection m_J of the angular momentum J on the magnetic field direction for the case of (D^0,X) is considered to be the sum of the projections on the magnetic field direction m_ℓ of the (D^0,X) non-rigid rotator quantum number ℓ_{rot} (m_ℓ) and of the $j = \frac{3}{2}$ hole angular momentum (m_j). The heavy hole has $m_j = \pm\frac{3}{2}$, while the light hole has $m_j = \pm\frac{1}{2}$ [88A1,89G1]. However, even at zero magnetic field, the excited rotator states have the light/heavy degeneracy removed by the quantization of the hole spin along the angular momentum direction [78R1].

The m_J final state values are taken to be those obtained by adding the projections of the angular momentum and spin of the single donor electron (e.g. $2p_-$, spin $-\frac{1}{2}$ would have $m_J = -\frac{3}{2}$).

(2) Secondly, TES replicas only occur strongly for initial states having ℓ_{rot} even. This postulate derives from the observation that the A and B transitions extrapolate to $\ell_{rot} = 0$ in the fan diagram of Fig. 4.8, and the assignment of $m_J = +\frac{1}{2}$ to the B transition initial state using the method of the postulate 1. That the TES transition only occur for ℓ_{rot} even is not unreasonable, since the existence of TES (in any semiconductor BE recombination) is

dependent not only on the angular-momentum selection rules, but on the overlap of the wave functions of the BE and the remaining electron excited final state. This postulate is also based on the observation that the (A_0, B_2) and (B_1, B_1^*) states most probably originate from the $\ell = 1_h$ rotator state in the fan diagram of Fig. 4.8, and these states do not display strong TES.

Proposed quantum number assignments for some of the lowest (D^0, X) states are given in Table 4.3. Further work will be needed to investigate the validity of such a scheme.

Table 4.3 Possible state assignments using the postulates of section 4.7. The (D^o, X) state is labelled by the principal transitions involving that state.

(D^o, X) state	ℓ_{rot}	$m_{\ell_{rot}}$	m_{j_h}	$m_J = m_{\ell_{rot}} + m_{j_h}$
(A, A^*)	0	0	$-\frac{3}{2}$	$-\frac{3}{2}$
(A_0, A_0^*)	1_h	+1	$-\frac{3}{2}$	$-\frac{1}{2}$
(B_1, B_1^*)	1_h	-1	$-\frac{3}{2}$	$+\frac{1}{2}$
(B, B^*)	0	0	$+\frac{1}{2}$	$+\frac{1}{2}$

CHAPTER 5 RESULTS AND DISCUSSION II: Donor Identification in GaAs by Fourier-Transform Photoluminescence

5.1 Introduction

Now that we have some idea of the behaviour of (D^0,X) states in a magnetic field, we turn to the applied side of this thesis: donor identification. As outlined in Chapter 2, a number of previous workers have shown the usefulness of PL as a means of identifying donor species in GaAs. The most thorough account to date is that of SBCC [89S1] which describes results for a number of samples grown by MBE and MOCVD. The use of dispersive spectroscopy for this application, however, means working at the resolution limit of the instruments, with the resulting problems of signal-to-noise ratio and spectral accuracy. In addition, the optical set-up required for the dispersive system may be quite complicated due to the necessity of collecting as much of the PL light as possible [89S1].

FTPL, on the other hand, can use a much simpler system. In the set-up used for this work, only one simple plano-convex lens was used to collect the luminescence, and initial alignment was easily achieved by imaging the internal light source of the interferometer onto the sample. The large signal strength obtained in this study often required closing the interferometer aperture below the size dictated by the desired resolution, in order to avoid saturating the detector. Most spectra were collected in a single interferometer scan, which varied from 30 seconds to $2\frac{1}{2}$ minutes in length, depending on the resolution. Even for figure-quality spectra, averages were rarely longer than 15 minutes.

As has been demonstrated by SBCC, a field of 12T is sufficient for the resolution of all of the known donor species (except Sn/Se) in GaAs in the TES region. Due to the expense of superconducting magnet systems, optical cryostats with operating fields higher than 12T are uncommon. For these reasons, all of the spectra which are reported here are for fields between 0 and 12T. This should enable other workers to use the results given here for characterization purposes.

The most commonly followed method of donor identification uses the central-cell splitting observed in the $2p_-$ TES transitions. The identities of the (D^0,X) states which are the origin of these $2p_-$ transitions has been addressed in Chapter 4.

As first observed in PL by SBCC, central-cell structure is visible in the principal transitions, due to the chemical dependent localization energies of the donor BE. This central-cell dependence of the (D^0,X) states augments the splittings of the central-cell of the D^0 final state, and makes the $2p_-$ splittings observed in PL larger than those observed in PTIS. When studying very high quality samples (*i.e.* ones with very narrow transition linewidths), the (D^0,X) 1s central-cell splitting is sufficient for donor-identification purposes, provided that the spectral resolution is high enough.

However, when samples on the other end of the purity scale are studied, even the $2p_-$ transitions begin to overlap. In this case resonant line-narrowing, as described by SBCC, is required, as the use of resonant excitation into the principal 1s transitions has been found to result in narrowed $2p_-$ TES transitions [89S1]. However, such resonant excitation can be rife with complications, as impurity-specific

resonant enhancement effects are observed for all (D^0,X) 1s states below the FE energy. Any single spectrum taken under resonant conditions will therefore not give a true representation of the relative concentrations of the donor impurities. In addition, interpretation of the actual identities is done slightly differently than is the case with non-resonant excitation. Thus, the resonant line-narrowing should be used only when absolutely necessary, and this will be discussed in detail in Chapter 6, where results on bulk SI GaAs will be presented.

The most straightforward method of performing rapid identification of donors in a number of samples is achieved by using the Faraday configuration. This removes the problem of orienting the sample with respect to the field, as the growth direction of epitaxial GaAs is almost always along the <001> crystal axis, or within a few degrees of <001>. Thus a sample holder need only allow the samples to lie flat, in an unstrained manner, and the field and <001> crystal direction will be very nearly parallel.

5.2 Donor identification in high-purity epitaxial n-type GaAs.

The high-field PL technique has been well proven as a technique for donor identification. The point to be taken in this thesis is that the use of FT spectroscopy at high field makes PL a superior method to PTIS in all respects, except perhaps for samples which contain a high concentration of defect or impurity transitions in the donor $2p_-$ region (such as are observed in some MBE grown samples). Even in this situation, the $2p_0$ TES may suffice. The FTPL technique also lends itself to situations where a large number of samples are to be

characterized, with the potential for simultaneous acceptor characterization. We now consider the case for performing donor identification in normal, high-purity epitaxial GaAs.

In high quality epitaxial samples, the identification of donors can be a straightforward measurement. (The following assumes Faraday configuration). A typical measurement would include a wide-band spectrum collected using above-gap excitation. Such a spectrum is shown in Fig. 5.1, taken at an ultra-high resolution of 0.025 cm-1 (~0.03 meV). The entire excitonic region is shown in Fig. 5.1(a), for the same low-acceptor sample shown previously in Figs. 4.2-4.4. An expanded view of the (D^0,X) principal region is shown in Fig. 5.1(b). Such high resolution is not absolutely necessary, but is included in this case to demonstrate the resolution of the Se/Sn from Si bound excitons even in the principal 1s A region. The wide-band spectrum is used to ensure that the crystal orientation is reasonably close to B ∥ <001>, and that the field is at 12T. Any differences from these conditions will result in relative shifts of the 1s transition energies. The transition energies measured by FTPL for the known donor impurities in GaAs are given for reference purposes in Table 5.1. The transition linewidths are also a measure of the sample quality, with line broadening resulting from higher impurity concentrations, and energy shifts resulting from strain in the sample, or possibly alloying effects.

The next step in the donor identification process is the collection of a spectrum of the $2p_-$ region, with cleaner spectra obtained by using an interference filter to remove luminescence at all other energies. Such a spectrum can be made more intense by pumping into the FE, which

Figure 5.1

(a) Wide, high resolution photoluminescence spectrum of high purity at B= 12 T for a sample with very low acceptor concentration. (b) Expanded view of the low-energy portion of the (D^0,X) region from the same spectrum as in (a). The resolution in the A lines of Sn/Se from Si is reported for the first time. Resolution is 0.025 cm^{-1}. The time required to collect and transform this spectrum was less than three minutes.

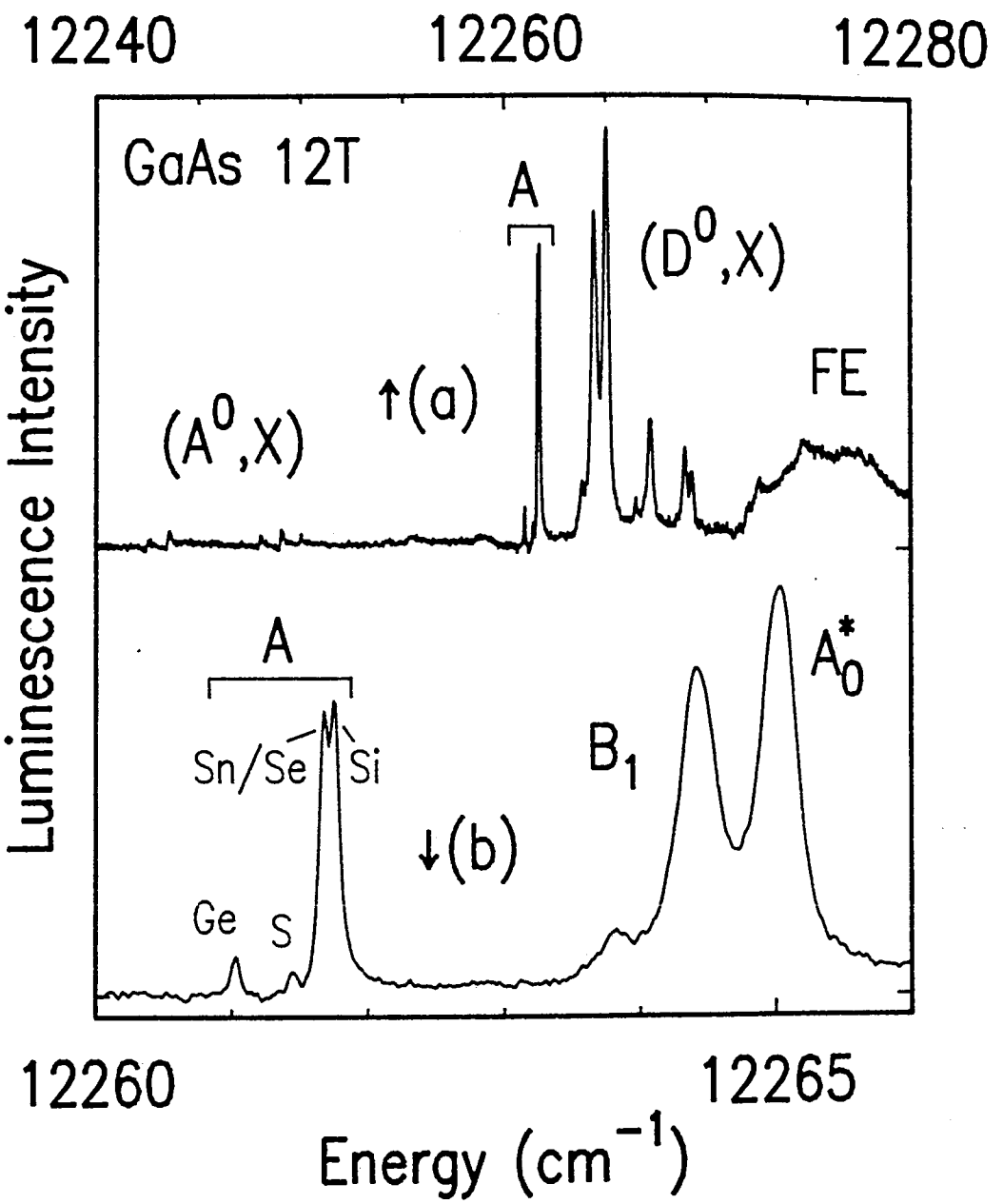
12240
12260
12280
GaAs 12T
A
(D0,X)
FE
(A0,X)
↑(a)
A
Sn/Se
Si
Ge
S
↓(b)
B1
A*0
Luminescence Intensity
12260
12265
Energy (cm-1)

Table 5.1 Energies and separations for species-dependent (D^0,X) PL transitions in GaAs at B = 12T. In the last column, the observed $2p_-$ shifts of all the donors are given relative to the Si line.

Donor Impur.	Energy (cm^{-1})			
	1s A	$2p_- a^*_-$	ΔE (A - a^*_-)	$2p_-$ shift
Ge	12260.9 ± 0.3	12221.6 ± 0.2	39.34 ± 0.05	-2.91 ± 0.02
S	12261.4 ± 0.2	12223.4 ± 0.2	37.98 ± 0.04	-1.16 ± 0.02
Sn/Se	12261.6 ± 0.2	12224.2 ± 0.2	37.41 ± 0.06	-0.348 ± 0.008
Si	12261.7 ± 0.3	12224.6 ± 0.3	37.09 ± 0.05	---
Te	12261.9	12225.2	36.8	0.60 ± 0.05

is located at ~12285 cm^{-1} and ~12350 cm^{-1} for the n = 1 and n = 2 FE states respectively at B = 12T. For the purposes of donor identification this is still considered non-resonant excitation, as it is non-selective. A $2p_-$ TES spectrum is given in Fig. 5.2(a) for the same sample as shown in Fig. 5.1. Fig. 5.2(b) contains the $2p_-$ spectrum for another sample, collected under similar conditions. The spectral line positions for the impurities in these and other samples are given in Table 5.1 for both the 1s A and the $2p_-$ a^*_- transitions.

In addition, the 1s A to $2p_-$ a^*_- energy separations are also given, with lower uncertainty, due to the insensitivity of this energy difference to changes in the sample orientation, or minor band-gap changes due to strains and alloying effects. This value is the most important measurement for donor identification purposes, and it will remain constant (at 12T) even if the sample orientation is not exactly <001>, provided the 1s A transition is properly identified. This insensitivity of the 1s to $2p_-$ energy difference to the various perturbations is a consequence of the spherical nature of the conduction band minimum in GaAs. The values listed in Table 5.1 for the 1s A to $2p_-$ a^*_- separation agree within experimental error in every case with the values taken from the graphs of PTIS transition energies at 12T [80A1,80A2,81A1], taking into account the electron spin-flip energy. This agreement is achieved using the value of 2.255 ± 0.008 cm-1 for the electron spin-flip energy at 12T given in Chapter 4.

For high purity samples, donor identification can be determined from a principal line spectrum. However, more reliable identification can be made using the $2p_-$ TES, with the 1s A to $2p_-$ a^*_- separation giving

Figure 5.2

Photoluminescence spectra of the $2p_-$ TES region in GaAs at B = 12T for (a) the same sample used for the fan diagram in Fig. 4.7 and (b) the same sample used for the orientation dependence diagram Fig. 4.8, and the PLE spectrum, Fig. 4.9. The resolution in the present spectra is 0.1 cm^{-1}.

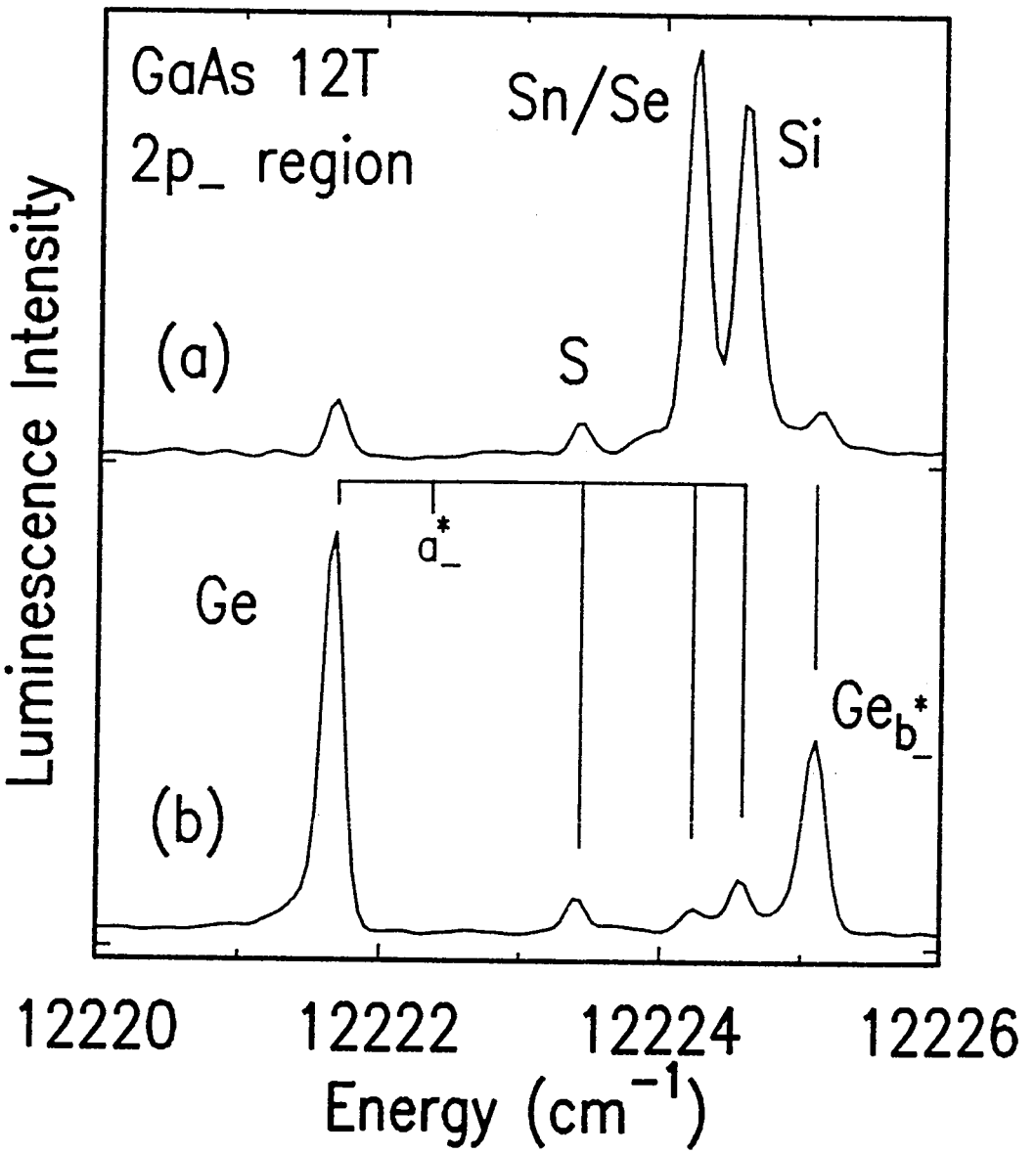
GaAs 12T
2p_ region
Sn/Se
Si
(a)
S
a*_
Ge
Ge_b*_
(b)
Luminescence Intensity
12220
12222
12224
12226
Energy (cm^-1)

the donor species conclusively when compared to the values in Table 5.1.

To further demonstrate the use of FTPL for donor identification, $2p_-$ TES spectra of two other high-purity epitaxial samples are shown in Fig. 5.3. The top spectrum was taken at relatively low resolution of 0.1 cm^{-1}. The bottom spectrum was taken at the highest possible resolution for the interferometer at this wavelength: 0.025 cm^{-1}. This sample is remarkable for MOCVD-grown GaAs, due to its complete lack of Ge.

5.3 Donor identification in p-type GaAs

One of the drawbacks of PTIS measurements is its inutility for identifying donors in p-type samples. This is attributed to the fact that PTIS is only useful for the identification of majority carriers [88B1], as well as to the absence of neutral donors in such samples. The situation for PL is different, however, as the creation of free-carriers is ensured by the use of near- or above-gap excitation, and some population of neutral donors will result, making donor identification possible via the (D^0,X) transitions. In addition, the (D^+,X) transitions exhibit a central-cell shift, as reported by others [83R1,89S1] and may also be used for identification purposes, but this subject will not be addressed here.

The wide-band PL spectrum of a p-type GaAs sample is shown in Fig. 5.4(a), in which the (A^0,X) recombination obviously dominates over that due to (D^0,X). Note the weakness of the (D^0,X) transitions. However, using the same technique as in Section 5.2, the identity of the donors can be obtained from the $2p_-$ transition when pumping into the FE.

Figure 5.3

Photoluminescence spectra of the $2p_-$ TES region in GaAs at B = 12T (a) taken at 0.1 cm^{-1} for a sample from a different laboratory than the other epitaxial samples presented here and (b) taken at 0.025 cm^{-1} for a sample with zero detectable Ge donors.

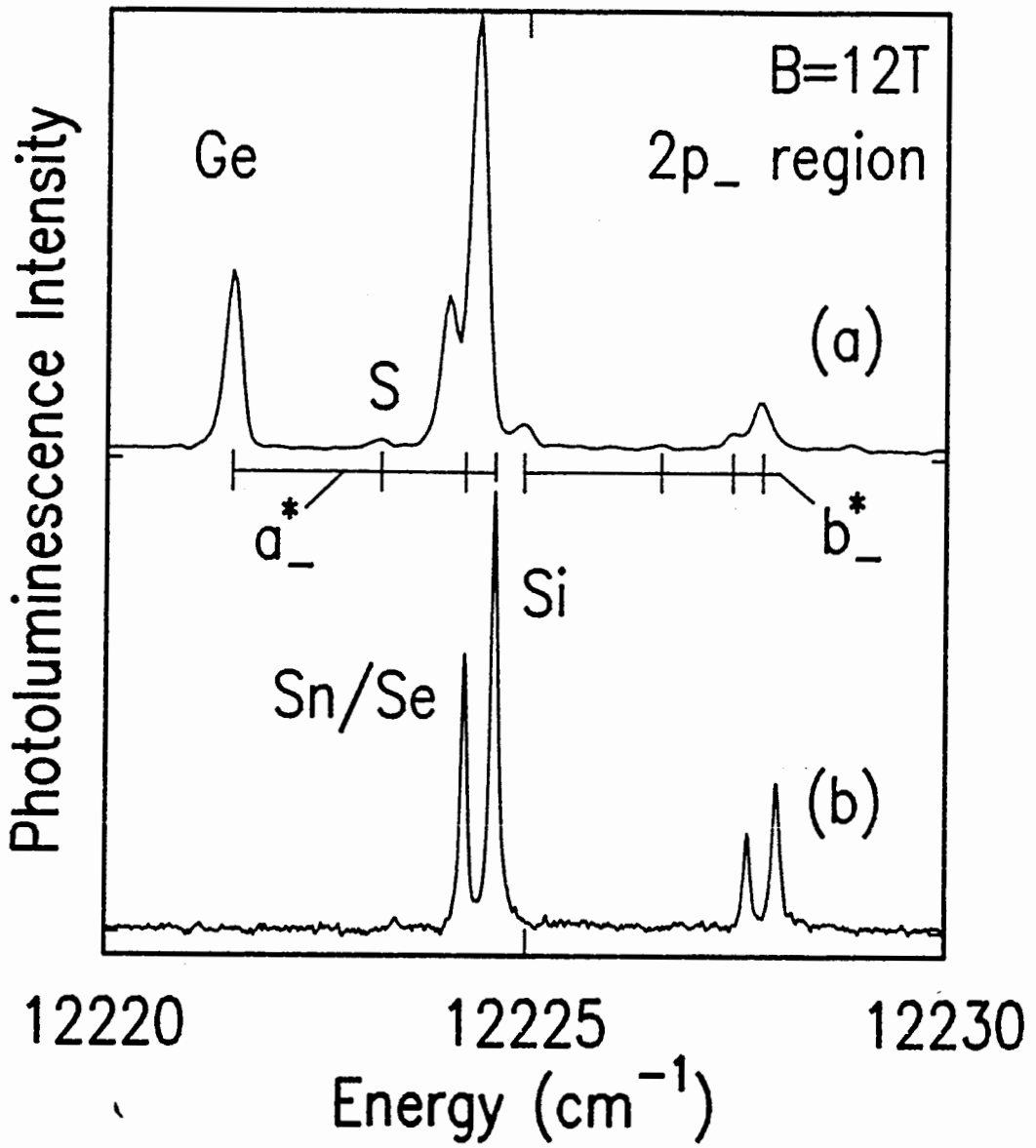
B=12T
2p_ region
Ge
S
(a)
a*_
b*_
Si
Sn/Se
(b)
Photoluminescence Intensity
12220
12225
12230
Energy (cm^{-1})

Figure 5.4

Photoluminescence spectra of a p-type GaAs sample at B = 12T showing (a) the principal 1s region, which is dominated by acceptor bound exciton emission and (b) the $2p_-$ TES region when pumping non-selectively at the FE energy. This sample shows the presence of Te donors, whose a^*_- transition occurs at the same energy as would the Ge b^*_- transition. However, since there is no Ge a^*_- transition present, and thus no Ge, the luminescence must be due to Te. The $2p_-$ TES region in (b) is selected optically by a high performance, narrow band pass interference filter. The broad background is common in p-type and bulk semi-insulating samples.

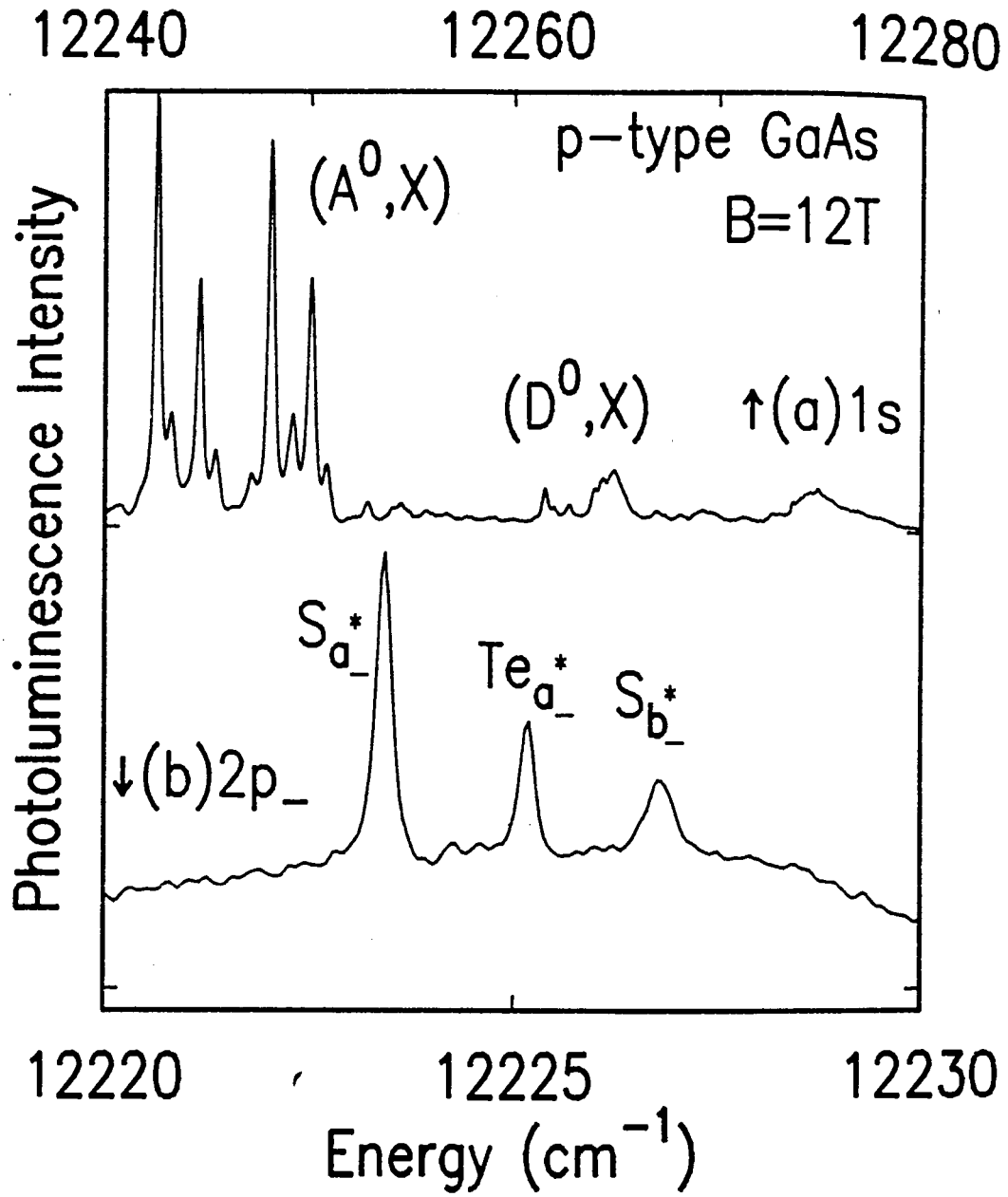
12240
12260
12280
p-type GaAs
B=12T
(A^0,X)
(D^0,X)
↑(a)1s
S_{a^*}
Te_{a^*}
S_{b^*}
↓(b)2p_
Photoluminescence Intensity
12220
12225
12230
Energy (cm^{-1})

Such a spectrum is shown in Fig. 5.4(b) for the same sample. The wide background follows the through-put of the narrow band pass interference filter, and is common in spectra for p-type and semi-insulating samples. The donors in this sample are seen to be S and Te. It is worth noting that the Te $2p_- a^*_-$ TES energy overlaps that due to the Ge $2p_- b^*_-$ TES. This is not a problem in this particular sample, due to the absence of Ge (note that there is no Ge $2p_- a^*_-$ TES). However, in samples with Ge *and* Te, circular polarization would be required to suppress the b^*_- transitions. The b^*_- transition due to S is also visible in this sample, indicating that the S luminescence may be coming partly from the substrate, and is visible due to the relatively weak nature of the (D^0,X) luminescence from the epilayer. Similar spectra have been obtained from other p-type samples.

5.4 Conclusions

In this chapter, methods for the identification of donors by FTPL in high purity epitaxial GaAs are described. The most important measurement for such purposes is the separation of the principal 1s A line from its $2p_- a^*_-$ TES counterpart, measured for each donor species. A measurement of this energy difference gives unambiguously the identity of the donor species present in both n- and p-type samples. The energy separations for all of the known shallow donors in GaAs is given in Table 5.1.

In Chapter 6, methods for identification of donors in bulk SI samples will be described. These methods are also useful for epitaxial samples with broadened transitions, which do not lend themselves to

non-resonant techniques.

CHAPTER 6 RESULTS AND DISCUSSION III: Application to Bulk GaAs

6.1 Introduction

The identification of donors in bulk GaAs (e.g. from a boule) is a more difficult problem than in higher purity material. This is because the impurity concentrations are sufficiently large and inhomogeneous to cause significant broadening of the transitions, both in the principal (D^0,X) 1s transitions and the corresponding $2p_-$ TES. This broadening requires the use of resonant excitation to narrow the luminescence transitions to the point where useful information can be extracted. Such narrowing has been reported previously by SBCC, where the narrowing was explained as being due to the slow migration time between donors, of the resonantly created BE, relative to the (D^0,X) radiative lifetime. However, as mentioned in Chapters 4 and 5, resonant excitation can not be applied at any arbitrary energy, as this may result in misleading, or even incorrect interpretation of the $2p_-$ spectra.

Given the impurity specific nature of the excited states, it is clear that resonantly exciting into these states may result in misleading intensity ratios in the $2p_-$ TES, such as was shown in Fig. 4.11(b), *i.e.* ratios which are unrelated to the true impurity ratios. PLE spectra are useful in demonstrating the impurity specific nature of the principal transitions. Two such spectra are shown in Fig. 6.1. The top spectrum is the same one as was shown previously, in Fig. 4.10, and represents the intensity of the Ge $2p_-$ a^*_- TES as a function of excitation energy. The bottom spectrum was collected simultaneously, and represents the intensity of the Si $2p_-$ a^*_- TES. The lines joining

Figure 6.1

Photoluminescence excitation (PLE) spectra for high-purity epitaxial GaAs. The intensity of the two-electron satellites are plotted as a function of excitation energy for (a) Ge a^*_- and (b) Si a^*_- transitions. Ge is the dominant donor in this sample, so some feedthrough due to Ge is visible in the spectrum for Si. The lines connecting similar spectral features highlight the impurity specific nature of even the highest (D^0,X) states.

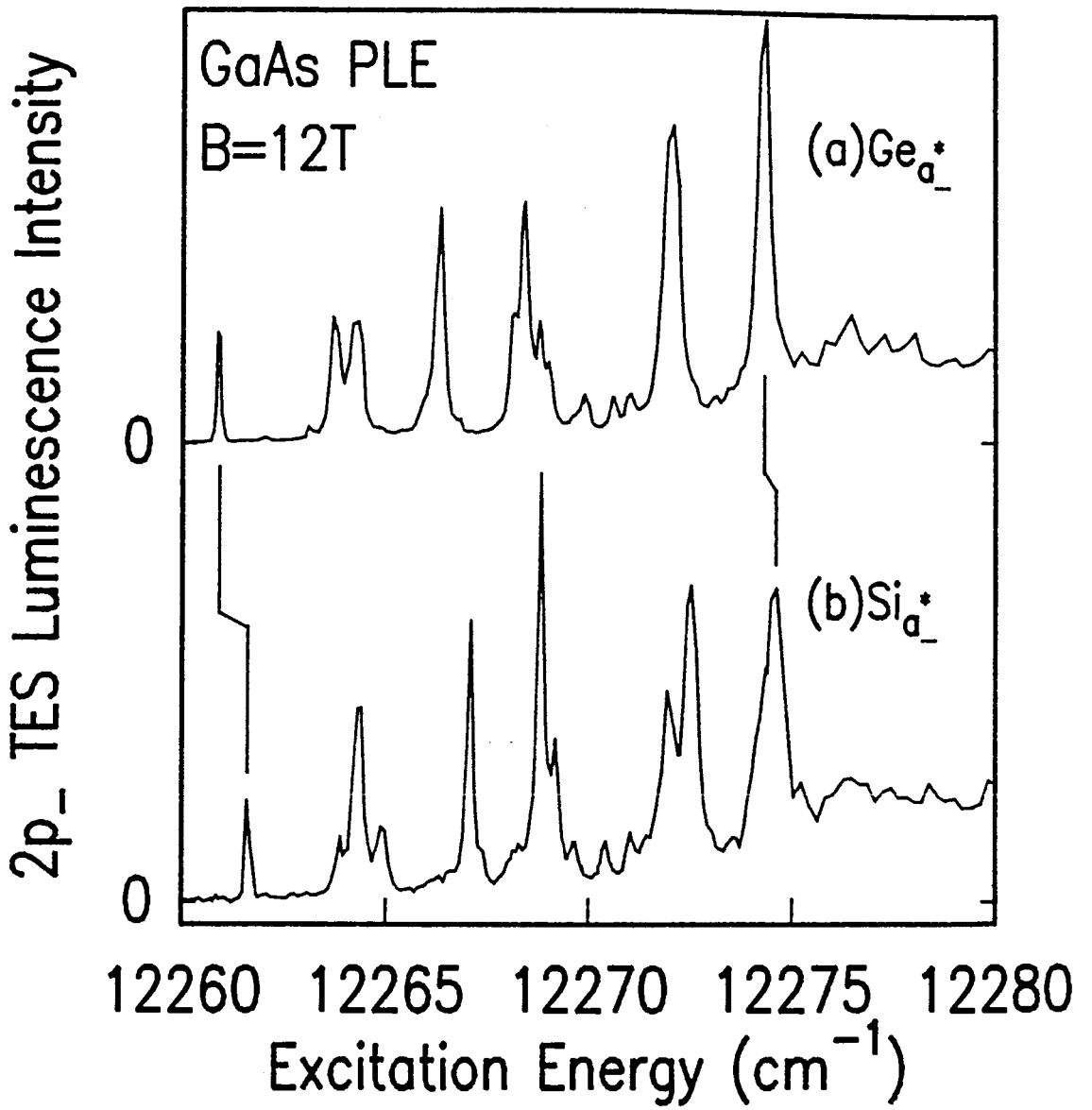
GaAs PLE
B=12T
(a)Ge$_{a^*_-}$
(b)Si$_{a^*_-}$
0
0
2p_ TES Luminescence Intensity
12260 12265 12270 12275 12280
Excitation Energy (cm^{-1})

similar spectral features highlight the impurity-specific shift of the spectra. Since Ge is dominant in this sample, some features do line up, but these can be attributed to transfer of excitons from Ge to Si binding centers.

As mentioned in Chapter 4, SBCC reported non-selective excitation into an excited state, labelled "G" in their PLE spectrum [89S1]. However, we do not observe a strong TES response when pumping at this energy, which is above the F^* line in Fig. 4.10, and postulate that this transition corresponds to FE absorption.

6.2 Results and Discussion

The problem of transition line broadening is typified by the comparison of the two spectra given in Fig. 6.2. The 12T photoluminescence spectrum of a high purity, MOCVD-grown GaAs sample is given for reference purposes in figure 6.2(a), where the principal 1s (D°,X) to crystal-ground-state transitions are shown. The labels are those described in detail in Chapters 4 and 5. The structure visible in the "A" and "C" regions is due to transitions from excitons bound to different chemical species. For comparison, the spectrum for a bulk SI GaAs sample is shown in figure 6.2(b). The broadening of the bound exciton transitions is obvious.

The corresponding ground-state to donor-excited-state $2p_-$ TES transitions are shown in Fig. 6.3. The transitions due to different impurities are labelled for the epitaxial sample in Fig. 6.3(a). The increase in the chemical shifts, which is the advantage of studying the TES luminescence, is sufficient to resolve all of the donor species for

Figure 6.2

Photoluminescence spectra for the (D^0,X) 1s region in (a) epitaxial GaAs and (b) bulk GaAs using non-resonant excitation.

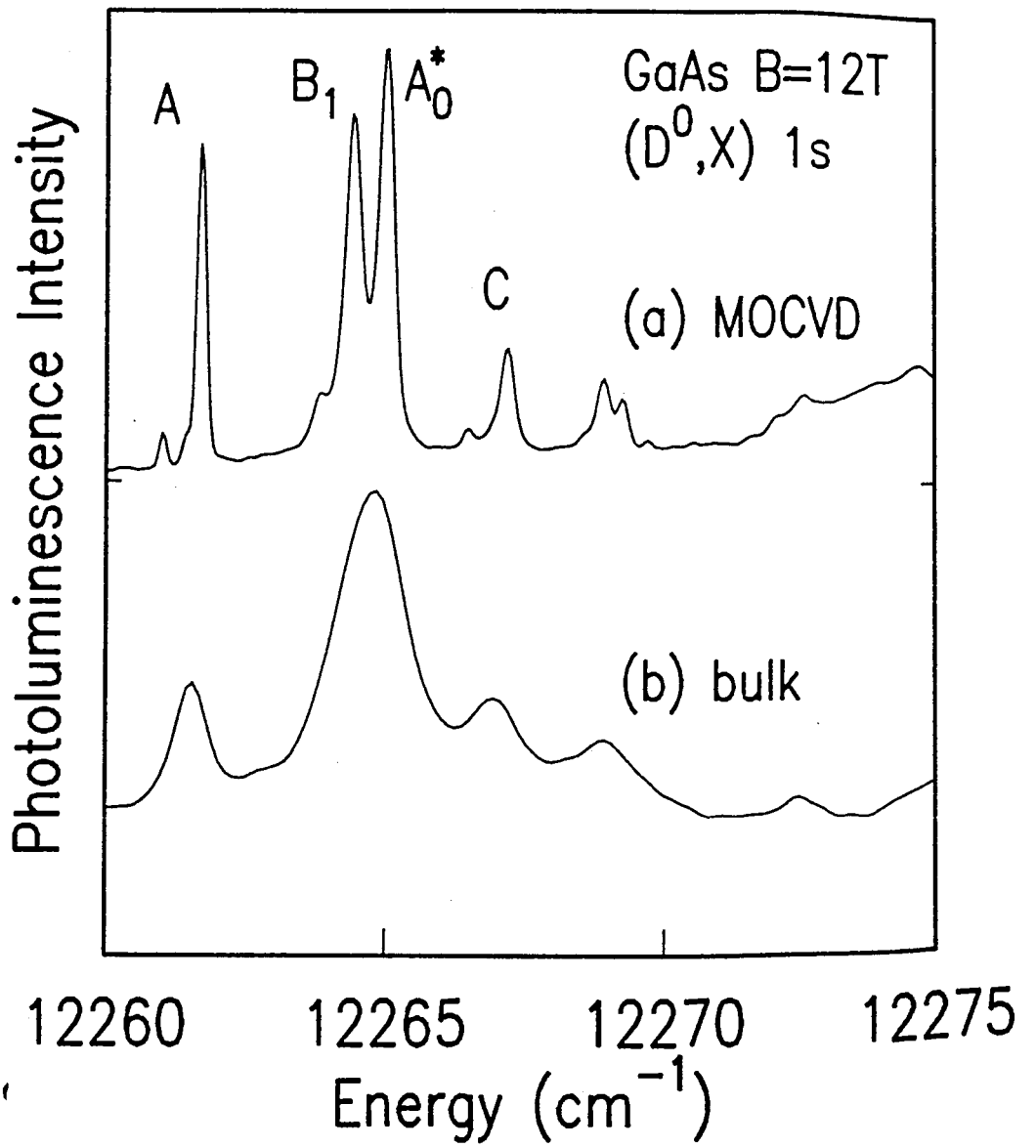
A
B1
A*0
C
GaAs B=12T
(D0,X) 1s
(a) MOCVD
(b) bulk
Photoluminescence Intensity
12260
12265
12270
12275
Energy (cm-1)

Figure 6.3

Photoluminescence spectra of the $2p_-$ TES region for the same samples as in Fig. 6.2. The presence of S in the bulk sample is evident, but other donors may be obscured by S and the background level. These spectra were collected with non-resonant excitation.

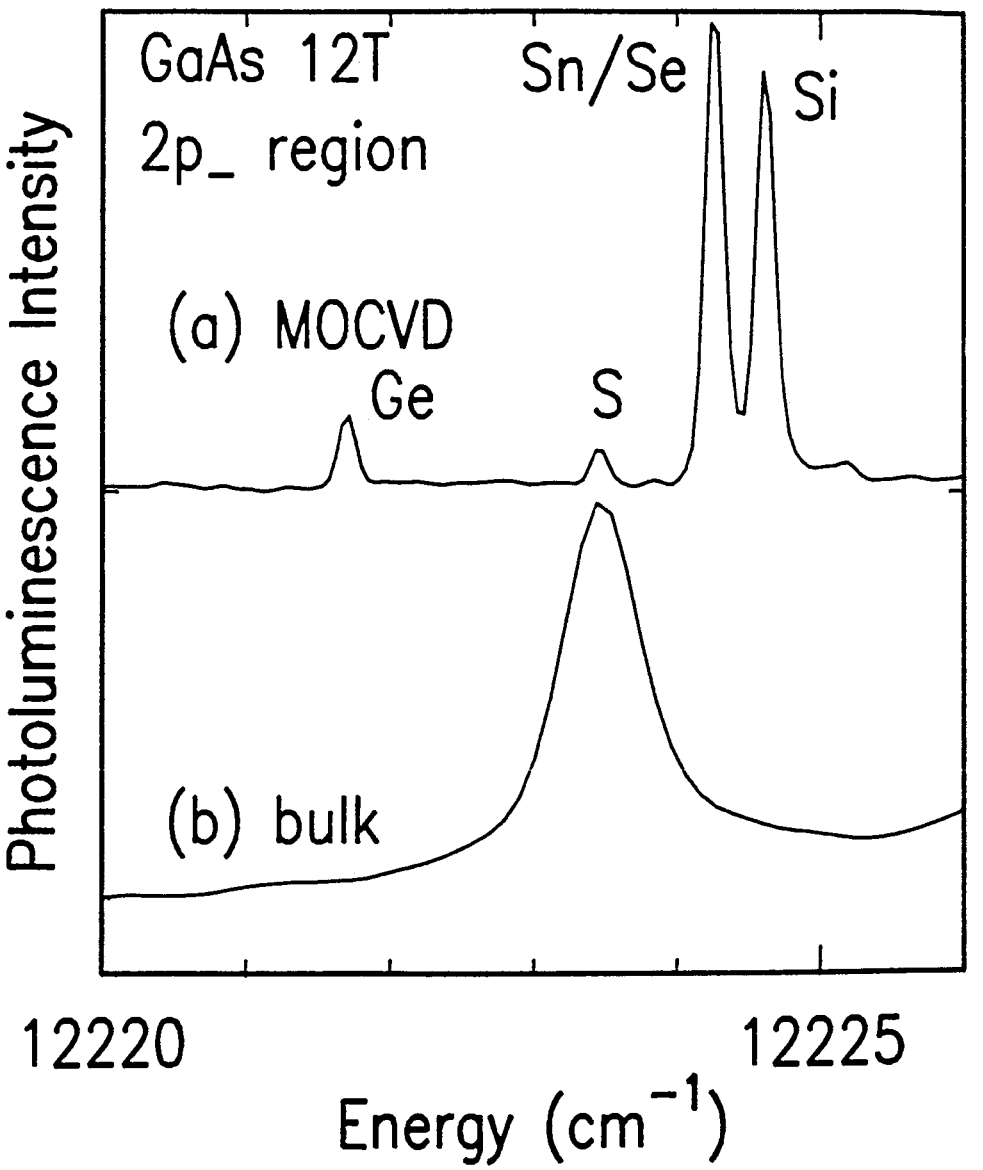
GaAs 12T
2p_ region
Sn/Se
Si
(a) MOCVD
Ge
S
(b) bulk
Photoluminescence Intensity
12220
12225
Energy (cm^{-1})

this sample, except of course Sn/Se. However, the same can not be said for the bulk SI sample whose TES spectrum is shown in Fig. 6.3(b). The bulk sample is seen to be dominated by S donors (Fig. 2b), however any other donors are obscured by the broadened transitions and the strong background. All of the spectra in Figs. 6.2 and 6.3 were collected with non-resonant excitation. The broadness of the transitions in Fig.6.3(b) suggests that resonant excitation is required.

Other researchers [88H1, 86H1] have used the PLE technique to enhance resolution and increase the luminescence intensity of donor-related transitions in bulk GaAs. They report selectivity in the amplitude of the TES response for different donor species, but not in the spectral position. Their results show only one known donor, S, in addition to a shallower spectral feature, which they label as an as yet unidentified donor. S was found in all of the bulk samples which they studied.

The process for (D^0,X) TES luminescence can be understood more clearly when one considers the process occurring under resonant conditions. When using resonant excitation, bound excitons (D^0,X) are being created on a subset of the inhomogeneously broadened distribution of donors. The result of this is the creation of bound excitons on different donor species, but having the same energy. This is different than the non-resonant high purity epitaxial case, in which excitons bound to different donors have different energies, as evidenced by the central-cell splittings in the principal transitions. Thus, for bulk GaAs, the laser to $2p_-$ TES splitting will be the same as that measured by PTIS (less the electron spin-flip energy), because the added

central-cell splitting of the bound exciton ground state has been nullified. Thus the donor species must be identified by their TES separation from the excitation energy, which corresponds to the principal line to TES separation measured separately for each donor in epitaxial material. These separations are those given in Table 5.1.

The bulk $2p_-$ TES also follow the laser energy, and thus do not, except when pumping at the peak of the 1s distribution, occur at the same energy as the non-resonant case. The intensity of the satellites will vary with the laser energy as it pumps a different proportion of the concentration- or strain-broadened 1s BE states. The peak $2p_-$ satellite intensity for a given donor species should thus occur for the same excitation energy as the 1s transition in higher purity material, assuming no band-gap shifts exist due to alloy effects. From this result, one can see that the presence of a particular donor species can be determined by pumping at one energy and measuring the corresponding separation between the laser and the $2p_-$ satellite.

To determine the relative concentrations of the various donor populations, one must pump resonantly at the peaks of each of the (D^0,X) populations and compare the intensities of the $2p_-$ response. This is accomplished by pumping the most populous donor peak first (determined as having the largest $2p_-$ response, e.g. S in Fig. 6.3(b)). Once its identity and $2p_-$ intensity have been determined, the pump energies for the other principal donors can be calculated from the splittings between the 1s (D^0,X) energies in Table 5.1. One can then pump the 1s "peak" of each donor individually, and translate the intensity of its $2p_-$ satellite, relative to the strongest, into a relative value for the

concentration. Absolute donor concentrations can be calculated if the total number of donors is known from some other measurement.

This technique relies heavily on the precise knowledge of the laser energy, and is easily accomplished with the aid of the wavemeter. The same results can be obtained, although not as conveniently, by observing the laser position in the spectra, and adjusting accordingly.

The enhancement of the $2p_-$ transitions in this way is really an exploitation of the resonant enhancement of BE transitions also observed [89S1] for the high purity materials described in Chapter 4. In this case, however, the resonantly enhanced "shoulder" dominates over the much broader true distribution.

The situation described above is shown schematically in Fig. 6.4. In figure 6.4(a) the case of high purity epitaxial materials with two donors in equal concentration, e.g. Ge and Si, is shown. The 1s to $2p_-$ splitting for each donor is shown, and correlates with that observed in PTIS. The TES splitting is the sum of the donor and the donor BE central-cell shifts, and is approximately 1.3 times that observed in PTIS, as reported by SBCC. The case of bulk material, where the transitions are broadened, is shown in Fig. 6.4(b). Excitons bound to different donor species are resonantly created at the same energy, thus the TES separation is identical to the PTIS-measured separation, and different from that shown in (a).

Similar narrowing effects can be obtained by pumping into the higher excited states as well, such as at the C transition energy. This supports the model of a resonantly enhanced (D^0,X) recombination, rather than the resonantly enhanced Raman scattering explanation of SBCC.

Figure 6.4

Schematic diagram of the principal 1s and $2p_-$ TES regions for the case of a sample with identical concentrations of Ge and Si donors for (a) high-purity epitaxial GaAs, and (b) bulk GaAs. Fig. (b) shows the effect of resonant excitation into the broadened distribution of donors in bulk material. The 1s to $2p_-$ separation is the same for the same donor species in each sample.

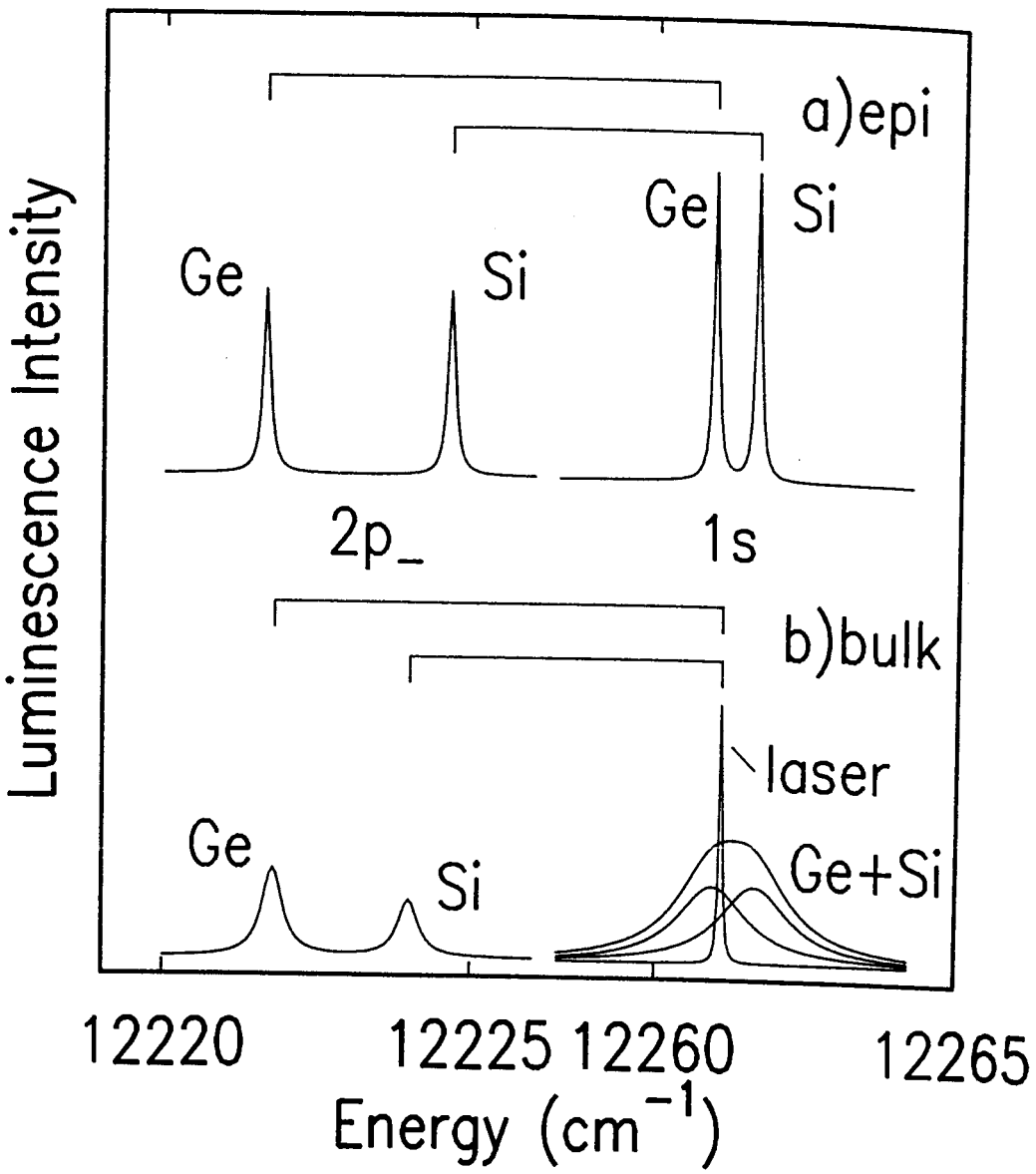
Luminescence Intensity
a)epi
Ge
Si
Ge
Si
2p_
1s
b)bulk
laser
Ge
Si
Ge+Si
12220
12225
12260
12265
Energy (cm^{-1})

Excitation at the C transition energy may be advantageous when thin epitaxial samples are being studied by this method, as the weaker absorption of the A transition may allow laser excitation to penetrate into the substrate.

Even though a particular (D^0,X) state is resonantly selected, some redistribution to other (D^0,X) states will occur due to thermalization or tunneling. This leads not only to the presence of lower energy TES transitions, but also to enhancement of TES transitions originating from higher energy initial states. One of the these processes may be responsible for the unidentified shallow donor transition reported in references 88H1 and 86H1.

Interpretation of resonantly pumped TES spectra using resonant excitation as depicted in Fig. 6.4 can result in rapid assessment of the presence of donor species in bulk GaAs. For quantitative measurements of the relative donor concentrations, the peak of each impurity-broadened principal transition must be resonantly excited, and the intensities of the TES response for each donor can then be compared.

We have done this for a number of bulk SI GaAs samples from a variety of sources. As reported previously [88H1,86H1], the dominant, and often *only*, donor was found to be S. A series of spectra for a bulk SI GaAs sample is shown in Fig. 6.5. This sample was chosen for demonstration purposes because it was one of the few which showed anything other than S. The non-resonant spectrum is shown in Fig. 6.5(a), while in Figs. 6.5(b)-(d), the resonant enhancement of three different donors in the same sample is shown. This excitation was applied in the "A" region of the principal transitions. The relative

Figure 6.5

The use of resonant excitation and FTPL for the identification of donors in a bulk GaAs sample containing Ge, S and Si. (a) the spectrum for non-resonant excitation. (b)-(d) the spectra for excitation at the principal A transition energies for Ge, S and Si respectively. The absolute intensities (not shown) give the Ge:S:Si ratio as 10:70:20.

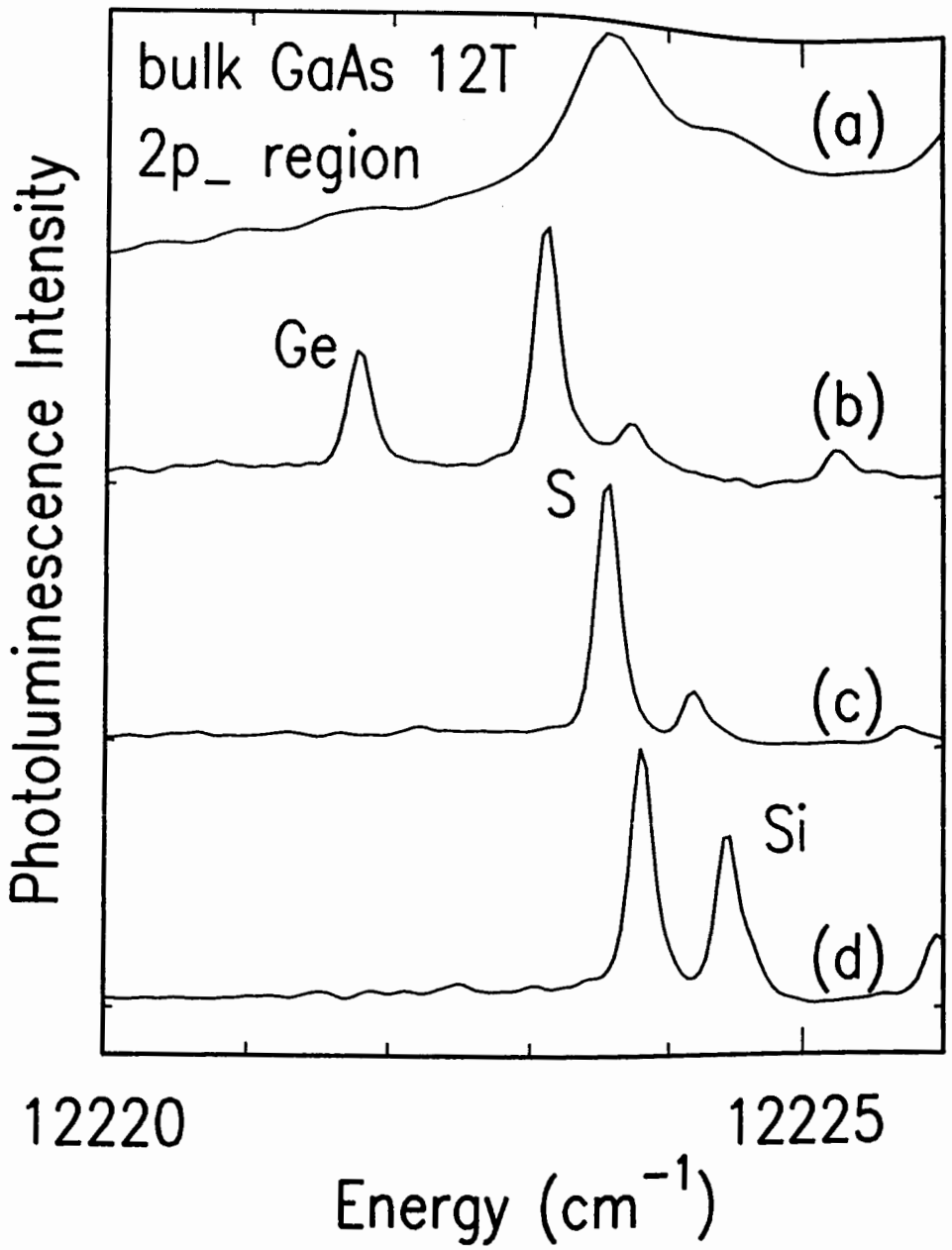
bulk GaAs 12T
2p_ region
(a)
Ge
(b)
S
(c)
Si
(d)
Photoluminescence Intensity
12220
12225
Energy (cm^{-1})

concentrations were found by taking the absolute intensity (not shown) of the TES response as each donor is resonated. In this sample the relative concentrations were measured to be 10:70:20 for [Ge]:[S]:[Si].

While it is necessary to pump each donor individually in order to obtain relative concentrations, this is not strictly necessary in order to determine the identity of the TES features. The identities can be obtained by measuring laser-to-TES separations for a single excitation energy, and comparing these values with the 1s to $2p_-$ separations measured very precisely for high purity epitaxial samples. The energy separations of the 1s A transitions and the $2p_-$ a^*_- TES at 12T for the 6 known shallow donor impurities in GaAs can be found in Table 5.1, in the previous chapter.

6.3 Conclusions

The above results demonstrate a reliable method for characterizing shallow donor impurities in bulk GaAs. This method relies on the high signal throughput and resolution capabilities of Fourier transform interferometry, as well as the intrinsic spectral accuracy of this method. In addition, the impurity specific energies of the ground and excited states of the donor bound exciton in GaAs has been demonstrated. This must be taken into account when interpreting resonantly excited spectra for donor characterization purposes. This method also relies on a precise and accurate knowledge of the excitation energy, demonstrating the convenience of a wavemeter. In agreement with previous publications [88H1, 86H1], the dominant donor in bulk SI GaAs was found to be S in all cases.

The contents of Chapter 6 have been submitted for publication [90B1].

CHAPTER 7 SUMMARY and CONCLUSIONS

7.1 Donor Bound Excitons in GaAs.

A comprehensive study of the shallow donor bound excitons in GaAs has been performed using Fourier transform photoluminescence. The superior resolution and SNR obtained with FTPL have been repeatedly demonstrated. The study has made use of PL spectra collected under varying conditions of magnetic field, excitation wavelength and sample orientation. The energetic positions of many of the (D^0,X) energy levels have been measured. This may allow further theoretical work on the behaviour of this system in a magnetic field. A tentative scheme involving angular momentum-related selection rules has been proposed.

As a result of this work, the donor electron spin-flip energy has been measured as 2.255 ± 0.006 cm^{-1} at B = 12T in our experimental apparatus. This translates into an electron g-value of 0.405 ± 0.008, taking into account uncertainties in the magnetic field strength. This is approximately ten percent lower than previous measurements, although in agreement with one of those measurements, due to its larger uncertainty.

In addition, the origins of the TES transitions have been positively identified. The $2p_- \; a^*_-$ TES transition is seen to originate from the same energy level as the principal 1s "A" transition and it newly identified spin-flip counterpart, A^*. The $2p_- \; b^*_-$ TES corresponds to previously hidden principal transitions which lie very close to the stronger A^*_0 and C transitions.

The energies of the 1s to $2p_- \; a^*_-$ separations have been measured with

precision unprecedented for the PL technique, and are found to agree well with the values extracted from graphs of PTIS transition energies *versus* magnetic field, when the above value for the electron spin-flip energy is added. This tabulation of the energy separations in Table 5.1 should prove useful for future donor identification work.

The FTPL technique has also been extended to include reliable donor identification in bulk semi-insulating GaAs, where the application of resonant line narrowing is necessary. A technique requiring knowledge of the 1s to $2p_-$ energy separations and the exact energy of the resonant excitation has been demonstrated.

7.2 Future Work.

The FTPL techniques promises to be very useful for future studies in GaAs and the related material InP. Of particular interest are the transition energies for InP in analogy with those given in Table 5.1. InP should also prove to be a revealing material for the study of (D^0,X) states in a magnetic field. The (A^0,X) states in both materials could also be studied by this technique, both for characterization purposes and to better resolve the issue of the zero-field splitting of the (A^0,X) states. Transitions related to the (D^+,X) states are also of some interest.

In general, FTPL and related techniques are demonstrated to have important advantages for semiconductor spectroscopy. Thus this technique should rapidly become the standard for optical studies in this field.

60H1 J.R. Haynes, Phys. Rev. Lett. **4**, 361, (1960).

69S1 G.E. Stillman, C.M. Wolfe, and J.O. Dimmock, Solid State Commun. **7**, 921 (1969).

70R1 J.A. Rossi, C.M. Wolfe, G.E. Stillman, and J.O. Dimmock, Solid State Commun. **8**, 2021 (1970).

71F1 H.R. Fetterman, D.M. Larsen, G.E. Stillman, P.E. Tannenwald, and J. Waldman, Phys. Rev. Lett. **26**, 975 (1971).

70F2 R.A. Faulkner and P.J. Dean, J. Lumin. **1/2**, 552 (1970).

71S1 G.E. Stillman, D.M. Larsen, C.M. Wolfe, and R.C. Brandt, Solid State Commun. 9, 2245 (1971).

72B1 R.J. Bell, *Introductory Fourier Transform Spectroscopy,* (1972), Academic Press, New York.

72F1 H.R. Fetterman, J. Waldman, C.M. Wolfe, G.E. Stillman, and C.D. Parker, Appl. Phys. Lett. **21**, 434 (1972).

72W1 A.M. White, I. Hinchliffe, P.J. Dean, and P.D. Greene, Solid State Commun. **10**, 497 (1972).

73D1 P.J. Dean, *Luminescence of Crystals, Molecules, and Solutions,* F.E. Williams (Editor), 538, Plenum, New York (1973).

75R1 D.C. Reynolds, C.W. Litton, T.C. Collins, S.B. Nam, and C.M. Wolfe, Phys. Rev. B. **12**, 5723 (1975).

76B1 A. Baldereschi and N.O. Lipari, *Proceeding of the Thirteenth International Conference on the Physics of Semiconductors,* Rome, 595 (1976).

76L1 D.M. Larsen, Phys. Rev. B. **13**, 1681 (1976).

76S1 W. Schairer, D. Bimberg, W. Kottler, K. Cho, and M. Schmidt, Phys. Rev. B. **13**, 3452 (1976).

77C1 E. Cohen and M.D. Sturge, Phys. Rev. B **15**, 1039 (1977).

77K1 Sh.M. Kogan and T.M. Lifshits. Phys. Stat. Sol. (a) **39**, 11 (1977).

77O1 M. Ozeki, K. Kitahara, K. Nakai, A. Shibatomi, K. Dazai, S. Okawa, and O. Ryuzan, Jap. J. Appl. Phys. **16**, 1617 (1977).

77S1 G.E..Stillman, C.M. Wolfe, and J.O. Dimmock in *Semiconductors and Semimetals*, R.K. Willardson and A.C. Beer (Editors). Vol. 12 (1977), pp. 169-290. Academic, New York.

78R1 W. Rühle, and W. Klingenstein, Phys. Rev. B. **18**, 7011 (1978).

80A1 M.N. Afsar, K.J. Button, and G.L. McCoy, Internat. J. Infrared and Millimeter Waves. **1**, 145 (1980).

80A2 M.N. Afsar, K.J. Button, and G.L. McCoy, Internat. J. Infrared and Millimeter Waves. **1**, 513 (1980).

81A1 M.N. Afsar, K.J. Button, A.Y. Cho, and H. Morkoc, Internat. J. Infrared and Millimeter Waves. **2**, 1113 (1981).

81A2 R.J. Almassy, D.C. Reynolds, C.W. Litton, K.K. Bajaj, and G.L. McCoy, Solid State Commun. **38**, 1053 (1981).

81R1 A.K. Ramdas and S. Rodriguez, Rep. Prog. Phys. **44**, 1297 (1981).

81K1 C. Kittel, *Introduction to Solid State Physics,* 6th ed., (1981), Wiley, New York.

82L1 Landolt-Börnstein, *Numerical Data and Functional Relationships in Science and Technology, New Series*, K.-H. Hellwege (Editor in Chief). Group III, Vol. 17 Semiconductors, Subvolume a (1982), Springer-Verlag, Berlin. ISBN 0-387-10610-3.

82L2 T.S. Low, G.E. Stillman, D.M. Collins, C.M. Wolfe, S. Tiwari, and L.F. Eastman, Appl. Phys. Lett. **40**, 1034 (1982).

82L3 T.S. Low, G.E. Stillman, T. Nakanisi, T. Udagawa, and C.M. Wolfe, Appl. Phys. Lett. **41**, 183 (1982).

82R1 D.C. Reynolds, C.W. Litton, E.B. Smith, and K.K. Bajaj, Solid State Commun. **44**, 47 (1982).

83R1 D.C. Reynolds, K.K. Bajaj, C.W. Litton, and E.B. Smith, Phys. Rev. B. **28**, 3300 (1983).

84D1 P.J. Dean, M.S. Skolnick, and L.L. Taylor, J. Appl. Phys. **55**, 957 (1984).

84L1 D. Labrie, T. Timusk, and M.L.W. Thewalt, Phys. Rev. Lett. **52**, 81 (1984).

84R1 D.C. Reynolds, P.C. Colter, C.W. Litton, and E.B. Smith, J. Appl. Phys. **55**, 1610 (1984).

84R2 J. Rorison, D.C. Herbert, P.J. Dean, and M.S. Skolnick, J. Phys. C. **17**, 6435 (1984).

85S1 B.J. Skromme, S.S.Bose, B.Lee, T.S. Low, T.R. Lepkowski, R.Y. DeJule, G.E. Stillman, and J.C.M. Hwang, J. Appl. Phys. **58**, 4685 (1985).

85S2 G.E. Stillman, T.S. Low, and B. Lee, Solid State Commun. **53**, 1041 (1985).

85T1 M.L.W. Thewalt, D. Labrie, and T. Timusk, Solid State Commun. **53**, 1049 (1985).

86G1 P.R. Griffiths and J.A. de Haseth, *Fourier Transform Infrared Spectrometry,* Chemical Analysis Vol. 83 (1986), Wiley, New York.

86H1 T.D. Harris and M.S. Skolnick in *Defects in Semiconductors,* H.J. von Bardeleben (Editor). Materials Science Forum Volumes 10-12 (1986), pp. 1219-1222. Trans Tech Publications Ltd., Switzerland.

87B1 S.S. Bose, B. Lee, M.H. Kim, and G.E. Stillman. Appl. Phys. Lett. **51**, 937 (1987).

87C1 P. McL. Colley and E.C. Lightowlers, Semicond. Sci. and Technol. **2**, 157 (1987).

88A1 A.R. Adams, K.C. Heasman and E.P. O'Reilly, in *Band Structure Engineering in Semiconductor Microstructures,* R.A. Abram and M. Jaros (Editors). NATO ASI Series B: Physics Volume 189 (1988), pp.279-301. Plenum Press, New York and London.

88B1 S.S. Bose, M.H. Kim, and G.E. Stillman, Appl. Phys. Lett. **53**, 980 (1988).

88H1 T.D. Harris, M.S. Skolnick, J.M. Parsey, Jr., and R. Bhat. Appl. Phys. Lett. **52**, 389 (1988).

88R1 N.L. Rowell, Infrared Phys. **28**, 37 (1988).

88S1 S.K. Shastry, S. Zemon, D.G. Kenneson, and G. Lambert, Appl. Phys. Lett. **52**, 150 (1988).

88W1 S.P. Watkins, G. Haacke, and H. Burkhard, Appl. Phys. Lett. **52**, 401 (1988).

88W2 S.P. Watkins, G. Haacke, H. Burkhard, M.L.W. Thewalt, and S. Charbonneau, J. Appl. Phys. **64**, 3205 (1988).

89B1 Sales brochure, Bomem Inc. 450 St. Jean-Baptiste, Québec, QC Canada G2E 5S5.

89G1 D. Gershoni and H. Temkin, J. Lumin. **44**, 381, (1989)

89H1 G. Haacke, S.P. Watkins, and H. Burkhard, Appl. Phys. Lett. **54**, 2029 (1989).

89L1 B. Lee, K. Arai, B.J. Skromme, S.S. Bose, T.J. Roth, J.A. Aguilar, T.R. Lepkowski, N.C. Tien, and G.E. Stillman, J. Appl. Phys. **66**, 3772 (1989).

89R1 D.C. Reynolds, K.K. Bajaj, W.M. Theis, P.W. Yu, and N. Chand, Appl. Phys. Lett. **54**, 159 (1989).

89S1 B.J. Skromme, R. Bhat, H.M. Cox, and E. Colas, IEEE J. Quantum Electron. **25**, 1035 (1989).

89S2 T. Steiner, Yu Zhang, S. Charbonneau, A. Villemaire, M.L.W. Thewalt, M. Maciaszek, and R.P. Bult, Can. J. Phys. **67**, 242 (1989).

90B1 D.J.S. Beckett, M.K. Nissen, and M.L.W. Thewalt, submitted to Can. J. Phys., Aug 14, 1990.

90C1 E.R. Cohen and B.N. Taylor, Physics Today, **43** (8), part 2: Buyers' Guide, p. BG 9. (1990).

90N1 M.K. Nissen, T. Steiner, D.J.S. Beckett, and M.L.W. Thewalt, Phys. Rev. Lett. **65**, 2282 (1990).

90S1 M.Said and M.A. Kanehisa, Phys. Stat. Sol. (b) **157**, 311 (1990).

90T1 M.L.W. Thewalt, M.K. Nissen, D.J.S. Beckett, and K.R. Lundgren, Mat. Res. Soc. Symp. Proc. **163**, 221 (1990).

90T2 M.L.W. Thewalt and D.M. Brake, to be published in *Proceedings of the 4th International Conference on Shallow Impurities in Semiconductors,* London U.K., August 1990.

90W1 S.P. Watkins and G. Haacke, submitted to J. Appl. Phys., (Oct. 1990).

APPENDIX: Comparison of Interferometric and Dispersive Spectra.

Throughout this thesis, it has been stated that interferometry is a technique superior to dispersive spectroscopy for PL of GaAs. To make a direct comparison, examples of spectra from both techniques are given in Fig. A.1. (The effect of increasing the magnetic field should also be noted.)

The upper spectrum (Fig. A.1(a)) was taken at B = 7 T using a Spex 3/4-m double grating spectrometer with 1200 groove/mm gratings (88W2,89S2). The resolution with the grating spectrometer was 0.02 meV (0.16 cm^{-1}) with the slits at 50 μm. The spectrum in Fig A.1(b) was collected from by FTPL at a moderate resolution of 0.1 cm^{-1}.

The improvement obtained with FTPL is striking especially when one considers that the interferometer resolution could still be increased by a factor of four. In addition, the spectra on the interferometer can be collected without need for calibration, which is a serious concern with the mechanically scanned grating instrument.

Better dispersive spectra have been demonstrated with much more complicated optical collection systems (89S1). However, extending the resolution of a grating system to that (routinely) achieved with an interferometer will inevitably lead to much lower signal throughput. Thus, the best dispersive results do not compare favourably with those obtained with interferometry.

Figure A.1

Comparison of magneto-PL spectra collected by dispersive and interferometric techniques. (a) PL of TES $2p_-$ region in a high-quality MOCVD GaAs sample collected at B = 7 T using a dispersive grating spectrometer. Resolution is 0.16 cm^{-1}. (b) PL of a similar sample collected by interferometric PL at B = 12 T. Resolution is 0.1 cm^{-1}.

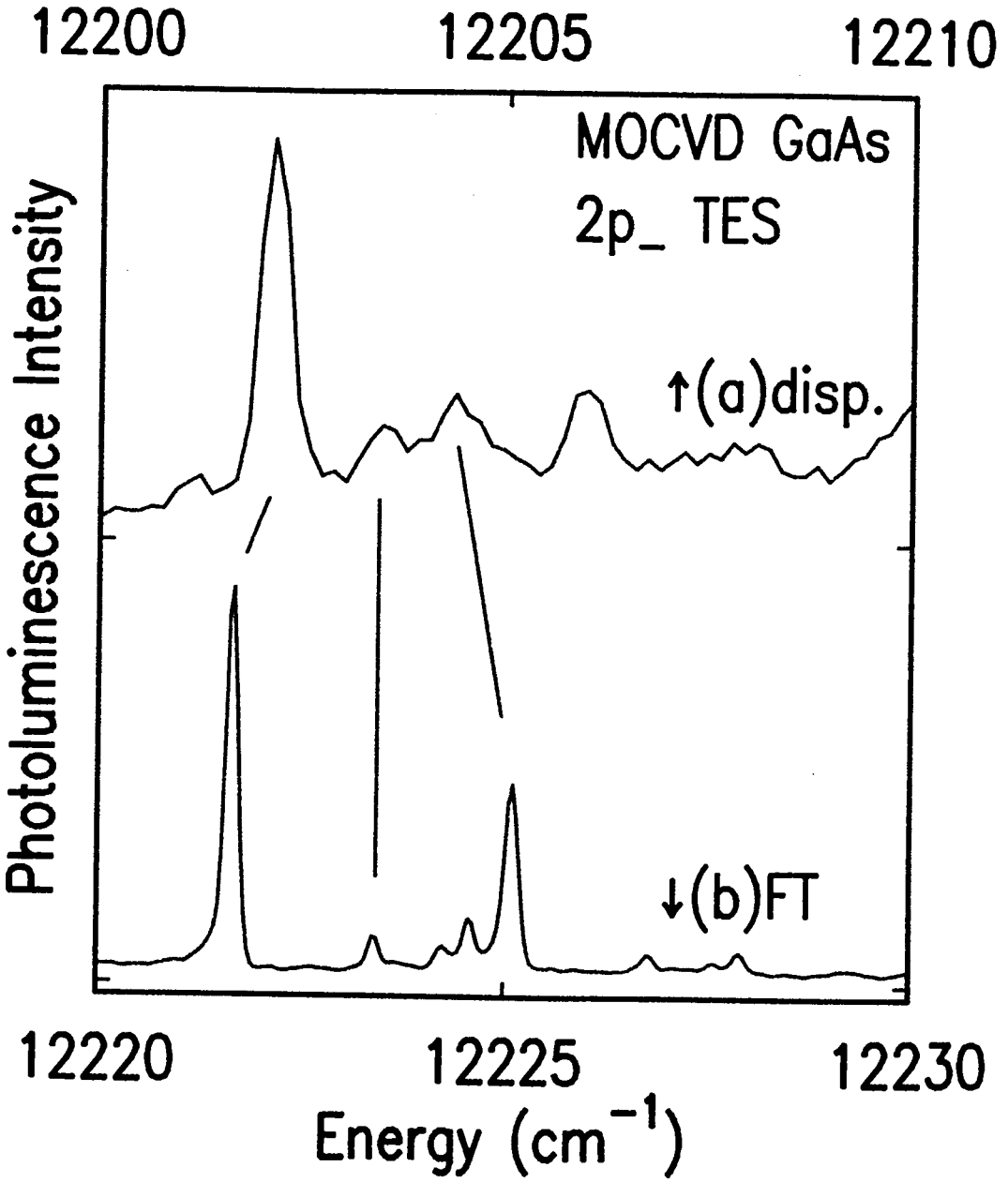
12200
12205
12210
MOCVD GaAs
2p_ TES
↑(a)disp.
↓(b)FT
Photoluminescence Intensity
12220
12225
12230
Energy (cm^{-1})